UNIVERSITY OF SOUTHAMPTON

FACULTY OF ENGINEERING AND PHYSICAL SCIENCES

DEPARTMENT OF MECHANICAL ENGINEERING

National Centre for Advanced Tribology at Southampton (nCATS)

A Study of Initiation Mechanisms of White Etching Cracking in Rolling Bearings

by

Ningxin Zhao

Supervisors:

Prof. Ling Wang [a], Prof. Philippa Reed [b], Prof. Walter Holweger [a,c]

a National Centre for Advanced Tribology at Southampton (nCATS), University of Southampton

b Engineering Materials Group, University of Southampton

c Basic Tribology, Competence centre of Surface Technology, Schaeffler Technologies AG & Co. KG, Herzogenaurach, Germany

Master of Philosophy

July 2020

UNIVERSITY OF SOUTHAMPTON

<u>ABSTRACT</u>

White Etching Cracks (WECs) in bearings are found to cause unexpected failures and can result in economic losses in many applications, such as wind turbine gearbox and automotive components. Although the problem of WECs is established as important and many researchers have studied the phenomenon, the effect of different drivers, whether the initiation point is subsurface or surface and the order of formation of cracks and white etching areas (WEA) are still the subject of debate. A better understanding of these particular issues will help to inform the reliability of roller bearings by improving their design through further mechanistic insight.

A systematic literature review was carried out first to assess previous relevant research related to WECS, such as the detailed microstructural features observed, proposed drivers of the phenomenon and initiation mechanisms in proposed bearing steel. In this project, the initiation mechanisms of WECs have therefore been further studied via experimental observation of a series of AISI 52100 steel bearing samples tested on an FAG-FE8 rig at Schaeffler under a contact pressure of 1.35 GPa over a range of test durations, where WECs at different stages were created. All bearing tests used the "WEC critical lubricant", a common lubricant to create WECs. Microstructure characterisation techniques, including optical microscopy, scanning electron microscopy (SEM) and energy-dispersive X-ray spectroscopy (EDS), were then used to characterize the different stages of WEC formation, with an especial focus on the initiation stages.

The bearings with the longest test duration that have surface damage were examined first to help to determine the area where WECs were likely to initiate. These areas in tested samples with shorter testing duration time were then observed in detail to find the earliest stages of WECs. By comparing the different microstructure characteristics of WECs at these different stages and comparing with prior knowledge in the literature, a growth mechanism of WEA related to a transitional area containing crack-like structures and an initiation mechanism of WECs related to the aligned/clustered carbide aggregation have been hypothesised.

Contents

Contents

List of Tables

List of Figures

List of Figures

List of Figures

Declaration of Authorship

I, **Ningxin Zhao**, declare that this thesis entitled

A Study of Initiation Mechanisms of White Etching Cracking in Rolling Bearings

and the work presented in it are my own and has been generated by me as the result of my own original research.

I confirm that:

1. This work was done wholly or mainly while in candidature for a research degree at this University;
2. Where any part of this thesis has previously been submitted for a degree or any other qualification at this University or any other institution, this has been clearly stated;
3. Where I have consulted the published work of others, this is always clearly attributed;
4. Where I have quoted from the work of others, the source is always given. With the exception of such quotations, this thesis is entirely my own work;
5. I have acknowledged all main sources of help;
6. Where the thesis is based on work done by myself jointly with others, I have made clear exactly what was done by others and what I have contributed myself;
7. None of this work has been published before submission.

Signed:

Date: 28/July/2020

Acknowledgements

Definitions and Abbreviations

AISI   American Iron and Steel Institute

ASB   Adiabatic shear bands

BSE   Backscattered electrons

DEA   Dark etching areas

EBSD   Electron backscatter diffraction

EDS/EDX   Energy-dispersive X-ray spectroscopy

FE8   FAG-FE8 test rig

FIB   Focused ion beam

HAGB   High Angle Grain Boundaries

HRC   Rockwell hardness c

ICCI   Ion channelling contrast image

IPF   Inverse pole figure

IQ   Image quality

KAM   Kernel average misorientation

L11   FAG L11 test rig

MnS   Manganese (II) sulfide

OM   Optical microscopy

OP-S   Collodial silica suspension

RCF   Rolling contact fatigue

SADP   Selected area diffraction pattern

SE   Secondary electrons

Definitions and Abbreviations

SEM	Scanning electron microscopy
SIM	Scanning ion microscope
SRR	Slide to roll ratio
STEM	Scanning transmission electron microscopy
TEM	Transmission electron microscopy
WEA	White etching areas
WECs	White etching cracks
WD	Working distance
WSF	White structure flaking

Chapter 1   Introduction

1.1   Background

Bearings are key components in all kinds of drivetrain applications, such as automotive, marine, and aerospace applications. As a result, the reliability of bearings involved directly affects the reliability of a drivetrain. White etching cracks (WECs) are sometimes found in bearings [1]-[5], which can lead to white structure flaking(WSF) [2], [3], [5] and result in significant economic losses to the industry. For example, it has been reported that some bearings in wind turbine gearboxes, whose designed life should be 20+ years, were replaced due to WSF within the first few years of service, with an estimated cost of £ 0.1-0.3 million per gearbox replacement [2], [6]-[8]. Further inspection of the failed bearings revealed that the failure was caused by WECs, as shown in Figure 1-1 [5]. WECs are distinctive and complex crack modes, which are boarded with material transformation called White Etching Area (WEA). Therefore, a better understanding of the initiation and formation mechanisms of WECs to increase the reliability of bearings is a critical industry need.
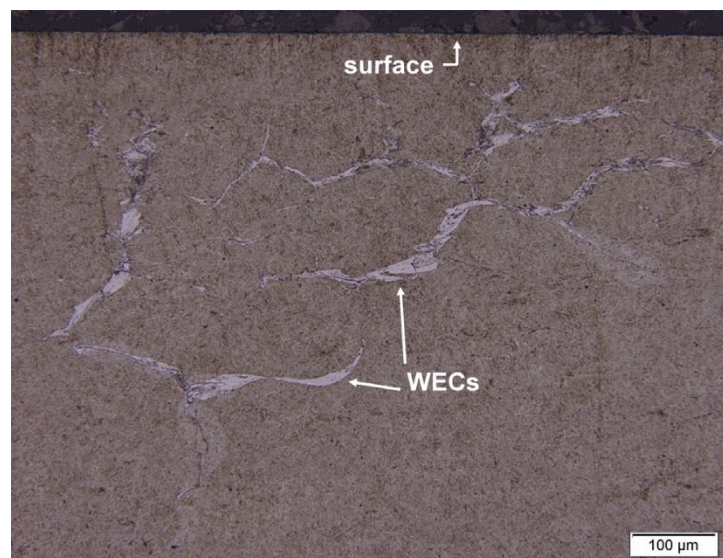
Figure 1-1. Optical images of WECs in the subsurface of bearings [5].

Over the last two decades, a large amount of research has been conducted to initially characterise WECs, then to create WECs in laboratory conditions, followed by a more detailed study on WEC formation and initiation mechanisms. While the general characteristics of WECs are now quite well understood, and many hypotheses on WEC

formation mechanisms have been proposed, their initiation process is still not very well understood. So far, the hypothetical root cause for WECs can be divided into local overload initiated by a complicated stress state and hydrogen released from the breakdown lubricant [2]-[4], [9], [10] and decomposition of water. Electrical current [1], [2], [11], [12], bad oil [1], [2], slip [1], [2], [13], [14] and high pressure are all considered potential drivers for WECs.

There are two main initiation mechanisms of WECs proposed in the literature based on the initiation area: subsurface and surface initiation. In the surface initiation mechanism hypothesis [15]-[17], WECs initiate from defects on the surface, where high-stress concentration causes lubricant film breaks. Subsequently, cracks will propagate from the surface into the subsurface. In the subsurface initiation mechanism hypothesis [1], [5], [9], [18]-[21] WECs initiate beneath the contacting surface; more specifically, they initiate from defects or stress concentration points under the contacting area. The initiated WECs grow and connect with each other into networks subsurface and then propagate towards the surface, resulting in axial cracking or WSF failures. However, all these mechanisms still require confirmation via further research.

Up to now, the initial stage of WECs has not been fully and exactly observed under different conditions. It has been confirmed that electricity is helpful to the growth of WEC. However, whether WECs are initiated by slippage or slippage-caused electricity is a problem. In this project, axial loading bearings are chosen because the slippage occurs between rollers and washers. WEC critical oil is an oil proven to cause WEC. Low pressure will be used to make the maximum shear stress shallow in the subsurface. This relationship is clearly illustrated in Section 3.5. It will be helpful to observe WEC near the surface.

1.2   Aims and objectives of the project

The main aim of this project is therefore to study the initiation mechanisms of WECs in AISI 52100 bearing steel by analysing the evolution of microstructure changes of WECs created in rolling contact fatigue tests. Advanced microstructural characterisation techniques, such as optical microscopy (OM), scanning electron microscopy (SEM), and energy-dispersive X-ray spectroscopy (EDS) are employed in this project.

The key objectives are:

- To understand the state-of-the-art WEC research through reviewing the existing literature systematically, especially focusing on the formation and drivers of WECs, which will help to determine the key detailed observations needed

- To first characterize the later stage of WECs via characterising failed bearings after longer testing times which will usually have obvious surface damage.

- To then characterize the early stage of WECs via characterising the appropriate areas in cross-sections of FE8 bearings after shorter testing times, which have no obvious surface damage, but where more experimental data will help to confirm the subsurface or surface initiation hypotheses of WECs.

- To propose an initiation and evolution mechanism of WECs based on detailed characterisation of the microstructures obtained under specific test conditions - WEC critical lubricant and slip by comparing the characteristics of WECs found at later and earlier stages.

Chapter 2   Literature Review

2.1   Bearing fundamentals

2.1.1   Rolling element bearings

Rolling element bearings refer to various types of bearings that use the rolling of a ball or roller to achieve small amounts of friction and constrain movement of one object relative to another. They are a widely used component in more than 90% of rotating machinery in industrial applications due to their advantages including lower starting and running friction, less maintenance and higher accuracy of shaft alignment.

Generally, rolling bearings comprise an inner race, an outer race, several rolling elements and a cage as shown in Figure 2-1. Based on the type of rolling elements, rolling bearings are commonly classified as ball bearing and roller bearing. The bearing shown in Figure 2-1 is an example of a roller bearing typically used in the wind turbine gearbox. The contact between the roller and the outer race is line contact, which is the same contact type studied in this project.

According to the applied load direction on the bearings, rolling bearings can be further divided into radial bearing, angular contact bearing and thrust bearing.
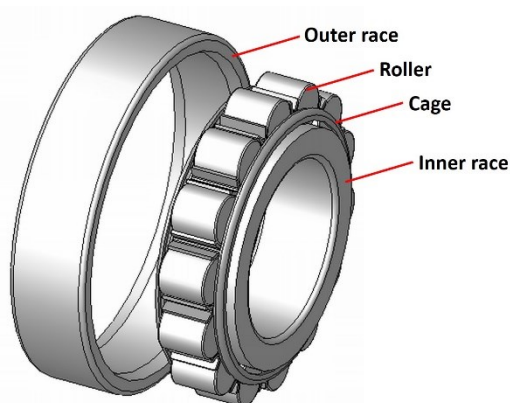
Figure 2-1. The structure of a rolling element bearing [22].

2.1.2   Bearing steel

The material for bearings needs to satisfy the requirements for contact fatigue strength, wear and corrosion resistance, hardness, toughness, elastic limit, dimensional stability and processability [23]-[25]. In order to ensure these requirements, the metallurgical quality of bearing steel needs strict control of the chemical composition and inhomogeneity of carbides and non-metallic inclusions. There are two types of steel mainly used for the rings and rolling elements-one is through-hardened chromium steel in martensitic or bainitic form, and the other is case-hardened steel having soft cores but hardened surface layers [26]. The American Iron and Steel Institute (AISI) 52100 through-hardened high carbon chromium bearing steel is the most widely used material in most bearing applications [26]. In this report, the races and rollers of all the bearings studied are made of AISI 52100.

In general, this kind of steel is supplied with an initial structure including pearlite and some proeutectoid cementite. The proeutectoid cementite located at the prior austenite grain boundaries forms a network, which is found to be unfavourable for rolling contact fatigue life when the contact pressure exceeds 5 GPa [26].

Typically austenitisation is developed at 840 ˚C for 20 min. Although the steel is completely transformed into austenite at higher temperatures, it will increase the austenite grain size [26]. Higher austenitisation temperatures result in a larger austenite grain size because more carbides dissolve. The austenite grain size is found to relate to the propensity for microcracking in the martensite formed afterwards. The austenite grain size should therefore be kept small enough to avoid cracking of untempered and high carbon martensite [27]. Short-austenitisation is a feasible process that achieves a finer austenite grain size used by industry. The cementite dissolution process can be sped up by cold working the steel prior to the short austenitisation [28].

During this austenitisation at 840 ˚C, some cementite may remain, where the volume percentage depends on the austenitisation time and the starting microstructure. This remaining cementite after heat treatment will however improve the wear resistance in the final microstructure.

The normal quenching process is down to 60 ˚C in oil to form martensite, resulting in a structure containing martensite and ~6 vol% of retained austenite and ~3-4 wt% of cementite particles [26]. This structure has a hardness of 59-66 HRC [26].

The tempering process, which occurs at 160 ˚C for 1-2 hours, improves the toughness of martensite, precipitating transitional hardening carbides like η-Fe_2C, χ-Fe_5C_2 and ε-$Fe_{2-3}C$ [26], [29], and decomposing some of the retained austenite.

2.1.3   Bearing basic rating life

The reliability of a bearing is an essential parameter in determining its lifetime. In general, L_{10}, also called the basic rating life, is widely used as a standard method for calculating the roller bearings' life.

The formula for L_{10} according to ISO 281 [30] is as follows:

$$L_{10} = \left(\frac{C}{P}\right)^p \tag{2.1.1}$$

where L_{10} is the basic rating life reached by 90% of a large group of tested bearings, C is the basic dynamic load rating, P is the equivalent dynamic load for radial and axial bearings, and p is the life exponent which is equal to 10/3 for roller bearings.

2.2   Rolling contact fundamentals

Contact areas in bearings are loaded continuously or cyclically under service conditions, thus resulting in surface/subsurface damage in these areas. Thus understanding the bearing surface contact conditions and stress distributions is important in the subsequent analysis of bearing failure root causes.

Line contact assumption is usually used in the analysis of contact in some rolling element bearings. Based on the assumption of the initial line contact between two contacting bodies, Hertzian contact theory calculates the local stress distribution based on four assumptions [31]. The four assumptions are 1)two contact bodies are elastic; 2)the contact surface is continuous and non-conforming; 3)the strains of the contact bodies are small and within the elastic limit; and 4)no friction on the surface is considered [31]. Hertz reasoned that some elastic deformation occurs where the load was applied resulting in a larger contact area to distribute the load so that the stresses are not infinite. When loaded, the contact area therefore becomes rectangular instead of a line. The model of roller-race contact and the surface compressive stress distribution for line contact is shown in Figure 2-2 [32] and Figure 2-3 [33]. Although Hertz's theory involves the condition of a frictionless contact

surface, Hertzian contact theory is still suitable to deal with the stress conditions with reasonable accuracy if the oil film thickness of a rolling bearing contact is large compared to the roughness of the contact components [34].
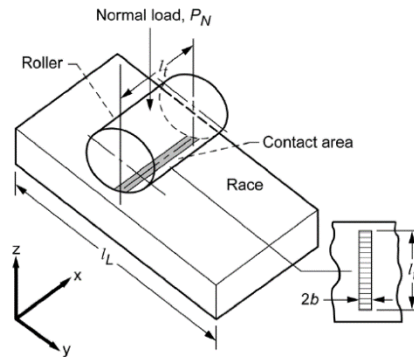
Figure 2-2. Roller-race contact model (line contact) [32].
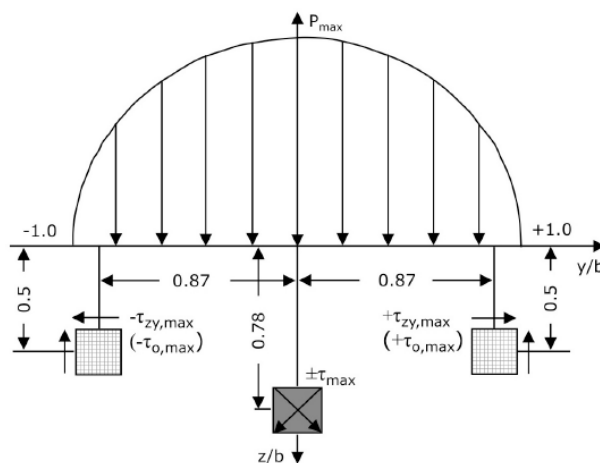
Figure 2-3. Maximum shear stress in the subsurface related to Hertz maximum contact pressure in line contact condition [33].

There are two types of shear stress in the subsurface of a rolling contact: 1) Orthogonal shear stress (τ_0), which is parallel or perpendicular to the surface; 2) Unidirectional shear stress (τ), which is at an angle of ±45° to the surface. It is well known that bearings typically fail due to rolling contact fatigue caused by continuously varying subsurface shear stress [35]. Two main shear stresses are commonly considered for bearing life analysis: orthogonal shear stress (τ_0) (based on the Lundberg-Palmgren model [36]) and the maximum shear stress (τ_{max}) (based on Zaretsky's model [37]). Both of them vary in proportion to the maximum Hertzian pressure (P_{max}) experienced by two objects as:

$$\tau = k \times P_{max} \qquad (2.2.1)$$

8

where the proportional constant k = 0.25 and 0.30 for the orthogonal and the maximum shear stress under line contact between steels (Poisson's ratio is 0.3), respectively. For roller bearings, the subsurface depths of maximum orthogonal and the maximum shear stress are 0.5b and 0.78b, respectively (b is the semi-width of the contact geometry in the rolling direction). In a real rolling contact, lubrication conditions and the level of sliding and rolling affect the subsurface stress fields. Sliding causes friction force on the surface and then causes shear stress acting along the surface. It is found that the maximum shear stress moves to the surface with an increase of friction force [38]. Therefore, it is necessary to consider the influence of sliding on the position of the initial crack.

2.3 White Etching Cracks

2.3.1 Bearing failures related to WECs

There are two failure modes seen in bearings that are related to white etching cracks (WECs). The first one is a kind of spalling that occurs at 1%-20% of L_{10} life [39]. It is termed white structure flaking (WSF) because the flaking cross-section region of the microstructure looks white after etching. Another failure mode is axial cracking, usually occurring in wind turbine gearboxes [15], [40]. The features of WSF and axial cracking on raceways and cross-sections of failed wind turbine gearbox bearings used in the high-speed shaft are shown in Figure 2-4 and Figure 2-5 [40] respectively.

It should be noted that there are similar microstructural changes seen around the flaking area in WSF and the axial cracking. The subsurface microstructural alterations (shown in Figure 2-4 (b) and Figure 2-5 (b)) in WSF and axial cracking are typical transformations seen from the original bearing steel microstructure to carbon supersaturated ferrite, known as a white etching area (WEA). The cracks bordered with WEA are white etching cracks (WECs).
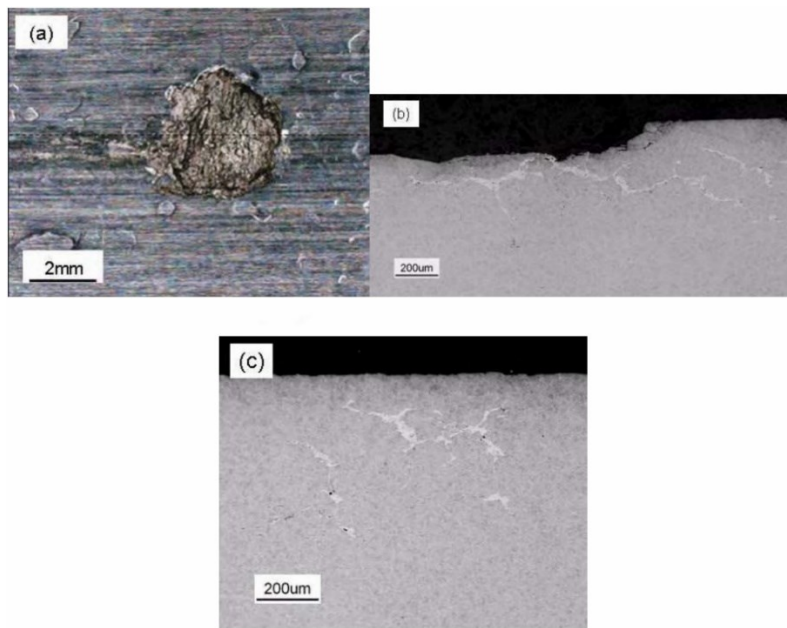
Figure 2-4. WSF on a failed wind turbine gearbox bearing (a) WSF on raceway surface; (b) cross-section of the flaking area in a, showing WECs in the subsurface; c) cross-section of the area with no flaking, showing WECs in the subsurface [40].
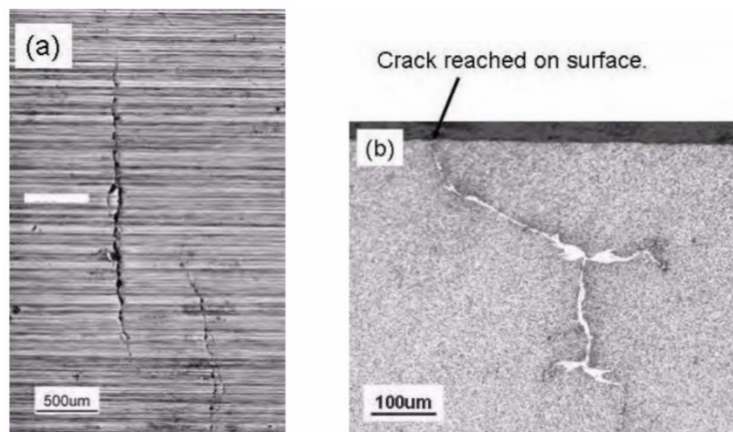
Figure 2-5. Axial cracking on a failed wind turbine gearbox bearing. (a) Axial cracks on the raceway surface; (b) The cross-section through the cracks [40].

WECs are usually observed in the subsurface of WSF and axial cracking, where they are bordered with a WEA up to 1.5mm depth under bearing contact raceways [2], [9], [41]. Depending on the position of the cross-section being observed, WECs are parallel or branching network systems ranging from micrometres to millimetres [2], [5]. In the plane parallel to the rolling direction, cracks generally run along the direction towards the core, which is more vertical. However, in the plane which is along the axial direction, most cracks are parallel with the surface; these cracks have fewer vertical branches [18], [42]-[44]. WSF and axial cracking have been observed to take place in the inner race of bearings [41], so

in most research, the inner ring was more focused upon to examine WECs. Although WECs have been investigated for decades, there is no clear consensus on the initiation mechanisms and drivers.

2.3.2 Microstructure of WEA

The altered microstructure of etched steel samples under a microscope, showing a "white appearance" due to the low etching response of the area to the etchant, is the WEA. It is an ultra-fine nanocrystalline carbide-free ferrite structure which has been evaluated in selected area diffraction patterns [1], [45]-[48]. It should be noted that the nature of its interface is complex. Between WEA and matrix material in butterflies (Detailed information about butterflies is in Section 2.5) the interface appears to change gradually while the boundary between the WEA and substrate in WECs is clear [2], [45].

In terms of the microstructure in WEA, needle-like structures [49], lamellar structures [45] and amorphous structures [46], [47] have been found and the grain size in WEA shows a clear trend where it increases in a gradient from one side to another from 10 nm to 300 nm. More detailed microstructure characteristics in WEA have been reported by other researchers. Grabulov et al. found that the grains of WEA have no preferential crystallographic orientation when analysed by electron backscatter diffraction (EBSD), shown in Figure 2-6 [45]. In Figure 2-6 (c) and (d), the different phases are identified by the automatic crystal orientation mapping in EBSD, and the black zone in an inverse pole figure (IPF) map shows that no preferential crystallographic orientation of grains was found in the WEA. Moreover, although there were no changes in microstructure observed in the bulk material, West et al.[10] reported a possible transition region which is gradually refined at the boundary of the WEA and matrix.

In terms of the hardness of the WEA, it is 10%-50% harder than the matrix [10], [41], [50]-[53]. This can be explained by the Hall-Petch relationship, which states that the yield strength of the material increases with the decrease of grain size. The equation for the Hall-Petch relationship is as follows:

$$\sigma_y = \sigma_0 + \frac{k_y}{\sqrt{d}} \quad\quad\quad (2.3.1)$$

where σ_y is the yield stress, σ_0 is the lattice friction to prevent dislocation motion, k_y is a strengthening constant, and d is the average grain diameter. In WEA, ultra-fine structures [10], [24], [41], [54], [55] ,voids, cavities [19], [45], [46] and microcracks have been observed [13], [19], [41], [45]-[47] . These ultra-fine nanocrystalline structures in WEA indicate very small grain sizes, thus resulting in higher yield strength and higher hardness.

In terms of the formation process of WEA, the spherical carbides elongate and deform in the early stages due to the cyclic stress, and then break up and finally dissolve [13], [50], [56]-[58] accompanied by the shear flow of carbides to the cracks and the interface of WEA/inclusion [46], [59], [60]. The diffusion of carbon into the microcracks reduces its surface energy and facilitates its stable growth [61].
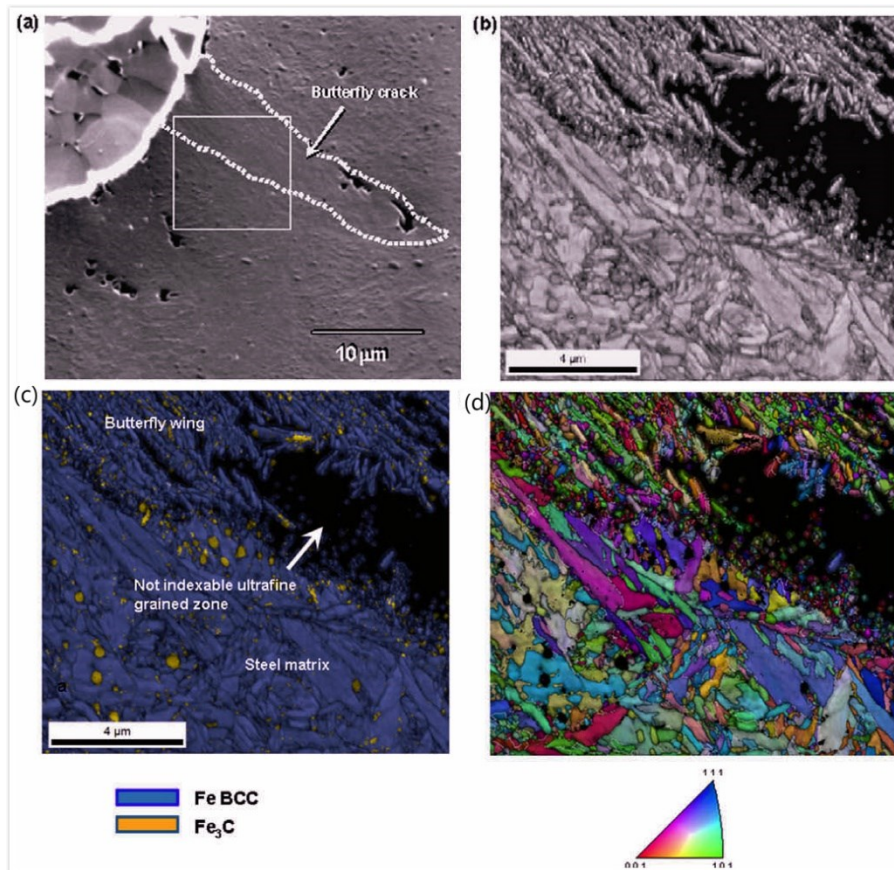
Figure 2-6. EBSD results on bearings with a similar composition to grade SAE 52100 and including artificially introduced spherical Al_2O_3 inclusions under high cycle rolling contact fatigue. (a) Image of the WEA in a butterfly wing near the inclusion. The butterfly will be discussed in Section 2.5. The marked area is investigated further in EBSD; (b) Image quality (IQ); (c) Combined IQ and phase map; (d) Normal direction inverse pole figure (IPF) map of the marked area in (a)[8].

2.3.3   The hypotheses of WEA formation

Harada et al. [13] proposed that acicular structures (Figure 2-7), resulting from the transformation of the microstructures from martensite into a mixture of dislocation cell structures and fine grains, are the initial stages of the WEA formation process. The acicular structures form at angles of 30° and 160° to the rolling direction, which indicates the direction of shear stress induced by slip. Micro voids formed near the interfaces of martensite/retained austenite and martensite/spheroidised carbide. The amorphous-like structure shown in Figure 2-8 [13] was seen in WEA, and microcracks were seen at the interface of the granular structure/amorphous-like structure and WEA/matrix. The WEA was produced using a disk on a roller-type rolling contact fatigue test machine. It was proposed that an amorphous-like structure formed first, then changed to WEA. Harada et al [13] proposed that the acicular structures and WEA were formed by localised plastic strain due to shear stress induced by the slip, resulting in the increase of dislocation density and localised shear in martensite. When reaching the critical dislocation density, the strain energy was released by the dislocation cell-like structures [62].
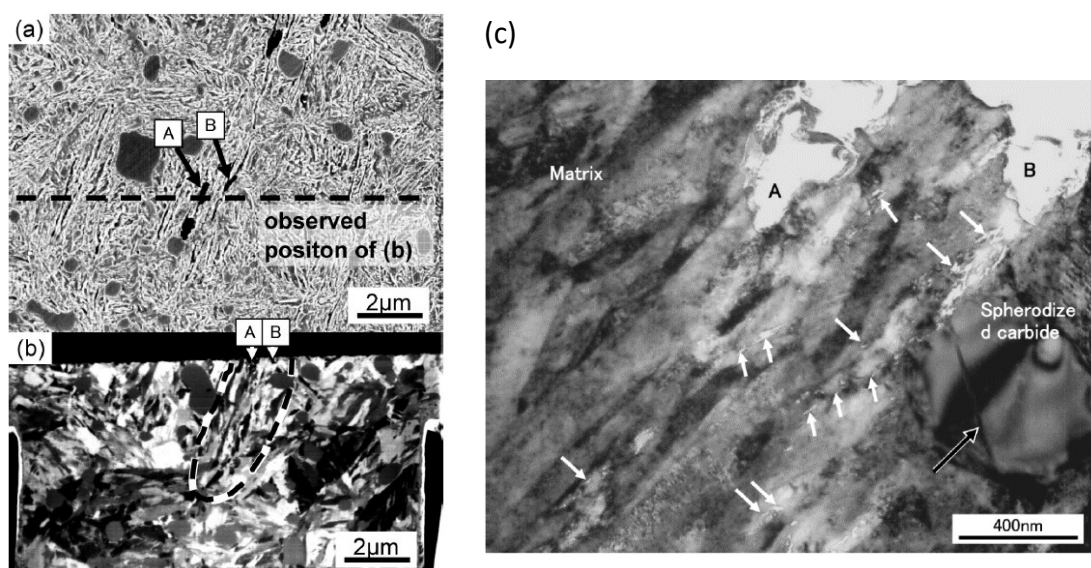
Figure 2-7. (a) The SEM observation of top surface, where acicular structures A and B are marked by black arrow (b) The SEM image of the cross section of the dotted line in (a). (c) TEM image showing the acicular structure in region A and B in (b). White arrows point to voids and black arrow mark the dislocation. The bearing made of high carbon chromium bearing steel, was tested under a maximum contact stress of 4.2 GPa, a slip ratio of 14% and traction oil conditions [13].
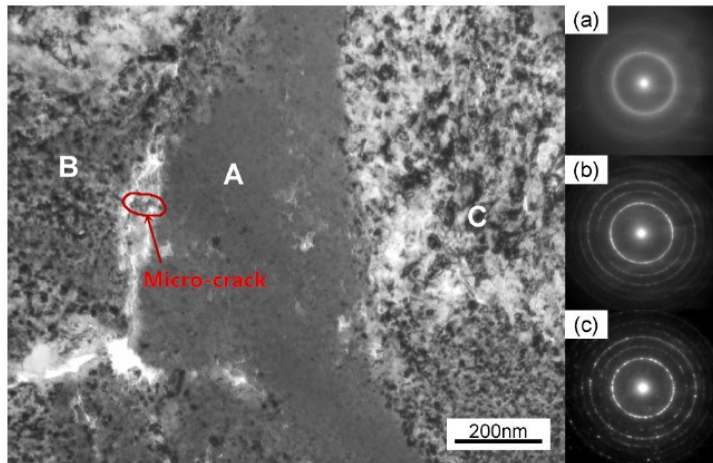
Figure 2-8. TEM image of WEA and selected area diffraction pattern (SADP) at different regions. SADP of A, B and C are shown in (a), (b) and (c), respectively. The halo rings in (a) indicate the structure is amorphous-like in area A. However, areas B and C have granular structures due to the mix of ring patterns and spot patterns [13].

Hydrostatic pressure forces the crack surface to close, resulting in nanocrystallisation due to crack face rubbing. This process has also been suggested to form WEA [59]. Where the area has a high hydrostatic compressive stress, finite element stress analysis shows that WEA will generate in a specific microcrack kink region [59]. Prerequisites of WEA formation were considered to be microcracks, which are suppressed by hydrostatic pressure, thus helping the accumulation of plastic strain to form WEA [63]. The hydrostatic pressure causes the dissolution of carbides because the density of carbides is lower than that of ferrite [64].

The order of formation of WEA and microcracks, or whether they grow together, has yet to be determined. Richardson et al. [65] found more evidence of cracks without WEA, supporting that microcracks form before WEA in 100Cr6 steel cylindrical roller thrust bearings under non-hydrogen charged conditions and with a maximum contact pressure of 1.5 GPa by using serial sectioning metallography techniques. West et al. [10] found a small crack not surrounded with WEA when examining the base material in prematurely failed 100CrMo7-3 steel bearings, as seen in the lower left in Figure 2-9(a)[10]. Based on this, the authors suggested that cracks form and grow before the formation of WEA.
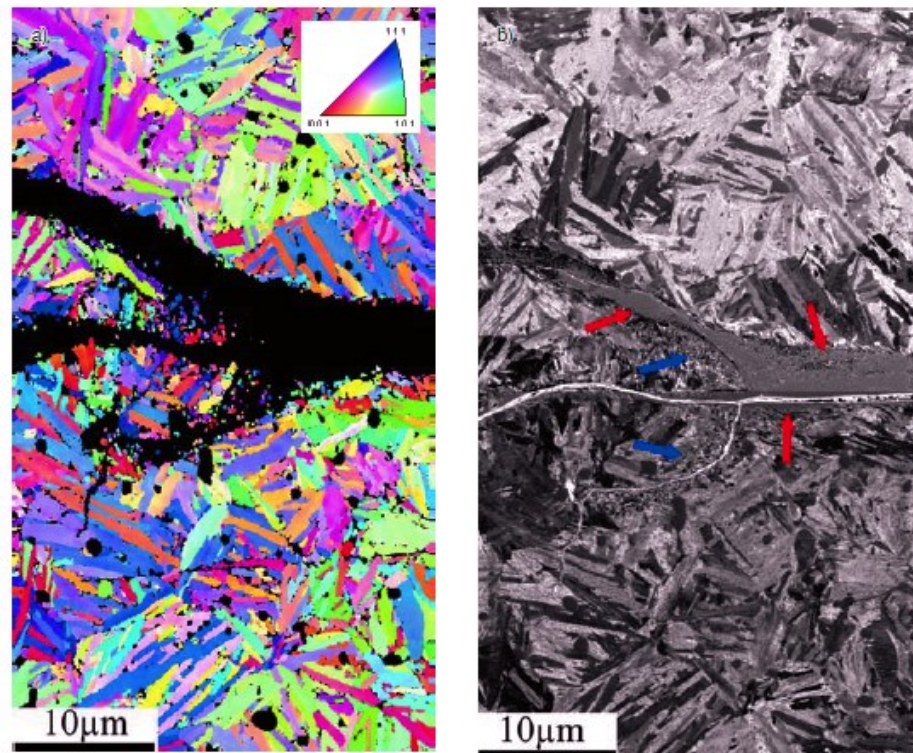
Figure 2-9. (a) Orientation map of EBSD results; (b) Ion channelling contrast image (ICCI) results on the same area. The direction of the lower-left branch of the crack is changes [10].

Some authors [2], [10], [46] found microcracks in WEA (Figure 2-10), while others[13], [47], [53], [66] considered crack-like linear structures as the pre-stages of WEA. Diederichs et al. [49] found a needle-like/elongated structure in WEA under the EBSD and STEM, which looks like microcracks after etching with Nital (Figure 2-11). Grains in this region are called needle-like grains. They believed that the needle-like grains had been wrongly considered as cracks in previous research[2], [13], [19], [47] after comparing the orientation contrast images and SE images of the etched region in the previous research. It was proposed that the needle-like grains could more easily be Nital-etched because of their lower carbon content [49]. In the EBSD analysis, these needle-like grains show the similar growth direction and orientation, see the inverse pole figure (IPF) map in Figure 2-12 (b), and lower misorientation when compared to the matrix, see Kernel average misorientation (KAM) in Figure 2-12 (c), which are similar to the characteristics of recrystallised material.
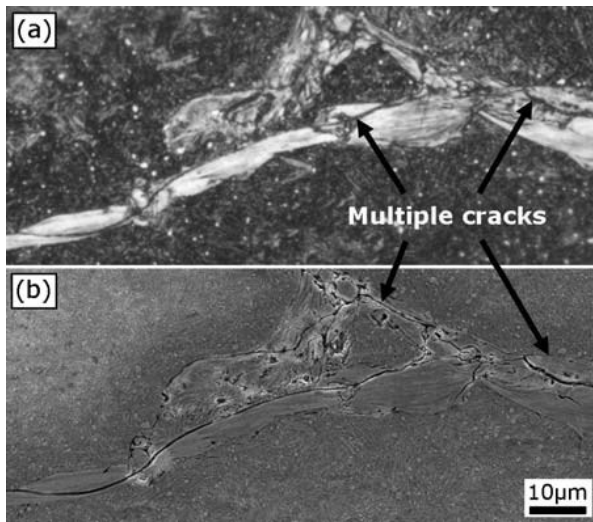
Figure 2-10. (a) optical and (b) SEM images showing multiple cracks in WEA [2].
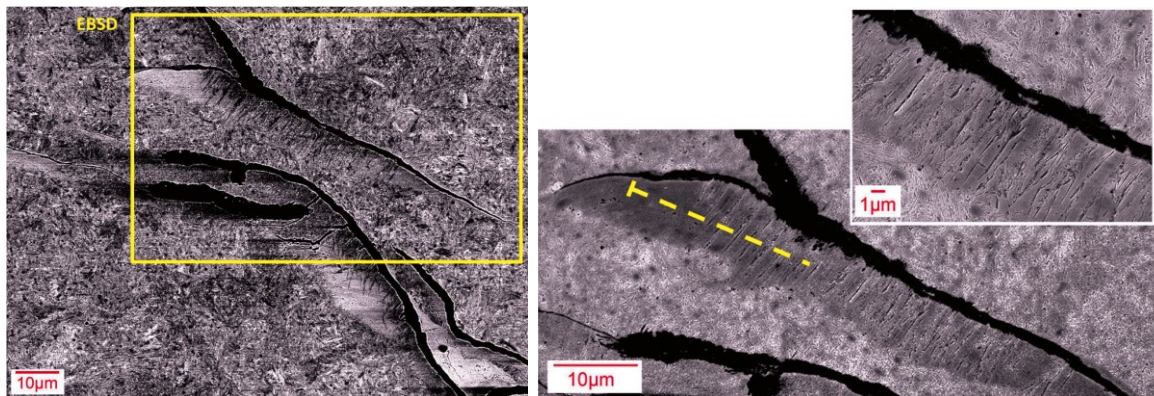
Figure 2-11. Orientation contrast image of a WEC region with an accumulation of long grains near the crack inside a WEA. The region for EBSD investigations is marked. Region marked in the left was imaged in Nital-etched condition after repolishing. Needle-shaped grain structures appear more affected by the etchant. The FIB lift-out region is marked with a yellow line [49].

Coarse grains are found in the area from the WEA to the surrounding matrix in butterflies observed in EBSD [46], [67]; however, these have not been found in WEAs in WECs. TEM studies demonstrated that nano-ferrite grains had different sizes [10] and would be coarser; the difference can be up to an order of magnitude, as the grain was away from the inclusion or stress raiser [45], [51]. Such findings support that the matrix structure breakdown by cyclic loading is a gradual process and the larger grains in lower-stress regions are not fully refined [51]. Furthermore, TEM studies of WEC/WEAs has found a randomly distributed grain size, regardless of position [67].
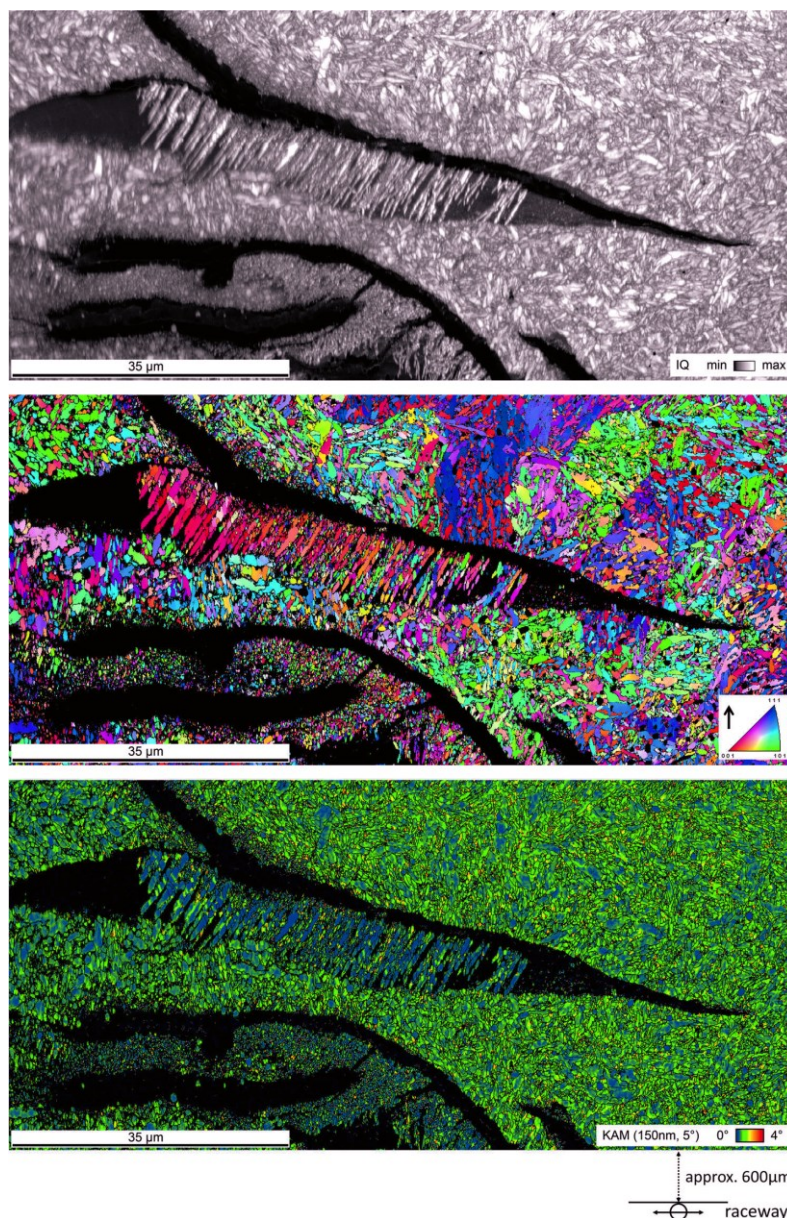
Figure 2-12. EBSD analysis of the marked region in Figure 2-11, step size 50 nm. (a) IQ-Map and (b) IPF-Map of α-Fe, the needle-shaped grains inside the WEA have similar orientations; (c) KAM-Map showing lower misorientations in the needle-shaped grains inside the WEA compared to the bulk material [49].

2.3.4   Initiation mechanism hypotheses of WEC

The initiation mechanism of WECs as well as their key drivers is still disputed in the literature. Most hypotheses are inextricably linked with their specific experimental conditions, such as additional loading, type of steel, bearing and tribological environment. In terms of the initiation site of WECs, it is hard to distinguish whether it is in the surface or in the subsurface because many WECs are found to contact with the surface but also

WECs are found subsurface. Based on these issues, these hypotheses can be broadly classified into surface initiation mechanism and subsurface initiation mechanism.

2.3.4.1   Surface initiation hypotheses

The surface initiation mechanism hypothesis suggests that the WECs initiate at the damage or cracks on the surface and then grow into the subsurface. In the surface initiation hypotheses, tensile stress induced mechanism and shear stress induced mechanism are the main surface initiation hypotheses.

In shear stress induced mechanism, the nascent microcracks induced by lower tensile stress tend to occur in the over-rolling direction of the contact surface [16]. Then nascent cracks develop under shear stress, which induces hydrogen release from penetrating lubricant, crack face rubbing and local fatigue ageing. Less WEA was observed near the surface, while more WEA was seen in the depth [16]. An example is shown in Figure 2-13, showing the WEC initiated by shear stress.

In tensile stress induced mechanism, cleavage-like axial cracks are formed in localised contact regions with high circumferential tensile stress, which reaches the maximum at the contact surface. An example is shown in Figure 2-5. The typical length of the axial cracks is 0.1-0.2 mm. The cracks initiate at material defects or stress raisers like inclusions. The cracks induced by tensile stress shown on the contact surface are different from that caused by shear stress, which looks like hairline cracks (Figure 2-13). However, some researchers found that cleavage-like cracks can be initiated subsurface, as shown in Figure 2-14. The surface axial cracks appear more often in rolled manufactured rings than in forged manufactured rings, it is suggested this is because the presence of MnS inclusions results in weak points near the surface layer [68].
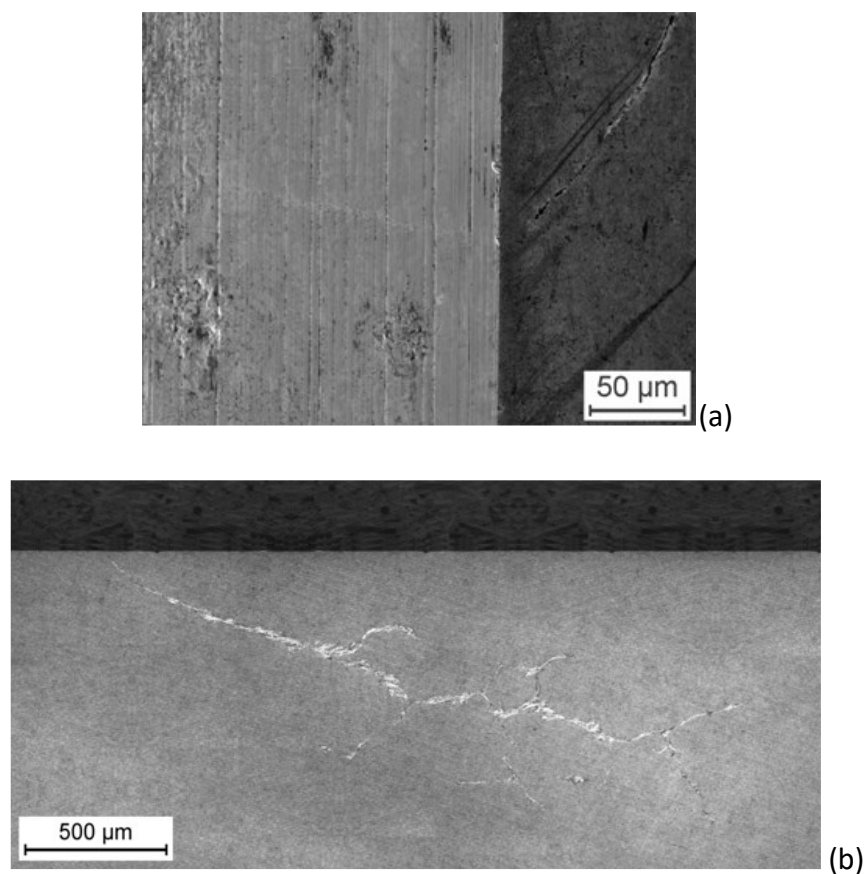
Figure 2-13. (a) an SEM image of crack shown on the contact surface. (b) OM image of the cross-section of the etched part of (a) [16]. The WECs was caused by shear stress.
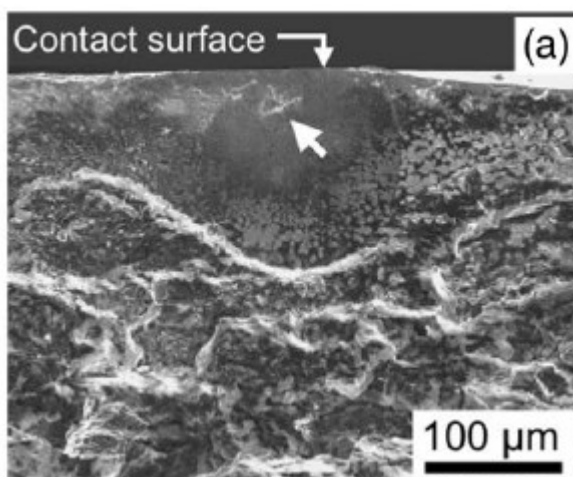
Figure 2-14. SEM fractography image of preparatively opened circular cleavage-like axial incipient cracks from an inner ring raceway of a failed taper roller bearing from an industrial gearbox [15].

Paladugu et al [17] proposed that high surface shear forces caused by the formed tribo-film in the sliding zone produced from oil additives in the "WEC critical lubricant", resulted in line cracks on the surface. The line cracks are similar to the axial cracks in the wind turbine gearboxes. The local intensity of contacts and the respective magnitude of the localised

surface shear forces determines the location and time to produce line cracks. These line cracks initiated and propagated perpendicularly down into the subsurface (10 μm to 20 μm from the surface) and then propagated on an incline, shown in Figure 2-15. WEA was formed by crack face rubbing only in the negative sliding zone due to the same direction of traction force and the movement of the raceway.
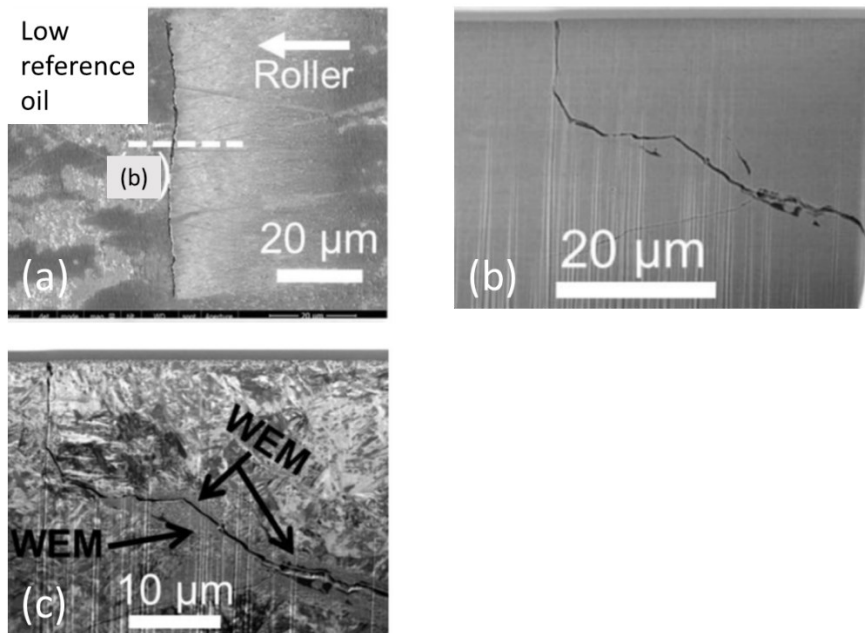
Figure 2-15. (a) SEM image of a line crack on the contact surface. (b) SEM image of the cross section in (a) after FIB milling. (c) SIM image of the location in (b) [17].

2.3.4.2   Subsurface initiation hypothesis

The subsurface initiation mechanism hypothesis suggests that WECs initiate in the subsurface and then grow into the contact surface, resulting in flaking. Different kinds of subsurface initiation hypothesis are proposed.

Non-metallic inclusions as a stress raising feature are suggested as one initiation site for WECs. Increasing evidence has been found to support this initiation process in different bearings under hydrogen charged or non-hydrogen charged conditions. Small/short inclusions are suspected to be initiators of WEC, as several studies have shown that many small/short inclusions interact with WEC. Evans et al. found that small/short inclusions (sulphide inclusions, globular manganese sulphide + oxide inclusions and globular oxide inclusions) with a diameter of 3 to 20 μm interacted with WECs from analysis of WTGBs and test bearings/samples [1]. These inclusions were judged to be possible WEC initiators because of the chemical composition of the inclusions, the depth from the contact surface

and the continuity of cracks near the inclusions. The induced tensile residual stresses, the hardness mismatch with the tempered martensite matrix and poor coherence/debonding between the oxide and the matrix could be the reasons for the existence of oxide in these inclusions [45], [69], [77]. Evans et al. [9] studied the same type of bearings under 1.2 GPa maximum contact pressure with slip. They found that many WECs had no interaction with a contact surface and were believed to be initiated at the non-metallic inclusions in the subsurface. Although some WECs interacted with the contact surface, they also interacted with inclusions and had few regions of WECs near the surface. Thin vertical cracks were found in the branch of the main WECs, which indicated how the WECs initiate at the subsurface and propagate to the surface.

Bruce et al. [21] similarly found WECs were attached to MnS inclusions with a length of 3-45 µm and depth of up to 630 µm from the contact surface in failed wind turbine gearbox bearings. Bruce et al. summarised the initiation stage and propagation at MnS inclusions, shown in Figure 2-16 [21]. Within the recorded inclusions, approximately 80% of inclusions were connected to WECs that appeared to have propagated from the inclusion tips. Each of the 80% inclusions had either one or two WECs that tended to propagate at much shallower angles (less than 30°) than traditional "butterfly wings", indicating that these MnS inclusions initiated WECs could not be caused by a concentration of unidirectional shear stress as "butterfly wings" are thought to be [2], [18], [26], [33], [68], [69] but are initiated due to Mode I loading of the inclusion tips at locations near to the maximum equivalent stress, which would explain their near parallel-to-surface propagation. A Mode I fracture may explain crack initiation at MnS inclusions and the growth of short cracks attached to the inclusions (loading is normal to crack growth direction). A Mode II/III fracture governs further growth of the cracks (loading is in-plane shear/off-plane shear) [18], [71].
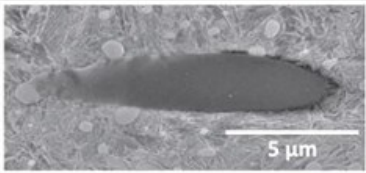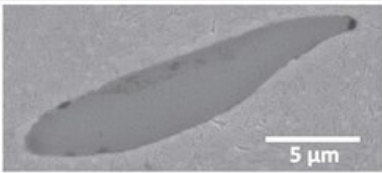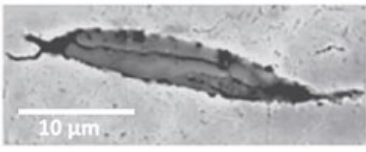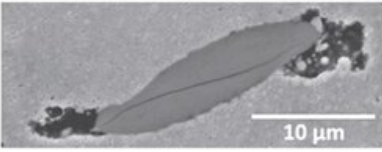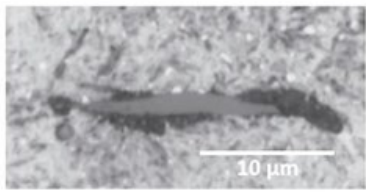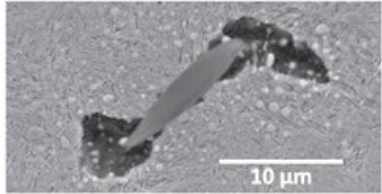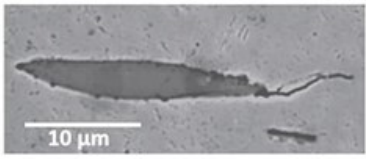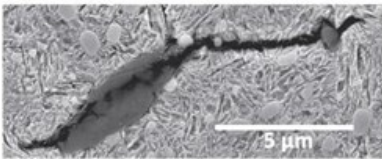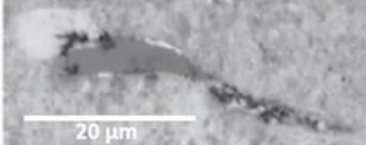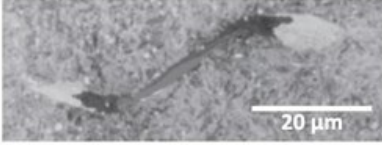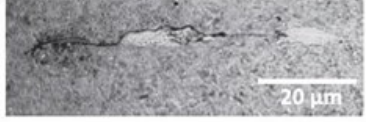
	Axial cross-section shape	Circumferential cross-section
Stage 0 Undamaged inclusion	5 μm	5 μm
Stage 1a Inclusion internal cracking	10 μm	10 μm
Stage 1b Separation of inclusion from matrix	10 μm	10 μm
Stage 2 Crack propagation into matrix from inclusion tip	10 μm	5 μm
Stage 3a WEA propagates from separation at inclusion tips	20 μm	20 μm
Stage 3b WEA develops adjacent to cracks forming WEC	20 μm	20 μm
Stage 4 Further propagation of crack and WEC into bulk material	20 μm	20 μm

Figure 2-16. The proposed stages of the initiation and propagation of WECs at MnS inclusions [21].
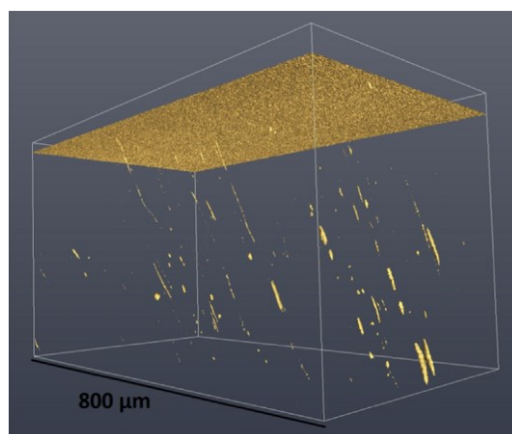
Figure 2-17. Inclusion locations: 3D representation of large MnS inclusion just below the raceway surface [72].

Danielsen et al. [72] analysed the subsurface away from the spallation of a type of cylindrical roller thrust bearing under 2.282 GPa maximum contact pressure running for 200 hours. They found some small globular inclusion-like points in WECs using 3D X-ray tomography, which indicates they have a relationship with crack propagation. However, the large MnS inclusions were found to be aligned in the direction and had no relation to the contact surface (Figure 2-17 [72]). The small globular inclusion-like objects were found in the matrix and had a high concentration along the crack surfaces. The WECs network they found had no contact with the surface, suggesting a subsurface initiation at the small globular inclusions of WECs.

Evans et al. [18] found that WECs could result from butterfly wing propagation. These authors conducted rolling contact fatigue tests using twin discs made from bearing steel and found butterfly cracks had initiated at material defects between 30 μm and 800 μm below the contact surface. Butterfly cracks will be discussed in Section 2.5. These "butterflies" were found to propagate into WEC networks, which themselves act as stress concentrators because of their comparatively high hardness, 30-50% higher than the surrounding matrix [41], [46], [73]. WECs, therefore, propagate themselves under high loading because of stress concentrations at the crack tip. Hydrogen embrittlement generated by lubricant ageing, water contamination or hydrogen initially present in the steel microstructure can accelerate this process [2], [43], [47] .

Another subsurface initiation hypothesis is that WECs are initiated by adiabatic shear banding (ASB) independent of or including defects/inclusions/other in impact load, and a crack forms after microstructural change. In through-hardened bearings, it is proposed that impact load generates rapidly propagated cleavage-like axial cracks under tensile stress, initiating at defects/inclusions/other at around a depth of 20-30 μm [74], [75]. The cleavage-like crack surface morphology has a flat plane, voids and nano-grains, and this morphology is classified as transgranular because of the absence of grain boundaries. Then, a v-segment crack forms below this depth due to a dual wave loading system. The shear stress caused the parallel cracks (relative to the contact surface) in v-segment, and the radial crack propagation is caused by tensile stress. The WEA is seen at the parallel/shallow-inclined cracks in the v-segment, which is considered as consequential damage. The thin straight nature of the parallel branches of WECs support that adiabatic shear banding caused their formation. Due to further development of WEA microstructural changes at the

supposed ASB borders, in many cases, the evidence for ASB having occurred is subsequently masked. The nature of WECs, which is a heavily distorted material produced by a sudden process, is reasonably explained by the fact that pulses are generated in the contact zone and cause ASB [76]. This type of pulse is evident in the exit region of the contact lubricated under elastic hydrodynamic lubrication conditions, or is a ballistic impact caused by cavitation. However, other researchers [77] showed that the impact effect of the rollers on the raceways in wind turbine bearings was not enough to cause ASB by simulations. ASB was not found in the bearings under high-strain rate tensile tests while WEA was found in the bearings under high-strain rate compressive tests [78]. This evidence questions the ASB initiation mechanism.

The hypothesis of electrothermal initialisation of the WEC is another proposed subsurface initiation mechanism [76], [79]. Local transient currents cause local electromagnetic induction through the contact surface, causing the electrothermal mechanism to trigger subsequent WEA microstructure changes. Chapter 2.4.4 discusses the reasons why a current exists in the bearing.

Local deformation can be associated with currents in the non-homogeneous microstructure of the steel due to changes in the electrical and thermal properties of elements of the microstructure [79]. If the carbides are surrounded with a relatively higher resistivity region and this area coincides with the high current density area, a resistivity heat source appears there. Many carbides in steel have a suitable environment that can withstand significant thermal stresses beyond the limits of plastic deformation when conducting current, or repeated pulses can accumulate stress. Such micro-deformation may result in the migration of carbon and chromium, the trapping of hydrogen, and possibly some other processes that will create micro-faults and lead to a network of fractures. Although it is not clear whether the resulting local stress is sufficient to cause crack initiation, the stress may be sufficient to initiate recrystallisation of the surrounding steel grains and create a WEA region, which may cause cracking thereafter. Ščepanskis et al. [80] established the model-based hypothesis of stress localisation at carbides in bearing steel in the presence of an electrical current. The stress may cause microstructure alterations even if its magnitude, combined with over-rolling stress, is not enough to initiate cracking. Therefore, the hypothesis supports the presented connection between electricity in bearings and WECs.

After studying the microstructures near the cracks, Gould et al. [82] observed three different types of microstructures which were identified generation along with the distance from the crack. The three different types of microstructures are: uniform WEAs, thin elongated DEA, and a region of mixing light and dark etching areas with some abnormally shaped carbides. Based on these three microstructures, Gould et al. [81] proposed an initiation mechanism of carbon migrating out of martensitic lattice under high local energy and shear stress in multiple stages. From thistheory, the first stage of WEC initiation is localised DEAs with no cracks (Figure 2-18). The formation of these DEAs may act as precursor to form WECs, which is consistent with the results of other researchers [46], [59], [60]. The next stage (Figure 2-19) is characterised with small and subsurface cracks, neighbouring with localised DEAs, but in this stage no WEAs were observed. The third stage found by Gould et al. [81] contains a crack with dark and white mixing etching area (Figure 2-20). The last stage observed consists of fully formed WEC with different microstructures in the nearby area (Figure 2-21). It is important to note that these four stages of WEC initiations were observed from different locations of different crack networks under the wear track of the rollers.
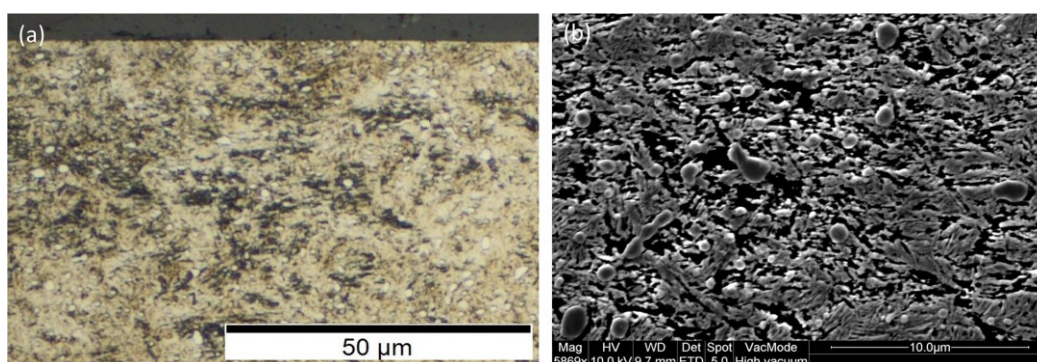
Figure 2-18. (a) An optical microscope image and (b) an SEM micrograph showing the DEA without the presence of a crack (stage 1) observed [82].
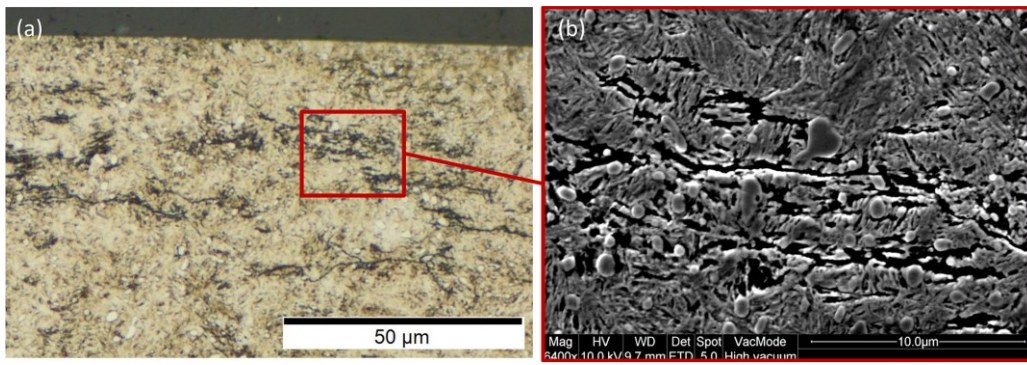
Figure 2-19. (a) An optical microscope image and (b) an SEM micrograph showing cracks through regions of DEA without adjacent WEA (stage 2) [82].
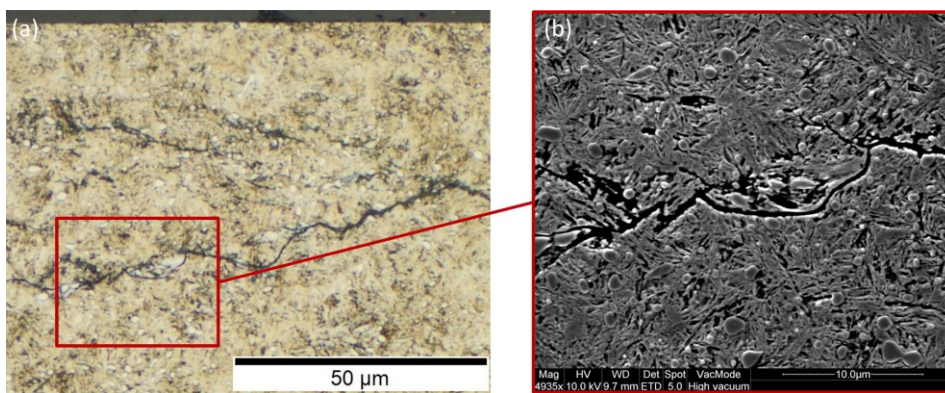
Figure 2-20. (a) An optical microscope image and (b) an SEM micrograph showing a crack with a small amount of WEA, DEA, and local carbide deformation (stage 3) observed [82].
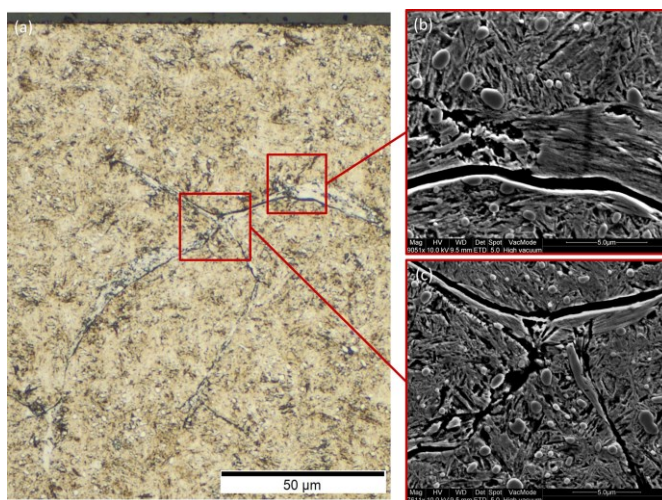
Figure 2-21. (a) An optical microscope image and (b) and (c) two SEM micrographs showing a WEC (stage 4) observed [82].

Rumpf [83] used the method analysing the development of microstructure change in different runtime bearings to study the initiation and propagation of WECs. Deep groove

26

ball bearings were tested under electrical current and critical lubricant conditions. She found vertical and horizontal small microcracks (less than 4 µm) without microstructure changes in the 10-hour bearing, which were considered to be an early stage of WECs (Figure 2-22). Microcrack-carbide interactions, for example microcracks cutting through carbides, were found in this early stage (Figure 2-23). In the bearings tested for 12.5, 15 and 17.5 hours, longer microcracks (up to 7 µm) without microstructure changes were found. Microstructure changes, including equiaxed grains at crack tips and small elongated grains, were firstly found in the 20-hour bearings (Figure 2-24). These stages can be considered as the early stage of WEA and the intermediate stage of WEC formation. After 20 hours, large WEC networks were found confirming that WECs propagated rapidly.
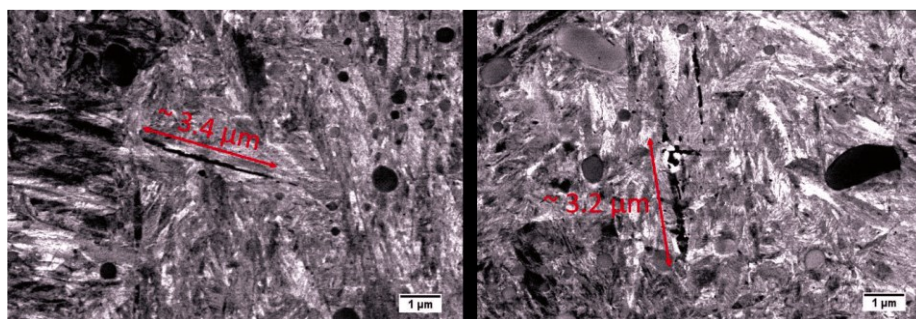
Figure 2-22. BSE images in SEM of the subsurface of 10-hour deep groove ball bearings [83].
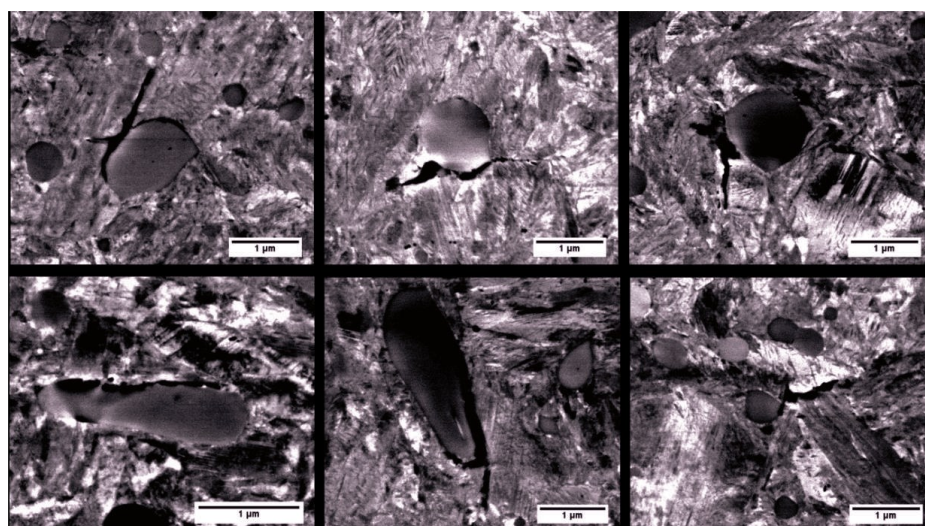
Figure 2-23. BSE images in SEM of microcracks-carbides interactions in the deep groove ball bearings tested between 10 and 17.5 hours [83].
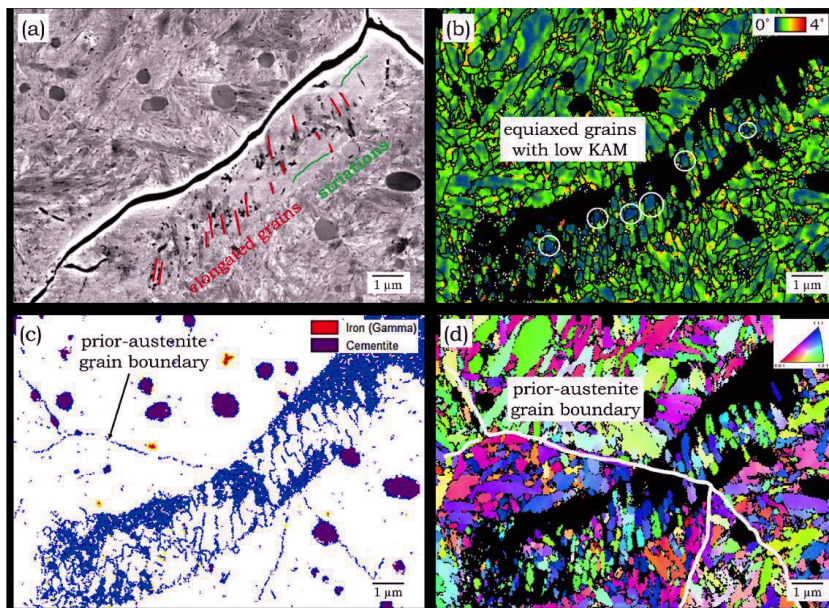
Figure 2-24. Elongated grains in WEA in the 20-hour deep groove ball bearings: (a) BSE image in SEM; (b) KAM (100nm,5˚) map; (c) non-martensite-martensite High Angle Grain Boundaries (HAGB) map; (d) Inverse pole figure (IPF) with respect to the normal direction during rolling [83].

Recently, Manieri [84] proposed a new mechanism of WECs based on analysing WECs on a triple-disc rolling contact fatigue test rig in AISI 52100 bearing steel. It was suggested that a specific time history of applied contact stress is the primary driver of WEC. Cracks in the subsurface are initiated under high-stress excursions of short duration firstly, and then the contact operates under moderate stress, causing the cracks to propagate very slowly and causing crack face rubbing. The final pitting failure occurs on the surface as long as the cracks propagate to the surface, whether or not if the cracks have the time to form WEA.

2.3.5   The formation order of WEC and WEA

Researchers continue to debate the formation order of WEAs and cracks. Some researchers believed that events imparting higher strain to the steel would result in instantaneous transformation and lead to WEAs with different hardness. Due to the hardness difference between the matrix and the transformed region, a crack initiates [85], [86]. In the previous Chapter 2.3.4.2, researchers [74], [75] who believe that WEAs can be interpreted as adiabatic shear bands generated by impact load, also considered the WEA forms first.

However, other researchers propose that a crack develops first [1], [10], [65], [66], [83] and then the crack surfaces rub in the following over-rolling cycles, leading to large local plastic deformation to form WEA [16], [43], [53], [65], [73], [87], [88] . According to the crack face

rubbing hypothesis, the WEA forms due to high adhesion and friction between the faces of subsurface cracks due to vacuum conditions and the absence of lubricant in the subsurface [89]. Solano-Alvaro and Bhadeshia [53], [90] used special heat treatment to produce microcracks in the bearings and conducted rolling contact fatigue tests on these bearings. They found that WEA formed around the former cracks and suggested that the formation of WEA is caused by crack face rubbing during repeated contact over-rolling. Richardson [65] found evidence of an increase in the amount of associated microstructural changes adjacent to the cracks by capturing the evolution of WEC formation. His detailed WEC characteristion analysis provided evidence that cracks could be a prerequisite to WEA, where a possible mechanism is crack face rubbing. However, conversely to this mechanism, Richardson [65] also found numerous small very near-surface WEAs without any visible crack; thus, the formation of the microstructural change to near-surface WEA does not require the presence of a crack. Rumpf [83] found evidence suggesting that cracks come first in the subsurface and the majority of WECs involved WEAs on only one side of a crack, suggesting that crack face rubbing could not be the dominant mechanism. Oezel et al. [91] also found that cracks are seen at the boundary of the WEA and the original martensitic matrix but believes that the WEA comes first because it contradicts the crack face rubbing mechanism.

In conclusion, the formation order of WEC and WEA cannot yet be confirmed. It seems that the results of Rumpf [83] are more reliable because she observed the microcracks without any microstructure changes in the initial stage and the formation of WEA in a later stage. However, because of the RCF test condition, the type of bearing and the material of the bearing differs among researchers, the formation order of WEA and WEC could then be affected, but this remains unconfirmed.

2.4 **Drivers of WEC**

This section explores the factors that affect the initiation and propagation of WECs in bearings. The root cause of WECs has always been the subject of debate among researchers. Understanding the proposed drivers of WEC formation will help design appropriate experimental approaches to identify WECs and hence to determine the acting WEC initiation mechanisms in the samples in this study. Hydrogen, lubricant and additives, slip,

electricity, impact loading and tensile hoop stress are key drivers proposed in the literature, and they are reviewed respectively.

2.4.1   Hydrogen

Some researchers believe that hydrogen diffusing into the components is the root cause of WECs, although there is disagreement around this [1]. Typically, hydrogen exists as of diatomic molecules (H-H), where the size is too big to diffuse into the steel matrix. However, during service, due to heat energy or chemical energy generated by mechanical work [2] or by electrical energy [92], hydrogen atoms may be generated through the dissociation of water [93], [94] and decomposition of lubricant [95], [96].

After hydrogen is generated, it is driven by further continuous hydrogen generation from water or lubricant oil entering inside cracks, and diffuses into the components through the nascent surface of cracks into the component; thus, the crack is opened further(as Figure 2-25 shows), which is called a hydrogen enhanced embrittlement mechanism [73]. This process will also cause change to WEA microstructures via hydrogen-enhanced localised plasticity mechanisms [73], [97]. A study on simulating the formation of WECs by using grain-boundary modelling and a semi-empirical quantum mechanical method (Austin Model 1) analyses the effect of local microstructure characteristics on the mobility of hydrogen at the area around the crack tip. This simulation work shows that the mobility of hydrogen at grain boundaries is much lower than that in the grain (neighbouring bulk) [98], [99], indicating the mobility of hydrogen diffusion at the crack tip is dominated by the neighbouring bulk area.
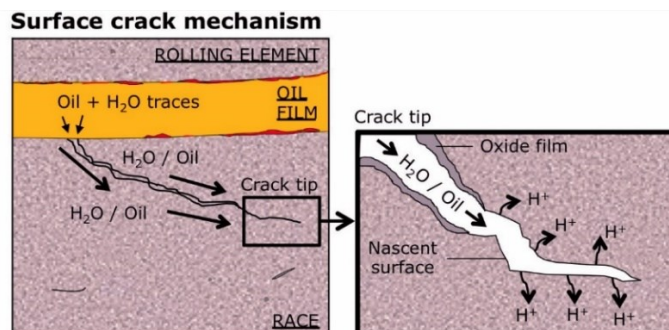
Figure 2-25. Schematic of hydrogen generation and diffusion into components through the crack surface [33].

However, this mechanism has not been entirely accepted, as it cannot fully explain the mechanisms of how hydrogen causes detrimental damage to steels [100]. Vegter and Slycke's work [43] indicates that hydrogen drives and accelerates WECs through promoting climb-controlled dislocation glide, which is usually very slow. As hydrogen generate, the concentration of hydrogen-vacancy pairs increases, as does their mobility, resulting in a higher possibility of a climb and causing creep deformation. This deformation, coupled with the attraction of hydrogen to point defects, will cause a self-generating damage localisation process [43].

Another mechanism describing hydrogen diffusion is that hydrogen ions generate from chemical reactions taking place at the boundary between the lubricant and fresh metal surface. Then they combine with electrons provided by nascent steels to form hydrogen atoms, which diffuse into the bulk material through the contact surface [101], [102]. Those diffused hydrogens then promote changes in microstructures and help the initiation and propagation of cracks. Figure 2-26 shows this process. Additionally, many studies demonstrate that hydrogen with a diffusion depth of 10-20 μm at wear-induced nascent surfaces can aid in the occurrence of cleavage-like axial cracks beneath the contact surface.
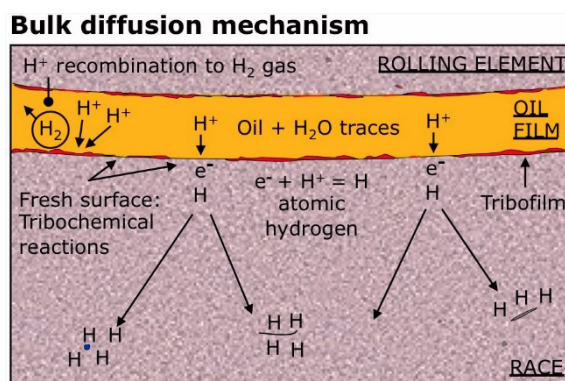
Figure 2-26. Schematic of hydrogen generation and diffusion into components through bulk diffusion [33].

In the laboratory, studies on hydrogen are normally conducted with samples pre-charged by hydrogen and in a hydrogen gas test atmosphere to study the effect of hydrogen on RCF life and WEC formation [25], [43], [103], [104]. Results show that slip bands and microstructural changes take place, only within hydrogen charged samples, and fatigue life and sample strength experience a decreasing trend with hydrogen charging [2]. In the RFC test, up to 4.2 ppm concentration of hydrogen has been observed to diffuse into steels [105]. During testing, it was observed that due to hydrogen redistribution, the local

concentration is much higher than that of the average level, as some hydrogen will be trapped in the matrix defects [94]. After tests, many researchers freeze samples with dry ice or even liquid nitrogen, stopping hydrogen from escaping, to examine the hydrogen content in the specimens [47], [63]. It is found that hydrogen concentration in the surface layer is particularly high.

As mentioned previously, researchers like Luyckx [74] disagree with the hydrogen theory, because they think this theory results from experiments conducted under very high contact stress (>3.2 GPa) in laboratories. Such high contact stress is normally not present in the real service situation of wind turbine gearbox bearing operations. Some reports also show that bulk diffusion hydrogen is unlikely to take place because WSF failed bearing raceways do not experience severe wear, and wind turbine gearboxes do not suffer from moisture corrosion and electric discharge damage during service [106], [107]. Other researches focusing on specimens from screw vacuum pumps, which are lubricated by fluorinated oil, have found extensive WECs in specimens [49]. This research further demonstrates that hydrogen is not required to initiate WECs, but it may influence the crack propagation [108].

2.4.2   Lubricant and additives

Another driver for WECs can be from lubricants. It is reported that by applying lubricant, benefits can be obtained such as the lubricant performing as a protective film, less wear-induced nascent surface and less hydrogen release due to slighter friction generating less heat [1]. Anti-corrosion lubricants or sulphonate lubricants especially have a significant effect. However, reports also demonstrate that anti-corrosion lubricant containing sulphur will enhance WSF because sulphur will stop the recombination of molecular hydrogen, resulting in more hydrogen ions diffusing into the bulk [109]. This is called the sulphur hydrogen poisoning effect. Those additives, being present in lubricants (e.g. anti-wear, like Zincdithiophosphates, Molybdenumdithiophosphates and anticorrosion, like Sulphonates based on Calcium, Sodium, and Magnesium) are critical and thought to be WEC drivers [110]. Researches show that in FAG-FE8 testing, bearings with such lubricants fail in about 16 to 40 hours, while those with pure base lubricants do not suffer from WSF before 1000 hours, even though the test conditions are the same [9], [76]. Moreover, it has been found that the oil under such fail lubricant conditions may result in thicker tribofilm than that resulted from the oil under normal work conditions. A tribofilm is defined as a thin solid

film formed due to the chemical reaction between the lubricant and the lubricated surface. The structure of a tribofilm is affected by its thickness, where a thicker tribofilm tends to be less homogeneous and increases the occurrence of tribochemical reactions on a primary crack surface [68]. Thus, hydrogen generation and diffusion are promoted. Additionally, WECs are found to generate only with highly heterogeneous tribofilms, while metal sulphonates are not necessarily demonstrated to be required for WEC generation [68]. Thus, the lubricant effect is linked to that of hydrogen. According to Paladugu et al.[111], about a 100 nm thick tribofilm was formed when using "WEC critical oil" (it was SAE 75W-80 oil in this research) in cylindrical roller thrust bearings. These researchers found a micro-sized line crack formed on tribo-surfaces due to the formation of a tribofilm, causing an increase of surface shear forces.

Other studies on large-scale bearings show that self-charging and discharging of lubricant result from the lubricant transportation in the contact region. This process may cause the appearance of local current flow or electromagnet from the contact region into the component, resulting in microstructure changes [76]. Such microstructure change can then lead to stronger hydrogen trapping and then decreased plasticity, aiding WEC formation [76].

2.4.3   Slip

Bearings during service will inevitably suffer from slippage due to misaligned rollers causing traction forces and the constraints from the geometry of roller and bearings [4]. According to previous literature [13], [58], [112] slip is reported as an essential driver for the formation of WECs and WEA, as well as a mechanism of increasing shear stress in the contacting regions. There are two main mechanisms for slippage driving the occurrence of WSF. One is that slippage can directly cause the generation of surface traction and shift shear stress to be closer to the surface [13], [113]. High frictional energy is generated in the slipping process and may accelerate surface fatigue, resulting in materials shearing and stress transportation and increased stress. This highly increases the probability of white structure flaking (WSF) occurrence. Another mechanism is that slippage affects the tribofilm formation, resulting in the formation of a new crack surface and release of hydrogen to further initiate or propagate cracks.

As mentioned previously, hydrogen charging can reduce the RCF life of bearings as it will aid WEC formation. However, research also shows that without slippage, WECs are unable to form even with hydrogen charging, because there will be insufficient energy provided [33], [68]. Previous reports show that the locations of WECs in the contact regions are linked to the PVmax value (a product of P expressed as bearing load and V expressed as surface velocity of the shaft), while the location of WECs always appear at the location of peak frictional energy [76]. It has also been found that WSF only occurs in those regions with the largest value of pressure multiplied by maximum slip velocity because these regions can provide the highest content of hydrogen [113], [114]. Furthermore, in the process of slippage, work is done to the lubricant and the temperature of lubricant increases, reducing the oil film thickness[115], [116]. This will cause wear of the bearing surface and hydrogen release.

Kruhoffer and Loos [117] found that WEC was preferentially formed in the negative slide zone where the washer is slower than the roller in the cylindrical roller thrust bearings. Paladugu [111] also found that the cracks became WECs only in the negative slide zone of thrust roller bearings, explained by the crack face rubbing mechanism. The traction force was applied in the direction of the raceway movement. Upon each load cycle, the crack faces rubbed each other and caused WEA formation along the cracks. Conversely, the applied traction force had the opposite direction to the raceway movement in the positive slide zone, and hence the crack faces tended to move away rather than rubbing. Gould et al. [82] found that the magnitudes of sliding (expressed as slide-roll ratio (SRR)) affect the formation of WEC in triple-disc fatigue tests. WEC was found under high magnitude of sliding condition with -30% SRR, rather than low magnitude of sliding condition with -5% SRR.

2.4.4 Electricity

Many authors have reported the presence of a current in the bearing. Nakayama and Nevshupa [118] reported that electricity due to charge-discharge affected the contact point. Chu and Cameron [119] reported the appearance of current is related to the lubricant. The current in the bearing may be related to the shaft voltages present in electric machines caused by winding faults, asymmetry of faults, unbalanced supplies, electrostatic effects, magnetised shafts or other machine members [120], [121]. The current can also be found

in the double layer effect associated with the polar additive [122] and static electricity on the surface of the lubricated bearing [123].

Loos et al. [124] showed that bearings could suffer from WEC-induced failure due to electrical loading, because the current flowing through bearings would change its microstructure. Lu and Qin [125] have recently demonstrated that electropulse-tempering would be a reason for martensite to decay to ultrafine-grained ferrite and nano-cementite (similar effects of change in microstructure in other alloys were shown in reference [125]). Such microstructure composition is usually related to WEA accompanying WECs [10], [45], [54]. However, there is no strong evidence showing that this changed microstructure produced subsequent cracks (like reported DEA or WEA). The published papers showed observations of some microstructure changes which could proceed WEC formation [51], [73], [81] . This may show a relationship between the presence of electrical loading and the premature WEC failures seen in bearings. In Rumpf's study [83], a ball bearing sample was tested in firstly 15 hours with electricity and more 50 hours without electricity. It was found that the morphology in subsurface of the sample was similar to the ball bearing sample tested in total 15 hours with electricity. This indicated that electricity was beneficial to the growth of WECs.

Previous research on the influence of electricity illustrate that arcing resulting from voltage helps the formation of a new crack surface, heavier wear conditions and more hydrogen release due to reactions induced by electrical energy; all these processes cause earlier occurrence of WECs or WSF [11]. Furthermore, as reported, when the voltage between two contacting surfaces increases up to hundreds of volts, spark discharging may take place, causing a new crack surface and hydrogen release [12]. Industries apply a ceramic roller or involve carbon nanotubes, which can either prevent electron discharge or continuously discharge electrons (stopping arcing taking place), to avoid this and reduce the influence of electricity. The application of these strategies effectively prevents the formation of WECs or WSF, even if electrical current is applied to the component during RCF tests or with other assumed drivers like water and lubricant, which help hydrogen release and are expected to promote WEC initiation and propagation [68].

Researchers studying the effect of these two types of currents have found that only a direct electrical current will affect the WEC initiation and propagation, whereas alternative current have no influence [76]. Moreover, as mentioned in the lubricant section, self-

charging and discharging of lubricant will cause current to flow into bearings and result in changes in microstructure and then lead to stronger hydrogen trapping and then decreased plasticity, aiding WEC formation [79].

2.4.5   Impact loading

Another important driver for WECs is impact loading. Especially in the unloaded zones, every time components are loaded, impact loading repeats [126], resulting in contact stress higher than yield strength. A study on a 750-kW wind turbine gearbox has reported that in normal service, loads can be 15% and 20% higher than the suggested value applied on planetary bearings or shaft bearings, respectively, because there are reversing torques and highly fluctuating loading taking place in the braking process [127]. Such repeated impact loading is reported to be a significant driver for WECs, because this process generates pressure peaks and these peaks will cause adiabatic shear bands (ASB) through high shear strain [128]. This is a dynamic failure mechanism with the appearance of a narrowband, in which there are nano-sized grains [129], [130]. Fortunately, according to Bhadeshia's research [26], even during extreme conditions like emergency shutdown, the impact velocity is far less than 1 m/s, which is much smaller than the velocity required for ASB formation (higher than 100 m/s). Additionally, impact loading has been proposed to promote the damage in subsurface non-metallic inclusions, which could propagate to WECs [131]. Bruce et al. [132] found the combination of impact loading and high levels of surface traction (due to slip) cause the microcracks in non-metallic inclusions. The damage increases with the increase of impact loading and surface traction.

2.4.6   Tensile hoop stress

Tensile hoop stress is also of interest, because it can lead to less resistance to WSF, resulting in reduced RCF life [58], [133]-[135]. Research was conducted to examine steel bearings in RCF tests, where fractography on post-RCF specimens shows that when applying higher tensile hoop stress, the process zone of crack propagation appears to be smaller than that under lower tensile hoop stress [133]. When a tensile hoop stress is applied to raceway rings, it can make the required stress for cleavage-like axial cracks lower. However, WEC propagation is reported to be observed in all kinds of specimens rather than just in bearings, which means that tensile hoop stress is not necessarily required for WECs [68].

Alternatively, the occurrence of vertically branched cracks beneath the contact surface takes place after the formation of WECs, and they connect to WECs; this evidence was observed in FAG-FE8 tests [9].

2.5   **Butterflies**

Butterflies are also a salient point when studying the initiation mechanism of WECs because it is suggested that the altered microstructure wing in butterflies is the same as the WEA in WECs [49], [69]. Whether WECs start with butterflies remains unclear. It has been reported that butterflies could grow to the surface and cause WSF [73]. Butterflies and WECs can exist in the same sample; however, the relationship between WECs and butterflies is unclear.

The "butterfly" (Figure 2-27) has been used by many researchers to describe two and four wing-like features, with cracks starting from the defects and propagating at 30°-50° and 130°-150° to the raceway in the direction of over rolling [2], [26]. The crack is called butterfly crack, distinguishing from other cracks. It can be assumed that the main reason for the orientation direction of the wings is shear stress that has its maximum value in this direction at the specific depth beneath the rolling surface [56]. Butterflies are three-dimensional structures that sweep around the initiator [41], [50], [61], [69], such as inclusions, voids [46], [52], [59] microcracks [59], [61], grain boundaries, and large carbides [50], [51]. They are cracks with altered microstructure wings in length of 10-250 μm [2], [50], [52], [59]. The WEA wings have large nano ferrite grains (50-100 nm) near the butterfly boundaries and small nano ferrite grains (10-50 nm) near the cracks [45], [46], [50], [51], [59].

Butterflies typically initiate at oxide inclusions or oxide-containing duplex oxysulphides, while titanium carbo-nitrides and manganese sulphides seldom initiate butterflies under normal rolling contact fatigue conditions [10], [51]. The difference between oxides and sulphide inclusions is that oxides exhibit poor or even no bonding to the steel matrix [45], while sulphide inclusions show a good bonding to the steel matrix [9], [11]-[13], [51]. Sulphide inclusions can encapsulate non-metallic particles, so they do not act as stress concentrators. However, MnS inclusions are reported to initiate more butterflies in the

literature. The adhesion property and coherence between the inclusion and the steel matrix is thought to be important in controlling the severity of the inclusion type.

Al-Tameemi et al. [136] found that the total length of inclusion and butterflies or microcracks were directly proportional to the length of inclusions. Therefore, larger inclusions are more detrimental to the life of the bearing. Butterfly wings and microcracks are longer in the axial direction.

Grabulov [137] proposed the three-stage embryonic butterfly formation process. In the initial stage, the oxide/oxide-containing inclusions are debonded from the steel matrix. In stage 1, the steel matrix near the inclusion has locally acquired a degree of accumulated micro-plastic damage during repeated cyclic interaction with inclusion. The high stored energy in the deposited material seam causes dynamic recrystallisation in stage 2. Then, continued rubbing and the related material transfer across the crack-like feature between the deposited and the undamaged microstructures, assisted by the diffusion bonding and debonding mechanism, leads to the emergence of a butterfly-wing feature in stage 3.
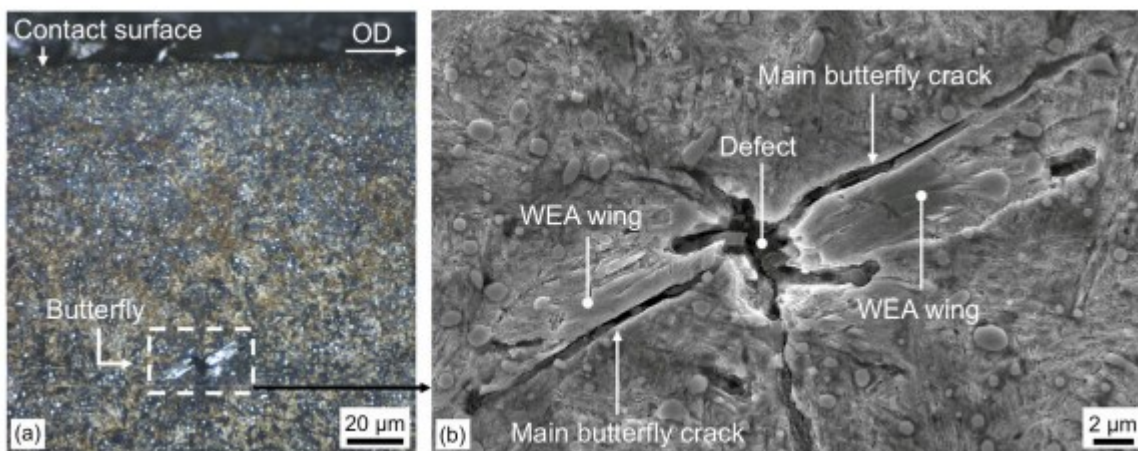
Figure 2-27. Images showing a typical butterfly. (a) Optical image; (b) SEM image [137].

2.6   Summary

This literature review assesses the research progress in establishing the characteristics, drivers and initiation mechanisms of WECs and WEAs, for example, their microstructures and the formation hypotheses. This literature reviews also explored the drivers that may promote the initiation and propagation of WECs. The mechanisms of WEC initiation on the surface or at the subsurface are explored as well, which will be used to design the

experimental approach in this study WECs. In the literature review, another phenomenon that was explored is butterflies, which is often mentioned in the context of WEC formation due to the WEA observed in the butterfly wings. The main findings are summarised below:

- Although WEAs seem to be smooth under an optical microscope, nano-fine structures, needle-like structures, lamellar structures and amorphous structures as well as voids and cavities, were found in the WEA when analysed in EBSD.

- Spherical carbides are elongated and deform due to cyclic stresses in the early stage of WEA, and then finally dissolve.

- Acicular structures formed due to shear-induced deformation of martensite were considered as the early stages of WEA formation, and amorphous-like structures are suggested to be formed before the fine grain structures of the WEA.

- The order of formation of microcracks and WEA is still debated. Instantaneous transformations due to higher strain on a bearing results in a WEA forming first. Most researchers believed that cracks form first and then the WEA forms due to crack faces rubbing. However, the rubbing face mechanism cannot explain the phenomenon that the WEA is found on one side of WECs. Evidence rejecting the rubbing face mechanism was also found.

- Several drivers, like hydrogen, slip, electrical current, lubricant, tensile stress and impact loading are proposed to initiate and form WECs. The influence of each driver on the initiation mechanism is still unclear. A combination of drivers is often used to create WECs in laboratory studies, further obfuscating this issue.

- Whether WECs are initiated from the subsurface or surface remains unclear. Non-metallic inclusions are proposed as one initiation point at the subsurface for the formation of WECs. Microcracks formed without microstructure changes in the subsurface are proposed as the initiation stage of WECs.

In the literature, researchers have mostly analysed fully-formed WECs found in failed bearings on a wind turbine or in the laboratory, to propose the initiation and formation mechanism of WECs. However, the initiation site needs to be found in the earliest stages of WEA or WEC formation to confirm whether cracks or WEA come first and whether a WEC is initiated from the surface or subsurface. However, the initial stage of WECs has not been fully observed and understood under different conditions yet. Early stage cracks of WECs under critical oil, electricity and high-pressure conditions in radial loading bearings were

found in the subsurface. Rumpf [83] has proven that electricity is beneficial to the growth of WEC, while whether slippage will result in the initiation of WEC is still a problem. In the current study, WECs will be created under WEC critical oil, slip and low-pressure conditions in axial loading bearings, because under axial loading, slippage will occur between the rollers and washers. The application of WEC critical oil and low pressure is to ensure the occurrence of WEC and make the maximum shear stress shallow in the subsurface, respectively. The focus then is to find the initiation mechanisms of WECs under these conditions by capturing the evolution of WECs from the earlier to later stages. Advanced characterisation techniques will be used to analyse bearings under different combinations of drivers for creating WECs. SEM approaches will be used to assess the microstructure of WEA.

Chapter 3   Materials, Experiments and Techniques

3.1   Introduction

The aim of the project is to understand the initiation mechanisms of WECs in AISI 52100 martensitic through-hardened bearing steel under WEC critical lubricant and slip by analysing the evolution of the microstructure changes causing WECs. A range of characterisation techniques including optical microscope (OM), scanning electron microscopy (SEM) and energy-dispersive X-ray spectroscopy (EDS), have been used in the research. This chapter describes the materials, fatigue testing, experimental methodology, microstructure characterisation techniques and theoretical calculations used for this research.

3.2   Bearings and Materials

Cylindrical roller thrust bearings, also known as axial cylindrical roller bearings, of type F-562831 shown in Figure 3-1, were used in this project because the design of this type of bearings can cause slippage between rolling elements and washers. Axial cylindrical roller bearings can support axial loading in one direction and have high rigidity and load capacity. The bearings have 15 steel rolling elements mounted in a plastic cage between two steel washer. The two washers are divided into housing locating washer (GS) and shaft locating washer (WS), which are installed on the housing and on the shaft respectively. The diameter of the rollers is 10.5 mm. The rolling elements experience one pure rolling point in the motion and slippage in the rest of the contact area because the rollers move relatively faster/slower than the washers (Figure 3-2). The outer part of the washer where the rollers move relatively faster is called the positive slippage zone and conversely the inner part of the washer where the rollers move relatively slower is called the negative slippage zone.
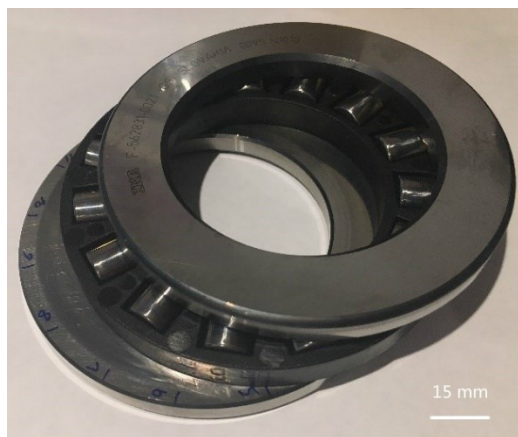
Figure 3-1. Image of the cylindrical roller thrust bearings of type F-562831.
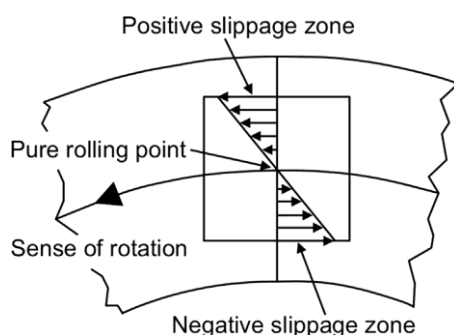
Figure 3-2. Slippage condition of cylindrical roller thrust bearing [9].

The washers and rollers of the bearings studied were manufactured in standard through-hardened AISI 52100 bearing steel. All samples examined were from bearings subjected to a standard heat treatment process including austenitisation at 830-860°C and quenched in oil to 60°C, followed by tempering at 170-220°C for 2 hours. The steel has a microstructure consisting of tempered martensite with homogeneously distributed primary spheroidized carbides $(Fe,Cr)_3C$, tempered carbides and approximately 10-12% retained austenite. The chemical composition of AISI 52100 (100Cr6) is shown in Table 3-1 from the official ISO 683-17 standards [138].

Table 3-1. Chemical composition of AISI 52100 [138].

C	Si	Mn	P	S	Cr	Mo	Fe
0.93-1.05%	0.15-0.35%	0.25-0.45%	0.025%	0.015%	1.35-1.60%	0.10%	remaining

3.3   **Rolling Contact Fatigue testing**

Rolling contact fatigue (RCF) tests were conducted at Schaeffler to reproduce bearings with WECs and experimental observations were carried out on these tested bearings at the University of Southampton. RCF tests were performed on a FAG-FE8 test rig to investigate WEC formation under a critical lubricant. The critical lubricant in this research was an extreme pressure semi-synthetic lubricant used for mechanical gearboxes and already proven to cause WECs. This testing system with bearings is shown in Figure 3-3. Operational speed was referenced as 750 rpm with varying running times. The axial load was 30 kN, resulting in the studied Hertzian stress level (~1400 MPa) on tested bearings in this research. Detailed information of the test parameters and the tested bearings are shown in Table 3-2 and Table 3-3. To characterize the early failure of WEC on a bearing, the bearing must first be tested to fail. This is the reason why the bearings were tested for 355 hours, 382 hours, and 389 hours. The 300h test time is selected because the time is relatively close to the time of bearing failure, and there is a greater probability of observing the middle or late stage of WEC. Then, from 200h to 50h, time was selected at every 50h interval, expecting to find the initial stage of WEC. The selection of 10h is because it is very close to the beginning, expecting to confirm whether WEC appears from the very beginning of the test.

A pure rolling condition exists at the centre of the rolling elements contact zone where there still exists significant slippage (up to 14%) arising towards the rolling element's ends (Figure 3-3) [139], [140]. This shows that the influence of slip should be considered in this test.
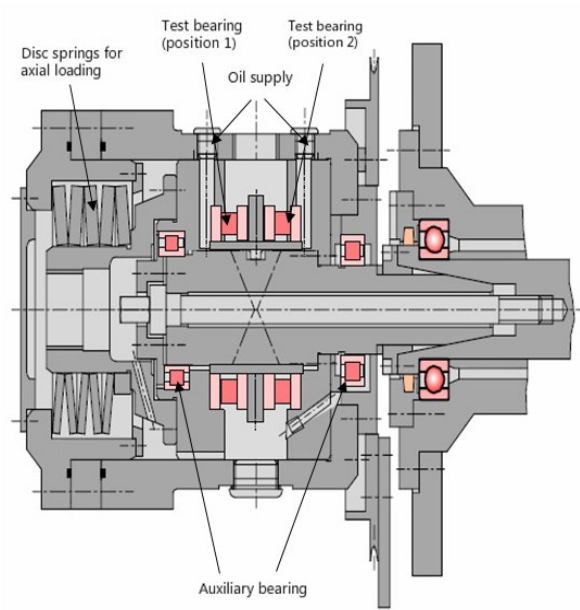
Figure 3-3. The schematic of the FE8 test rig set up.

Table 3-2. Test condition parameters of FE8 bearings and calculated critical stress. (Noted the calculation procedure see Chapter 3.5)

Test rig	FAG-FE8
Test bearing	Cylindrical roller thrust bearings of type F-562831
Material of washers and rollers	AISI 52100 through-hardened martensite
Lubrication	WEC critical lubricant
Speed	750 rpm
Axial load	30 kN
Hertzian stress	~1400 MPa
Viscosity ratio kappa	0.45
Temperature	100℃
Calculated maximum shear stress (τ_{max})	410MPa
Calculated depth of maximum shear stress	~100 μm
Calculated depth of maximum orthogonal shear stress	~62 μm

Table 3-3. List of run time and cycles of FE8 bearings tested under the condition shown in Table 3-2.

	Run time (h)	Cycles (x10^6)
1	389	17.51
2	382	17.19
3	355	15.98
4	300	13.5
5	170	7.65
6	130	5.85
7	70	3.15
8	10	0.45

3.4   **Experimental Methodology**

This part describes the methods and techniques used for microstructure characterisation of WECs. Based on the literature [39] [40], the spalling was mostly caused by the WECs. Then the parts with surface damage were mostly cut to find subsurface WECs. Therefore, in this research, surface damage was firstly checked for choosing where to cut further. Also, if the WECs were found to connect to the surface damage, it could prove the hypothesis of surface initiation mechanism of WECs in the literature. There could be other techniques to estimate the location of WECs in subsurface , like Barkhausen test in the literature [76]. However, if the Barkhausen test can confirm subsurface WEC is still on debate.

The evolution process of WECs can be assessed by systematically comparing characterisation studies and backtracking from the well-established WECs formed at a later stage of bearing damage to an earlier stage. Bearings tested under 355 h, 382 h and 389 h have visible surface damage, which are considered as a later stage of WEC formation. Bearings tested under from 10 h to 300 h, having no visible surface damage, can offer insight into the earlier stage of WECs. Combining assessment of the different characteristics found in the earlier and later stage of WEC formation, RCF test conditions and the proposed initiation mechanisms in literature, the initiation mechanism of WECs under this specific condition can be identified. The cutting and observation methods are shown in Figure 3-4. Only the cross-section of the bearings was analysed because it can show the inner and

outer race in one plane. The following section describes the specific experimental steps which are shown in the flow chart (Figure 3-5). Each step corresponds to section 3.4.1 - 3.4.4 respectively.
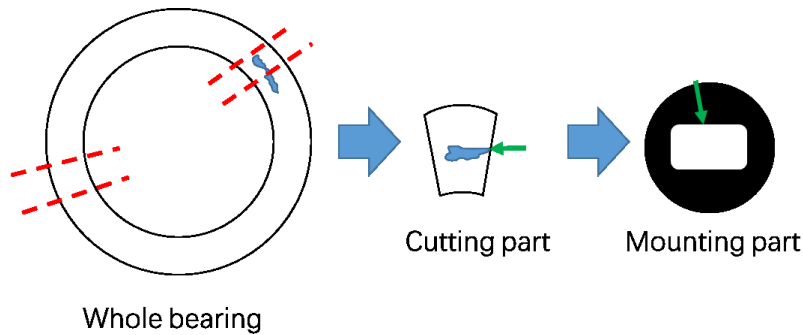
Figure 3-4. The method of cutting bearings. The blue area shows the surface damage on the contact surface and red dash lines show the cutting position. The green arrows point to the same plane of the sample.
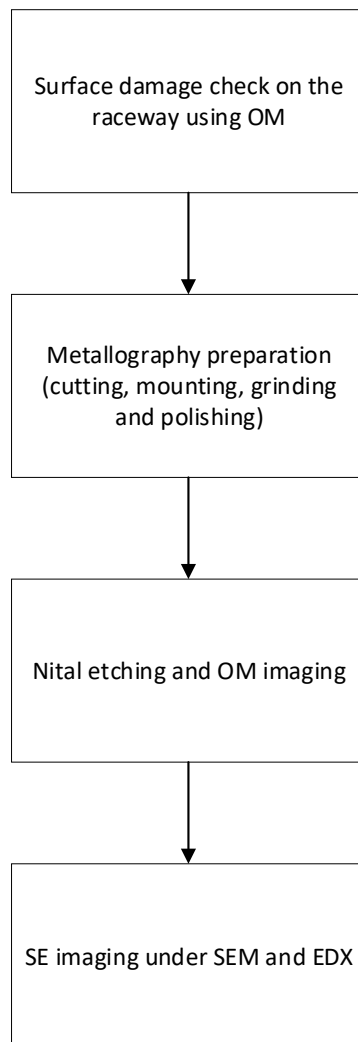
Figure 3-5. Flow chart of experimental steps.

3.4.1   Surface damage check

Before the metallography preparation, the surface of bearings was checked under the optical microscope (Olympus, BX51) in order to find possible surface damage, where WECs are likely to exist in the subsurface. The aim of this step is to locate positions in the bearing that should be analysed.

3.4.2   Metallography preparation

Metallography preparation including cutting, mounting, grinding, polishing and etching is essential before further analysis of the subsurface of bearings under OM and SEM. To capture characteristics more clearly, the samples should be prepared as well as possible (to avoid contamination or scratches on the surface).

Firstly, a cutting process was performed on the cutting machine (PRESI, Mecatome T210). A precision saw with circular diamond discs cutting blade was used. The cutting speed was 0.05mm/s and the rotation speed of discs was 4000rpm. Water was used as a lubricant and coolant during the cutting process, to avoid creating high temperatures in the samples, which may cause structural changes in the steel. The aim of this step is to expose the subsurface characteristics required to be observed, such as WECs.

After cutting specimens from the bearings, they were hot-mounted into conductive Bakelite resin mounting powder, which can also be used under SEM, to make the small specimens easier to handle for the following grinding and polishing steps. Automatic hot mounting press machine (ATM, OPAL 410) was used. Samples were heated for 4 minutes at 180 ℃ and cooled for 6 minutes. The pressure used was 5 bar (500 kPa).

Grinding was conducted with Silicon carbide (SiC) papers with successive grit sizes of 120, 800, 1200 and 4000 and lubricated by water. Specimens were then sequentially polished under diamond suspensions of 6 μm, 3 μm, 1 μm and 0.25 μm on corresponding polishing cloths. The same machine (Struers, TegraPol-15) was used for grinding and polishing.

3.4.3   Nital etching and OM imaging

In order to reveal the changes of microstructure characteristics, specimens were etched. Before etching, specimens were cleaned with ethanol in an ultrasonic bath to remove the

particulate residue related to the final polishing step. 2% Nital solution (Nitric acid in ethanol) was used to etch for a few seconds.

After etching, the samples were cleaned with ethanol and optical microscopy (using an Olympus, BX51) was used to initially observe WECs or cracks, which helped to determine the location that should be further analysed in the SEM.

3.4.4   Scanning Electron Microscopy and energy-dispersive X-ray spectroscopy

The microstructure of the WEC and initiating features were further observed by using SEM after the OM imaging. In this study a JEOL JSM 6500F field emission SEM equipped with a combined EDX/EBSD system was used. The SE imaging was performed at an accelerating voltage of 15 kV and about 10mm working distance.

Energy-dispersive X-ray spectroscopy (EDX/EDS), an element composition analysis method, was also used. The method analyses the energy of X-rays emitted when the samples are hit by the electron beams to obtain the element distribution of a point, a line or a selected area. For this study, EDS can be used to define the composition of inclusions related to WECs.

3.5   Calculation of the line contact parameters

The calculations in this session are carried out according to Hertz's contact theory [31], which has been introduced in Section 2.2. In the axial cylindrical bearings, the contact between rollers and washers is a line contact. When a load is applied on the bearing, the contact line becomes almost a rectangular shape, shown in Figure 3-6, where the "b" and "l" are contact half-width and contact length respectively. Based on Hertz's contact theory, these two values can be calculated based on the diameter of the two contact objects and material properties of contacting system.
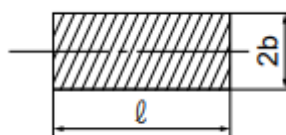
Figure 3-6. The contact shape for line contact. "b" is contact half-width and "l" is line contact length.

Calculated maximum Hertzian contact stress

The contact half-width b and the maximum Hertzian contact stress P_{max} for the contact between two rollers is calculated as follows [31]:

$$b = \sqrt{\frac{2F}{\pi l} \frac{(1-v_1^2)/E_1 + (1-v_2^2)/E_2}{1/d_1 + 1/d_2}} = 0.1243 \text{ mm} \qquad (3.5.1)$$

$$p_{max} = \frac{2F}{\pi bl} = 1366 \text{ MPa} \qquad (3.5.2)$$

Where l is the line contact length, F is the contact load, d_1 and d_2 are the diameter of Roller 1 and Roller 2, E_1 and E_2 are the Youngs' modulus of Roller 1 and Roller 2 and v_1 and v_2 are the Poisson's ratios of Roller 1 and Roller 2.

In the contact between roller and washers in this project, the value of d_1 and d_2 are the diameters of roller and washers, which means that they are equal to 10.5mm and $+\infty$ respectively. The value of contact line l is determined by the traces left by sliding, which was measured as 7.5 mm, see Figure 3-7. The value of contact load F is 2 kN because there are 15 rollers in cylindrical roller thrust bearings to support the total applied axial load of 30 kN. Both rollers and washers used are made of AISI 52100 bearing steel, whose material properties are reported in [141] (Poisson's ratio v =0.3, Elastic modulus E = 210 GPa). Values of all these parameters are shown in Table 3-4.

Table 3-4. Diameters and material properties of roller bearing contacting system.

d_1	10.5mm
d_2	$+\infty$
contact line l	7.5 mm
contact load F	2 kN
Poisson's ratio v	0.3
Elastic modulus E	210 GPa
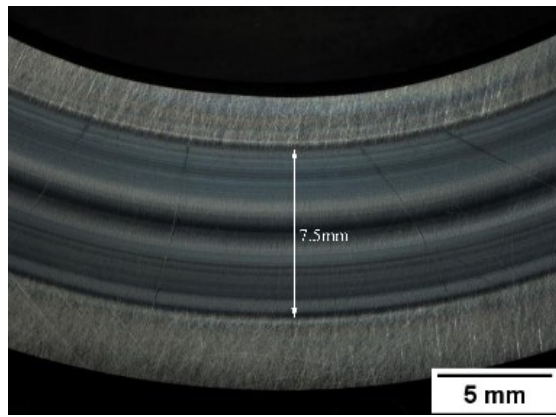
Figure 3-7. Measurement of length of contact line.

Equations of maximum shear stress and the depth of some equivalent shear stresses are listed as follows.

Calculated maximum shear stress [31]

$$\tau_{max} = 0.3 \times p_{max} = 410 \text{ MPa} \tag{3.5.3}$$

Depth of maximum orthogonal shear stress [36]

$$z_0 = 0.5 \times b \approx 62 \text{ μm} \tag{3.5.4}$$

Depth of the maximum shear stress [37]

$$z_{max} = 0.78 \times b = 96.954 \text{ μm} \approx 100 \text{ μm} \tag{3.5.5}$$

Chapter 4   Results and discussion

4.1   Surface damage

Due to the surface initiation mechanisms of WECs proposed in the literature, the characteristics of the surface damage is important. Firstly, all the bearings were analysed under the optical microscope to check the surface damage. There were eight tests carried out for different test durations (10h, 70h, 130h, 170h, 300h, 355h, 382h and 389h) and each test had two bearings tested. Thus 16 bearings were analysed in total. Bearings tested for more than 300 hours had visible surface damage.

Figure 4-1 shows the method used to confirm the location, length and width of the surface damage. The outer side edge of the rolling contact track area (wear track) is chosen as the baseline. The minimum distance between the surface damage and this baseline is used to determine the location of surface damage on the washer, marked by the red line. The length of the surface damage along the circumferential direction is determined as the width of the surface damage, marked by the blue line. The length of the surface damage vertical to the circumferential direction of the surface damage is determined as the length. In the following sections, the length of the surface damage is chosen to describe the size of the surface damage because it is larger than the width in 95% of the examined bearings.
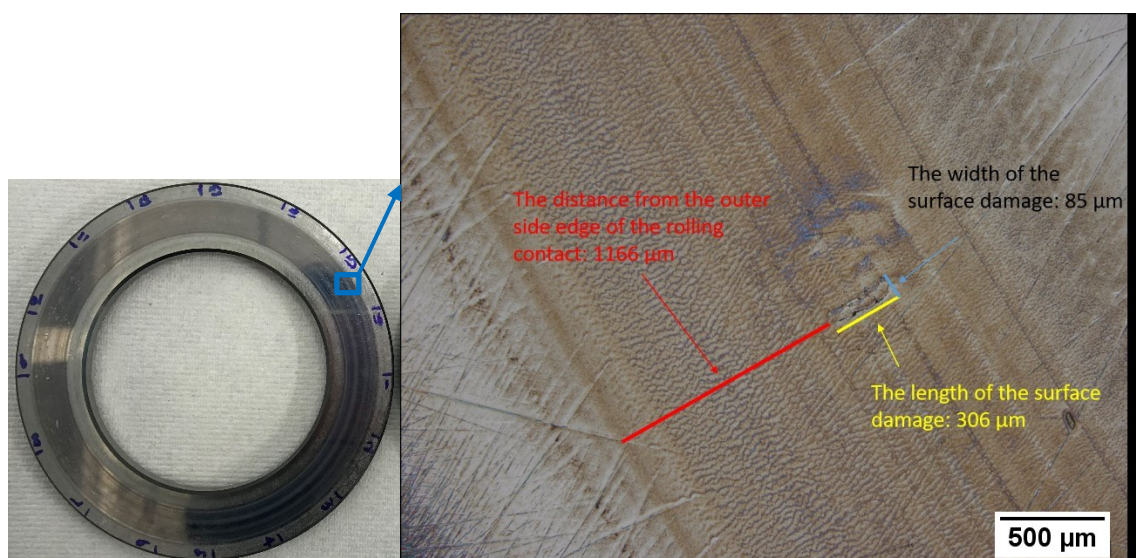
Figure 4-1. Illustration identifying the locations, length and width of the surface damage.

All the bearings were first checked under an optical microscope to search for surface damage. It should be noted that bearings tested above 300 hours have obvious damage

Results and discussion

which was seen easily by eye (>1000 μm). Surface damages at different size scales are shown in Figure 4-2. The distribution of sizes of the different surface damage observed for bearings tested above 300 hours and below 300 hours are shown in Figure 4-3.
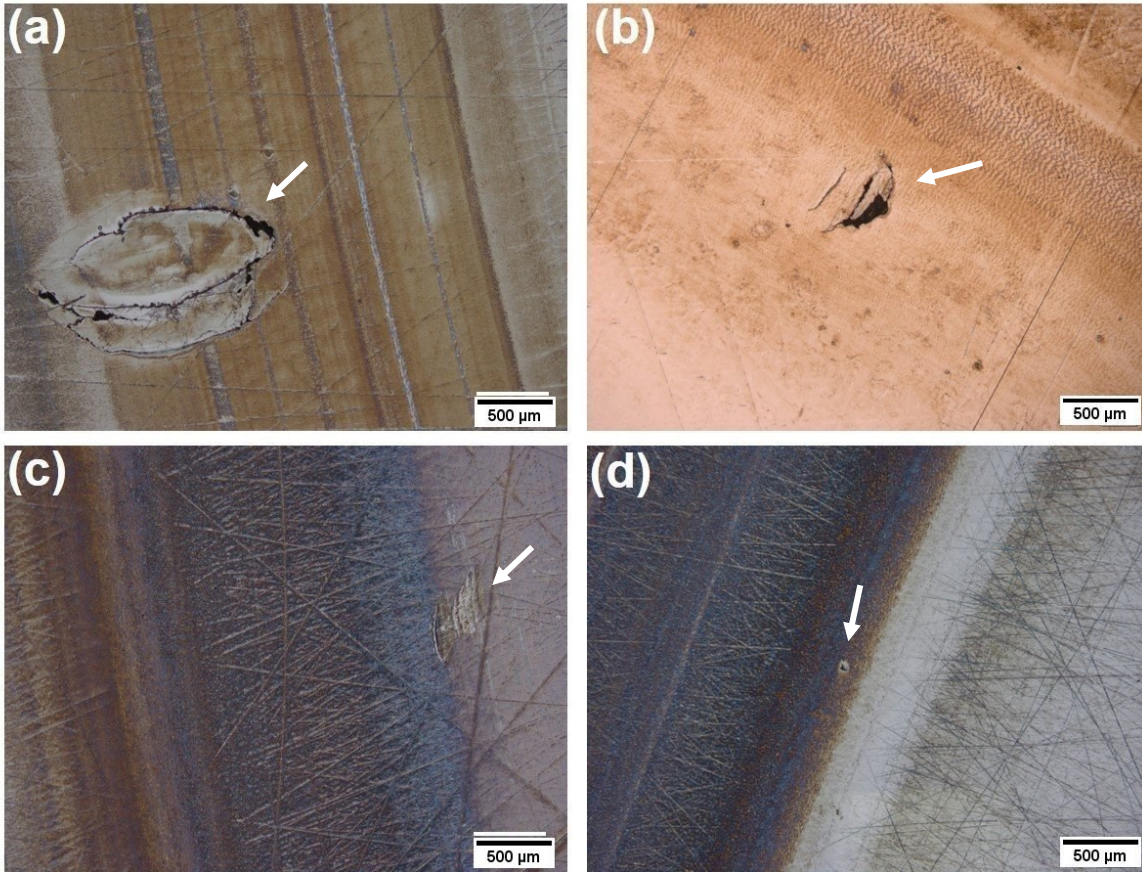
Figure 4-2. OM images of surface damage, marked by white arrows, in the size of (a)>1000 μm from 389-hour tested bearing; (b) 500-1000 μm from 355-hour tested bearing; (c)100-500 μm from 130-hour tested bearing; d) <100 μm from 70-hour tested bearing.
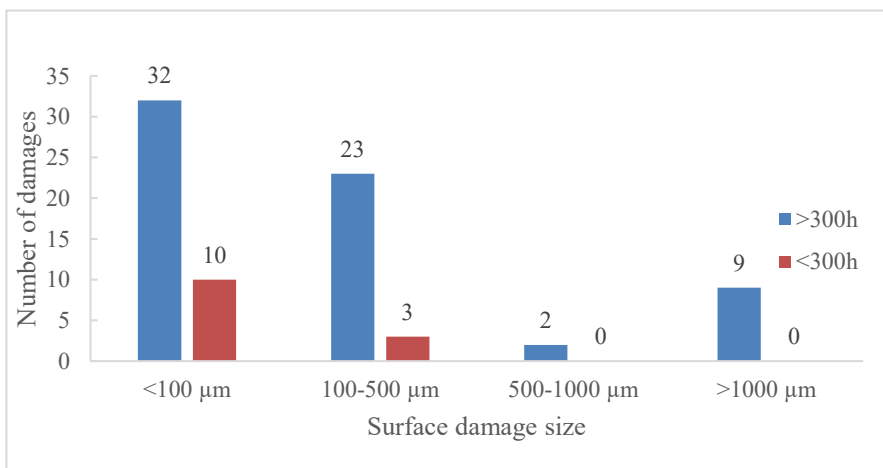
Figure 4-3. The numbers of different surface damage sizes observed on bearing washers under two groups of testing conditions: above 300 hours testing and below 300 hours testing.

The location of surface damage sites on GS and WS washers are represented by polar coordinates whose zero point is the centre of bearing. The angle θ is the polar angle, where the location of 0 degree is the start of manufacture the label back on the washers (Figure 4-4). All locations of these represented surface damage sites are shown in Figure 4-5 and Figure 4-6, the x-axis represents the polar angle θ and the y-axis represents the distance d between the surface damage site and the centre of the roller, although the value of d here used the minimum distance between surface damage and the baseline in Figure 4-1. It should be noted that the location of the midline of the wear track area corresponds to 3.75mm in Figure 4-5 and Figure 4-6. When the value of d is lower than 3.75mm, the surface damage is seen as located in the inner part of washer, which accounts for 73% and 64% of the total surface damage for the bearings tested above 300 hours and below 300 hours respectively. This means that surface damage is more located near the inner part of the wear track, especially the inner edge. This is because that the ratio of slip and roll increases when the location is away from the middle line of the wear track. The inner part of the washer is defined as the negative slip region and is more susceptible to damage according to [82], [111], [117]. In the literature, Paladugu [142] also found more damages at the extreme ends of the contact line in the same type of bearings under 1.9 GPa contact stress and critical oil in an FE-8 test rig. In the bearings under very lower hours of testing, (such as 70 hours) surface damage is also examined.
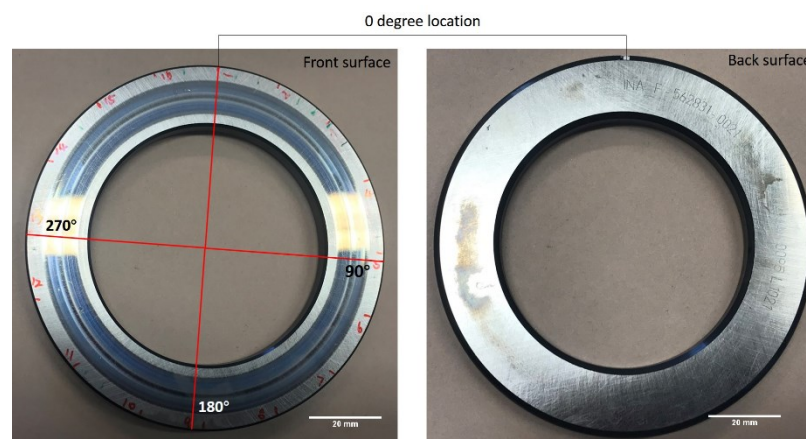
Figure 4-4. Illustration of the angle setting on a washer.

In the bearings tested above 300 hours, the surface damage on GS washer is 28% more than that on WS washer; while in the bearing tested below 300 hours, the surface damage on GS washer and WS washer are similar. From the current results, GS washer is more prone to surface damage than the WS washer in this research. Because the whole

phenomenon of WECs is quite sensitive to the surface quality of the washers WECs although they are subsurface cracks [142], bearings were cut mostly based on the location of surface damage occurred to find the WECs and the GS washers were cut first.
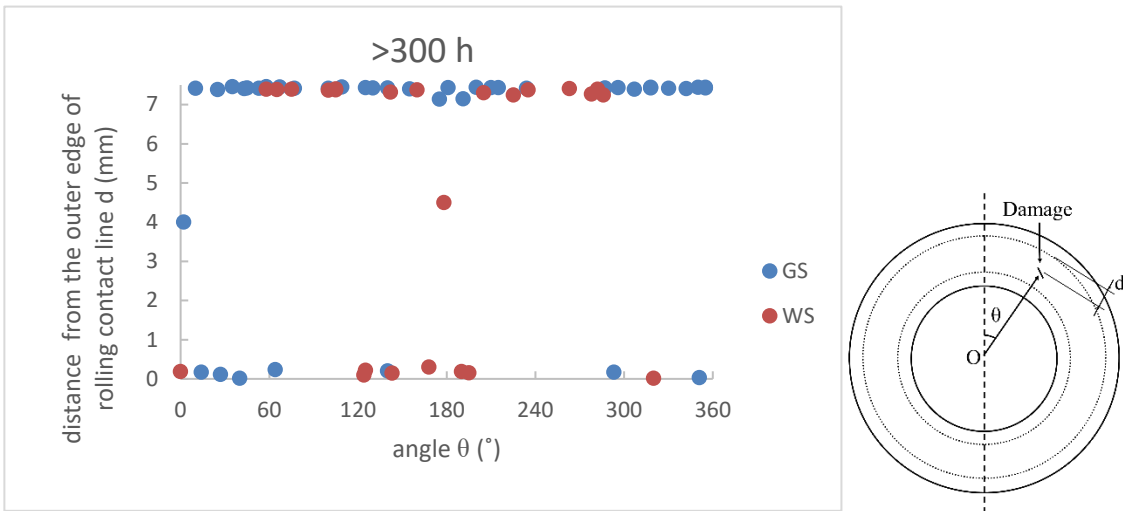
Figure 4-5. The distribution of surface damage on washers of bearings (>300 hours testing).
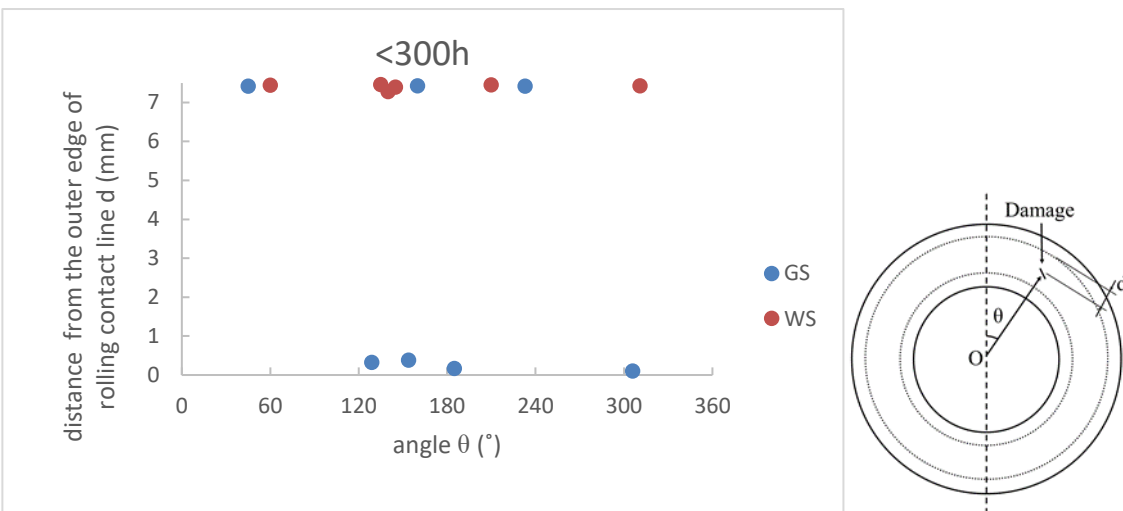
Figure 4-6. The distribution of surface damage on washers of bearings (<300 hours testing).

4.2   Characteristics of WECs and WEA

A series of WECs and WEAs were found after sectioning the bearings. Their location and microstructure characteristics are shown in this section. The relationship between the location of surface damage and WECs/WEA is also discussed.

4.2.1   Location of WECs/WEA

Depth

The circumferential location of WECs was not recorded. The axial location of WECs, which is the depth, was recorded in Table 4-1. Six WECs were found and the range of each WEC's depth are shown in Figure 4-7. The blue line and the purple line in the graph represent the calculated depth of maximum shear stress and the calculated depth of maximum orthogonal shear stress respectively. From the graph, it can be seen that three WECs have a narrow depth range and the other three WECs have a wide depth range. In Figure 4-7, two WECs reach the depth of maximum shear stress, and two WECs are observed close to the depth of predicted maximum shear stress. The rest two WECs are located at a depth more than 200 μm under the surface and with a wide depth range. This could be due to the only one cross-section of WECs found. WECs are a network and branched structure. The 3D structure of WECs could go much deeper in the later stages of formation as shown in the literature [152]. Although the number of WECs found is limited, there are still more than half of WECs reaching or approaching the depth of maximum shear stress. It can therefore be suggested that WECs are more likely to occur near the depth experiencing maximum shear stress, which is 100 μm.
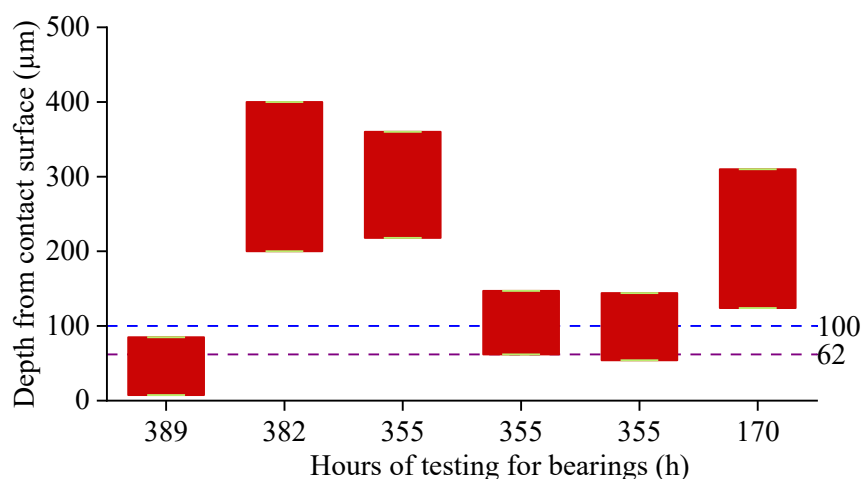
Figure 4-7. Graph of the depth ranges of WECs. The blue line is the value of calculated depth of maximum shear stress and the purple line is the value of calculated depth of maximum orthogonal shear stress.

Results and discussion

Relationship between surface damage and WECs

The location of WECs is represented by the distance to the outer edge of the rolling contact line. Information on the WECs/WEA found in the bearings is shown in Table 4-1. The length of WECs was measured by using the method shown in Figure 4-8 (c). The found WECs usually were not straight and branched. The length of WECs was the sum of all the branched lengths. If the crack was not straight, the length of that crack would be replaced by the length of the straight line which is parallel to it. It seems that the location of WECs are distributed between the outer and inner contact line quite randomly, indicating not necessarily related to the surface damage. The surface damage is more often located near the inner/outer edge of the wheel wear track. In addition, the observed WECs do not connect to the surface in images of the section surface and the location of some observed WECs are far away from the observed surface damage, see Figure 4-8. Above all, there may not be a direct relationship between the surface damage and the WECs.

(a)

(b)

(c)
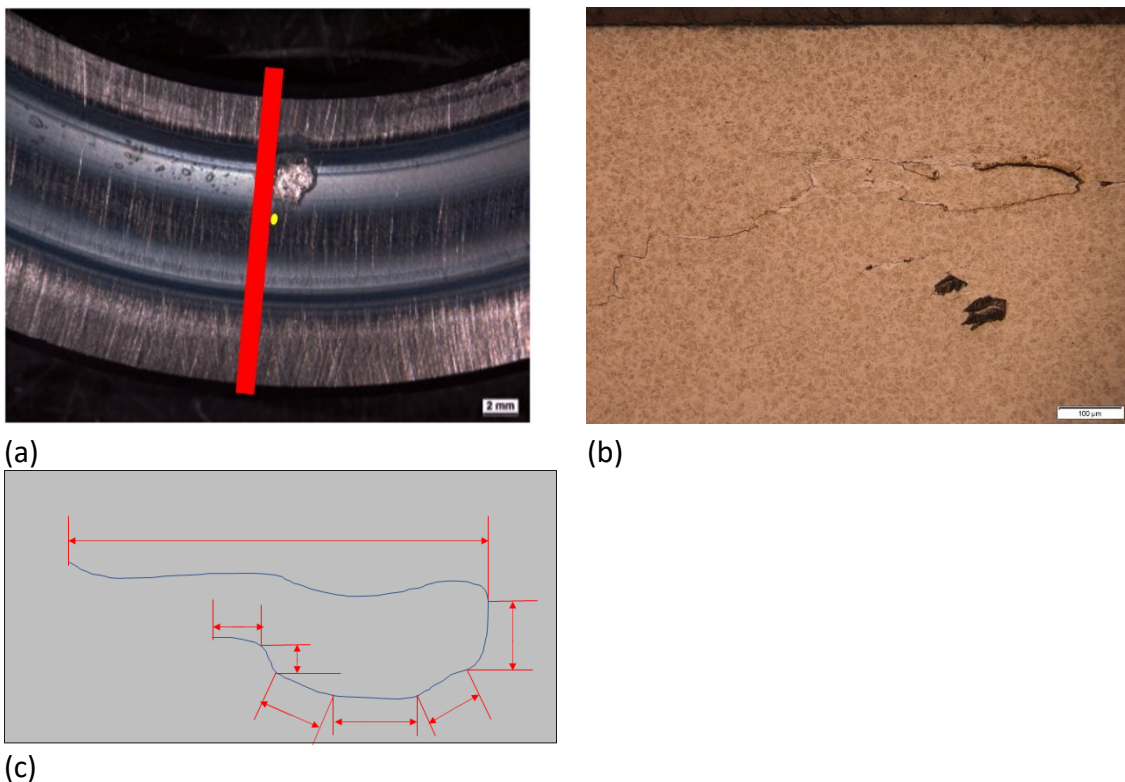
Figure 4-8. Observation of 382-hour test bearing: (a) Top surface image, where the location of the found WEC is marked by yellow point, (b) etched cross-section and (c) the method of measuring the length of WECs.

In Table 4-1, three WECs are close to the contact surface. This could be because the shear stress shifts to the surface due to the slippage. There are still half of WECs in deeper area due to the limited view of one cross-section of the WECs. Building 3D pattern of WECs through serial sectioning technique is beneficial on observing the whole picture of WECs. More WECs are found to locate near outer edge rather than inner edge, which is contradictory to the literature review. One explanation is that the WECs found in this condition are not caused by crack face rubbing mechanism. The limited number of found WECs is also a possible reason.

Table 4-1. The summary information of WECs.

Bearings	Depth (μm)	Length (μm)	Distance away from outer edge of contact line (Total length is 7.5 mm)
389h	7.5-85	1045	3.3mm (outer)
382h	200-400	1500	4.4 mm (inner)
355h	218-360	208	3.3 mm (outer)
355h	62-147	998	2.5 mm (outer)
355h	54-144	330	3.7 mm (outer)
170h	124-310	650	7.0 mm (inner)

4.2.2　　Microstructure of WEC

In the bearings tested for more than 300 hours, later stage WECs including multiphase structures in the subsurface were found, like shown in Figure 4-9. Numerous cracks were observed to be parallel to the contact surface in the axial cross section of washers. Figure 4-10 shows the SEM image of a later stage WEC. Coarse structure, smooth structure and no carbides were found in the WEA. Deformed carbides and intact carbides were found in the area between the WEA and the matrix and the WEA area respectively. This indicates that the dissolution of carbides could be part of the process of formation of the WEA. All

these observed WEC features have been seen in previous literature [10], [41], [49], [59], [61], [64], [143], [144]. These features confirm the formation of WECs under these test conditions and help to predict the initiation point of WECs in the earlier stages of bearing tests.
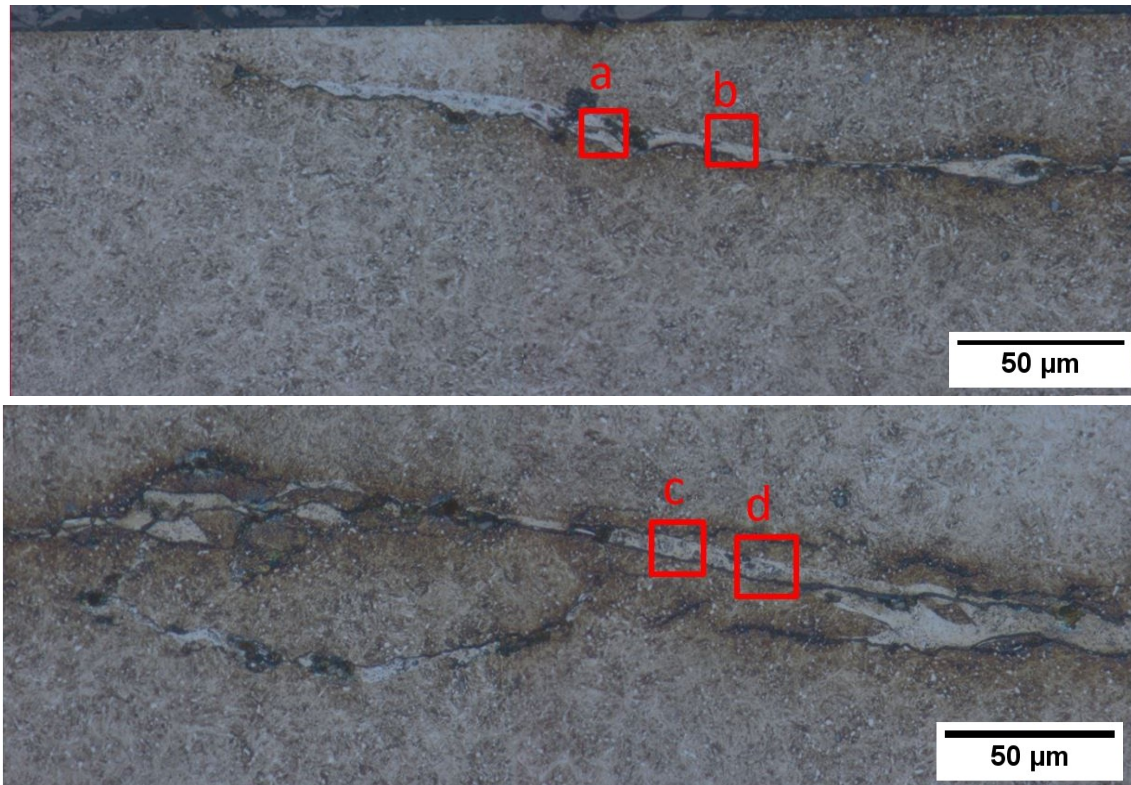
Figure 4-9. Optical images of cross-section of etched 389-hour test bearing. Area a, b, c, d will be further analysed in SEM.
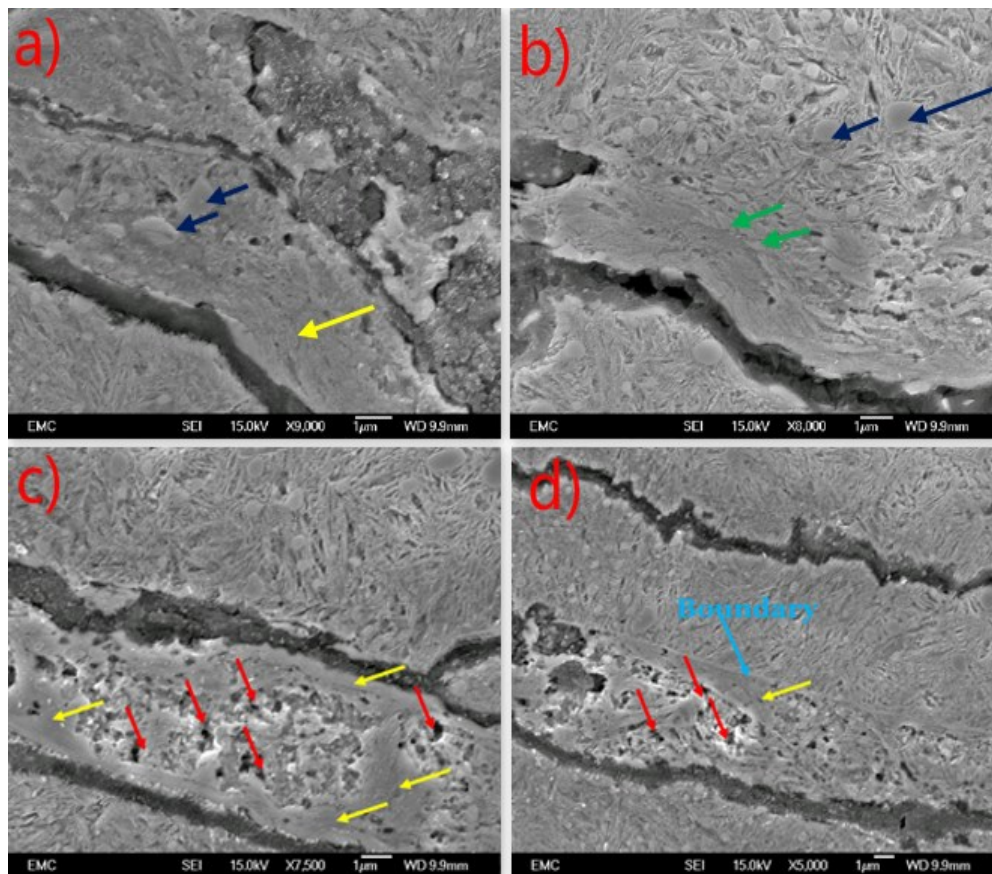
Figure 4-10. SEM image of cross-section of etched 389-hour test bearing corresponding to the area a, b, c and d in Figure 4-9. The green, deep blue, yellow and red arrows represent deformed carbides, intact carbides, smooth structure and coarse structure respectively.

4.3   **WEC initiation mechanism: Carbide aggregation**

Carbides have been reported to affect the fatigue life of bearing materials, especially the size and the distribution of carbides [26], [145]-[147]. Spheroidized carbides help to increase the fatigue life of bearing steel by strengthening the tempered martensitic matrix and the grain boundaries [147]. In carburized steels, network carbides along the grain boundaries have been reported to decrease the bending and tensile properties and led to cracks [148]. Large carbides were found together with the cracks, which may be at the boundaries or in the middle of the carbides [149]. A cluster of carbides was found to be more harmful to bearing steel than a single carbide due to the concentration of stress. Guan et al. [146] used a continuum damage accumulation model incorporated into a Voronoi finite element model to study the crack nucleation and propagation caused by a cluster of carbides in M50 bearing materials. They found that the edge of the carbide was the site of the maximum stress concentration and a high stress appeared in the matrix

between the carbides. The boundary of the carbides or the location between two carbides was found to be the site of crack nucleation. Then the cracks propagated and grew towards the clustered carbides. They also reported the critical depth affecting the crack nucleation for the chromium carbides is equal to the length of the contact half-width [146].

In this project, accumulated carbides, which could affect the initiation of WECs, were found in the experimental observation of the etched cross section. In bearings tested for less than 300 hours (i.e. the expected earlier stages of WEC initiation), accumulated carbides at depths between 30 μm to 200 μm are found to become more and more evident with increase in test duration time. In the undamaged areas of all samples and in samples with shorter testing times, the carbides are seen to be evenly distributed in the matrix. A typical example is the 10-hour tested bearing, see Figure 4-11. Accumulated carbides started to be found in 130-hour tested bearings, see Figure 4-12. These phenomena can be observed by optical microscope because they showed white after etching. After further analysis in the SEM, it is clear to see that they are clusters of carbides composing of two or more carbides. Two manifestations of these aggregations of carbide were found: the first is a linear or clustered arrangement of carbide; the second is the combination of two or more carbides into one apparently larger carbide. In the 170-hour and 300-hour tested samples, these linear/clustered carbide accumulations were also observed and were more significant, see Figure 4-13 and Figure 4-14.
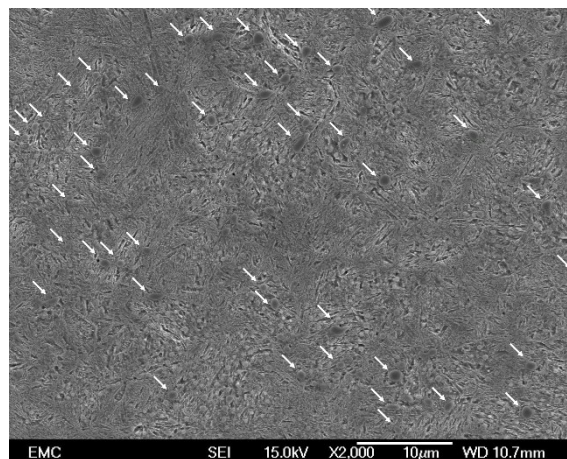
Figure 4-11. SEM images of microstructure of 10-hour tested bearings.
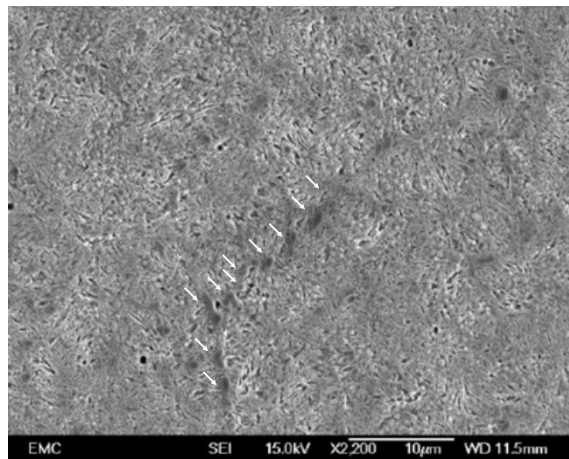
Figure 4-12. SEM images of the carbides aligned or clustered in 130-hour tested bearings.
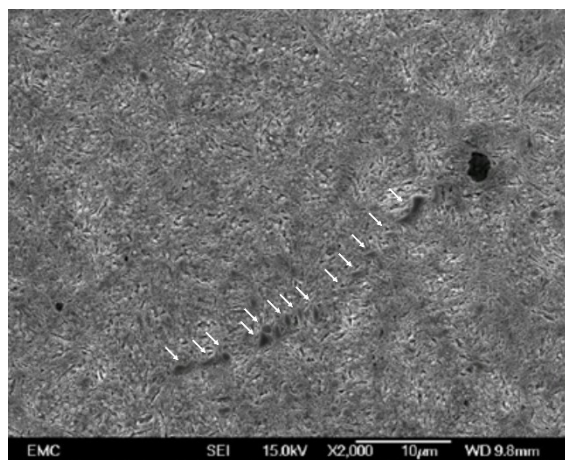
Figure 4-13. SEM images of the carbides aligned or clustered in 170-hour tested bearings.

(a)   (b)
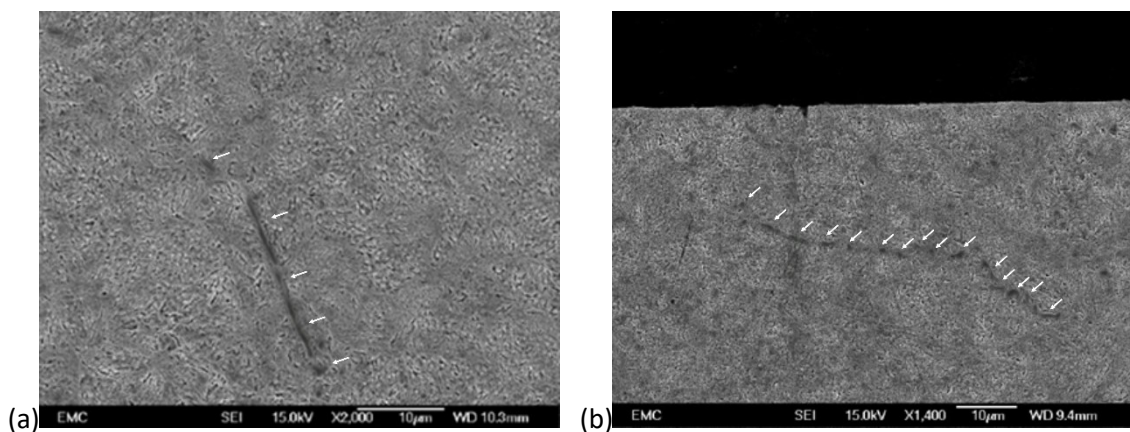
Figure 4-14. SEM images of carbide accumulation in 300 hours tested bearings.

In the bearings tested for 382 hours, mature WECs were observed, see Figure 4-15. In this image, small cracks with a carbide aggregation was also observed and the crack propagates along the direction of the carbide aggregation

Results and discussion

Figure 4-16 shows the increase of the average maximum length of accumulated carbides with the increase of testing duration time. Similarly, the average total length of accumulated carbides also grows with time (Figure 4-17). Both of these indicate the accumulation of carbides becomes more significant over time. It should be noted that there are no error bars for data corresponding to 170h because only one accumulated carbides phenomenon was captured.
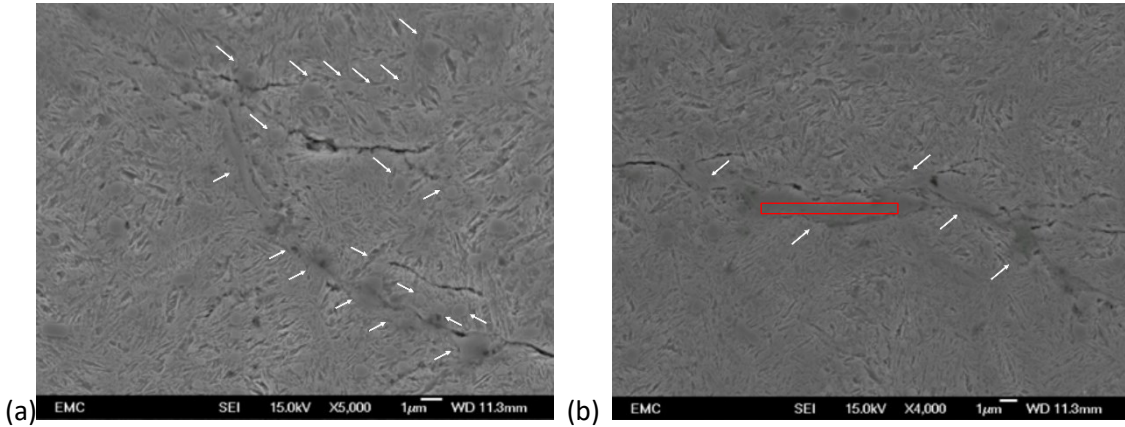
Figure 4-15. SEM images of the cracks related to carbide aggregation in 382 hour tested bearings.
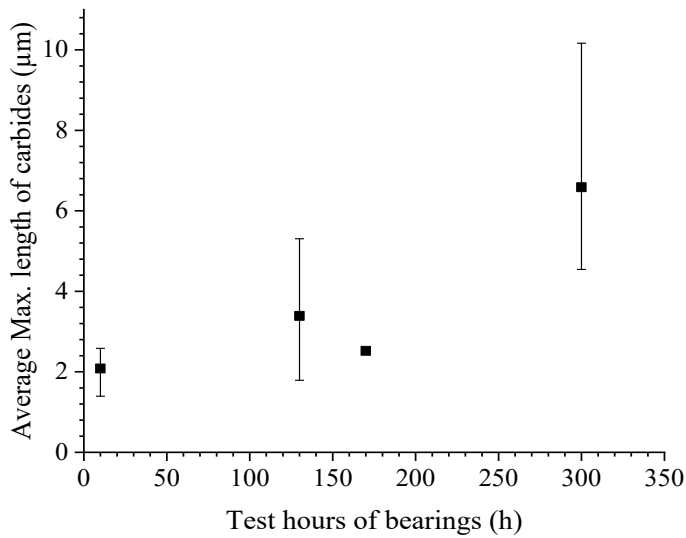
Figure 4-16. The relationship between average maximum length of carbides and the test hours of bearings.
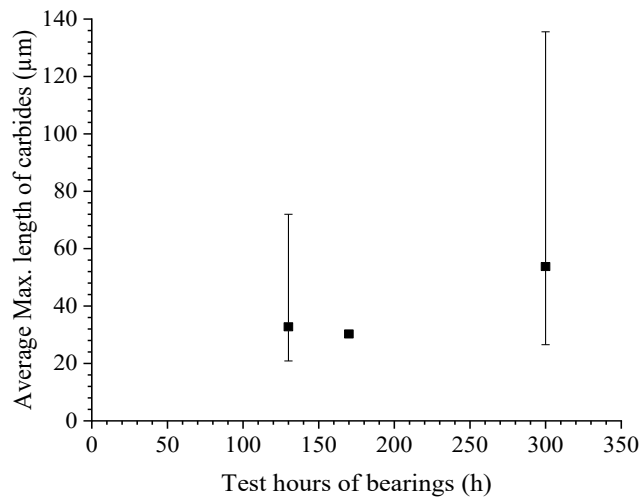
Figure 4-17. The relationship between average total length of accumulated carbides and the test hours of bearings.

Mostly accumulated carbides were found in high magnification SEM images, like Figure 4-12, Figure 4-13, Figure 4-14 (a), in which there is no boundary of the contact surface. Therefore, it is hard to identify the exact depths of the accumulated carbides. However, there was a finding that as long as the observed area went deeper, the amount of accumulated carbides tended to increase. While after exceeding a critical depth, the carbides tended to be less accumulated. Since stated previously, it is hard to identify the accurate depths of accumulated carbides in a high magnification SEM image, so the depths of the observed area were estimated. The observed carbide accumulation with the shallowest depth is the one in Figure 4-14 (b) with the value of 24 µm. For locations deeper than 300 µm, no carbide aggregation was found. Therefore, all observed carbides were located in the depth range of 24 to 300 µm, which is within the depth range of WECs occurrence. Then these carbides were thought to relate to the initiation of WECs. The observed carbide aggregation changing from less to more and from more to less as the depth increasing is consistent with the change in shear stress along with the depth. More accumulations of carbides were found in the region appearing higher shear stress. It could be guessed that the accumulation of carbide is related to shear stress. This indicates that a relatively higher shear stress level in the subsurface seems to be an important factor leading to the accumulation of carbides. Some literature indicates that large primary carbides or clusters of carbides may act as stress raisers like non-metallic inclusions and lead to damage like butterflies [150]. Therefore, it can be suggested that this carbide

aggregation may act as important stress raisers in the higher shear stress region and thus resulting in the initiation of cracks.
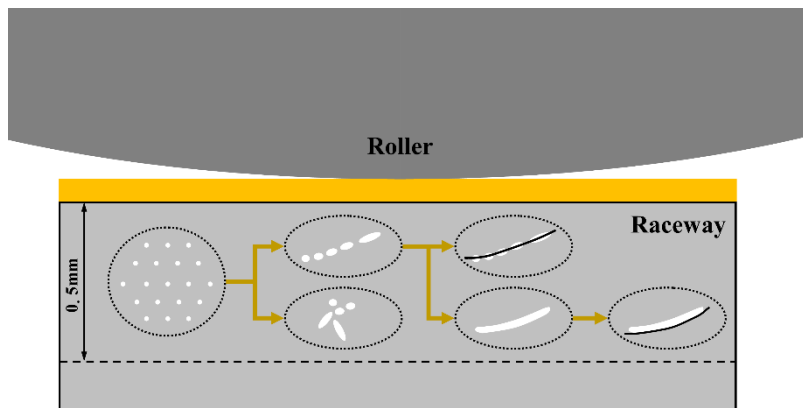
Figure 4-18. The schematics of the carbide aggregation leading to WECs.

The mechanism of carbide aggregation is not confirmed, but it may be related to mechanical and electrothermal reasons. A first hypothesis is the dislocation assisted carbon migration mechanism triggered by the special stress history of the cyclic rolling contact. [151]. In this research, the detailed rolling contact conditions are believed to trigger this mechanism and lead to carbide nucleation at the ferrite band boundary. During the process of experiencing rolling contact conditions, carbon will continue precipitating at these nucleations along the direction of dislocation glide and lead to the eventual coalescence of carbides. A second hypothesis is that localised transient current flow caused by self-charging and discharging of lubricant results in local electromagnetic induction to the subsurface. Accumulation of carbides would then be caused by localised resistivity heat due to the difference of conductivity properties of carbides and martensite [79], [80].

4.4   Growth mechanism of WEA

As an important part of WECs, the formation process of WEA may be related to the crack initiation mechanisms of WECs. Previous results about the WEA have indicated the microstructure characteristics and its change during the formation process, e.g. the dissolution of carbides [13] [16], [46], [137], but the growth mechanism of the WEA is still unclear.

In this project, WEAs containing significantly different volumes of carbides were observed by SEM in the 355-hour tested bearing sample, these can be considered as WEAs at

different stages, see Figure 4-20. Fine and smooth areas of WEA were thought as the later stage of WEA because it does not contain visible carbides. WEAs containing intact carbides as well as deforming carbides were thought to represent the earlier stage of a new WEA formation, see Figure 4-21.

Two kinds of boundaries between WEA and matrix were observed, including transitional areas containing "crack-like structure" and clear boundaries. It is observed in Figure 4-20 that a transitional area containing "crack-like structure" exists in both the earlier and later stage of WEA while that containing clear boundaries only exists in the later stage of WEA. The area between matrix and formed WEA, with carbides and more lined structures, is identified as a transitional area. The lined structure is identified as a "crack-like structure". It should be noted that the specific structure of the "crack-like structure" was not determined in this study because it requires confirmation by EBSD and XRD tests. In terms of the growth of WEA, clear boundaries are unlikely because the microstructures of the matrix on the other side of the WEA don't change. In contrast, a transitional area containing a "crack-like structure" is more likely to be the potential growth direction of the WEA. The reason for this is that there are many small voids and micro-cracks located at these transitional areas, which may be due to the change of volume related to the dissolution of the carbides, for both formed WEA without carbides, see Figure 4-21 (b), (c), (d), (e), (g), and the earlier stage of a new WEA with intact carbides, see Figure 4-21 (a), (g). In Figure 4-21, the spheres pointed by red arrows are intact carbides within the WEA. In the WEA, the pores circled by yellow mark are voids. The purple circles show the WEA with no carbides, which indicates that carbides were dissolved. The green area shows the transitional region between WEA and matrix, and the white arrows point to the "crack-like structure".

In the previous literature, there is a proposed growth mechanism of WEA named as the crack face rubbing mechanism. However, it seems not applicable to this case because the potential growth direction of WEA, the transitional area, shows no relationship to the crack face due to the significant distance between them. Based on the current findings, another growth mechanism of WEA can be related to "crack-like" structures which are near to where the carbides exist. In other words, the crack-like structure is here identified as the pre-stage of WEA.

Results and discussion

The detailed crystal structure of the crack-like structure is not determined due to the limitations of the resolution of EBSD available in the University of Southampton. However, some reasonable conjectures can be made based on previous literatures. H. Uyama [47] studied the pre-stage of WEA and found the small line structure shown in Figure 4-19, which is similar to the crack-like structure observed in this project. This small line structure was confirmed by him as an ultra-fine grained structure and proposed to be caused by in-charged hydrogen, which may occur in the samples studied in this project due to the decomposition of lubricant. H. K. Danielsen observed some grains in WEA at a similar size scale (10 nm) to these small line structures and confirmed them as equiaxed grains [152]. In addition, Rumpf found equiaxed grains formed next to the WEA, and the grains were of ferritic crystal structure [83]. Based on this, the "crack-like" structure found in this research can be conjectured to be ferritic grains but this requires to confirmation by high resolution EBSD.
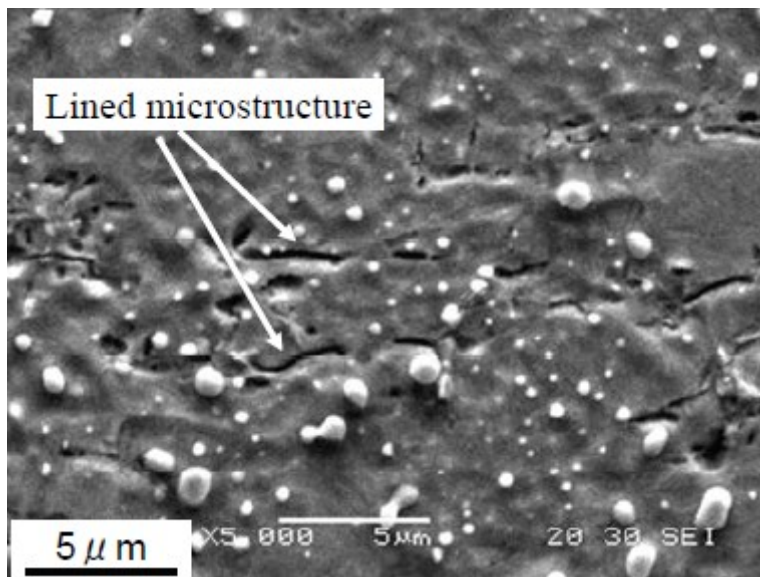
Figure 4-19. SEM image of small line structure. The specimens were hydrogen-charged using 0.3 mass% NH$_4$SCN aqueous solutions and under clean lubrication conditions and a maximum contact pressure 3.8GPa. The specimens were made of JIS-SUJ2 bearing steel, which is similar to AISI 52100 [47].

The flow chart of the proposed growth mechanism of WEA related to "crack-like" structures is shown in Figure 4-22. The only evidence of the observation of the "crack-like structures" obtained from this work is the SEM images shown in Figure 4-21, and the "crack-like structures" are thought to be ultra-fine grained structures based on the literature [47], [83], [152]. EBSD characterisation on the "crack-like structure" needs to be

conducted to identify the structure. TEM will be used to characterise the dislocations. These further research will help to confirm the proposed WEA growth mechanism. Based on the above conjectures about the likely crystal morphology of the crack-like structure, the growth mechanism of a new WEA from formed WEA can be divided into three steps and are here stated in greater detail:

Step1: Diffusion of carbon from formed WEA into matrix

A lot of dislocations accumulate at the boundary between the matrix and the formed WEA under cyclic loading. They may absorb carbon, thus leading to significantly higher concentration of carbon than that in the matrix. This large difference of carbon content between boundary and matrix may lead to carbon diffusion from the WEA into the matrix to form an adjacent area with a strong carbon enrichment.

Step2: Formation of transitional area in the matrix

There is a local stress field in the area around the boundary between the WEA and the matrix, the adjacent area with strong carbon enrichment, due to their different hardness [10], [41], [50]-[53]. In an area with localized strain, the dislocation density will continue to accumulate with further cyclic loads until reaching a certain dislocation threshold, where ruptures like micro-cracks or equiaxed grains may occur to release the energy [153], [154]. The crack-like structures, observed in this research and assumed to be ferritic grains, may reflect this kind of ruptures. Because carbides easily nucleate and precipitate at ferritic grains [151], the existence of these crack-like structures will lead to the generation of some new carbides and stabilise the nanocrystalline ferrite microstructure at the same time [155]. As a result, the transitional area containing both crack-like structures and new carbides observed in this project was formed.

Step3: Development of transitional area into earlier stage of a new WEA

During the process of formation of the transitional area, the difference of carbon content between the transitional area and boundary with many dislocations will decrease, leading to the cessation of carbide nucleation and thus resulting in the destabilisation of the nanocrystalline ferrite microstructure (crack-like structure). As a result, most of these crack-like structures will transform to other microstructures and the earlier stage of a new WEA with carbides will form. Under the stress field produced by rolling contact conditions,

carbides in these newly formed "earlier stage" WEA will dissolve and thus develop into formed WEAs over some time.
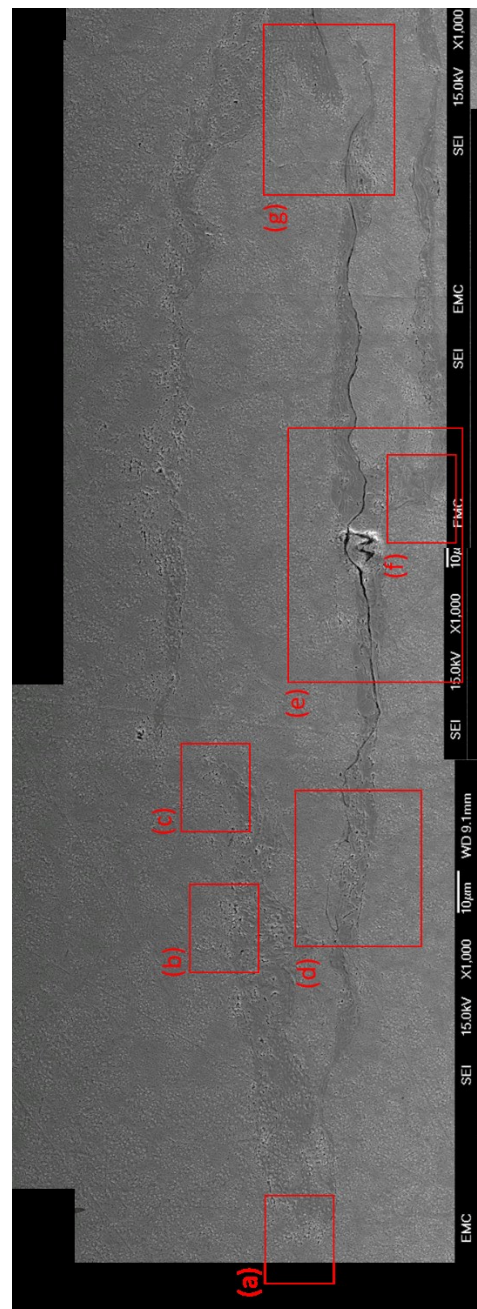
Figure 4-20. SEM image of large WECs in 355 hours tested bearings. The area marked with red will be observed in higher magnification.

(a)

(b)

(c)

(d)

(e)

(f)

(g)
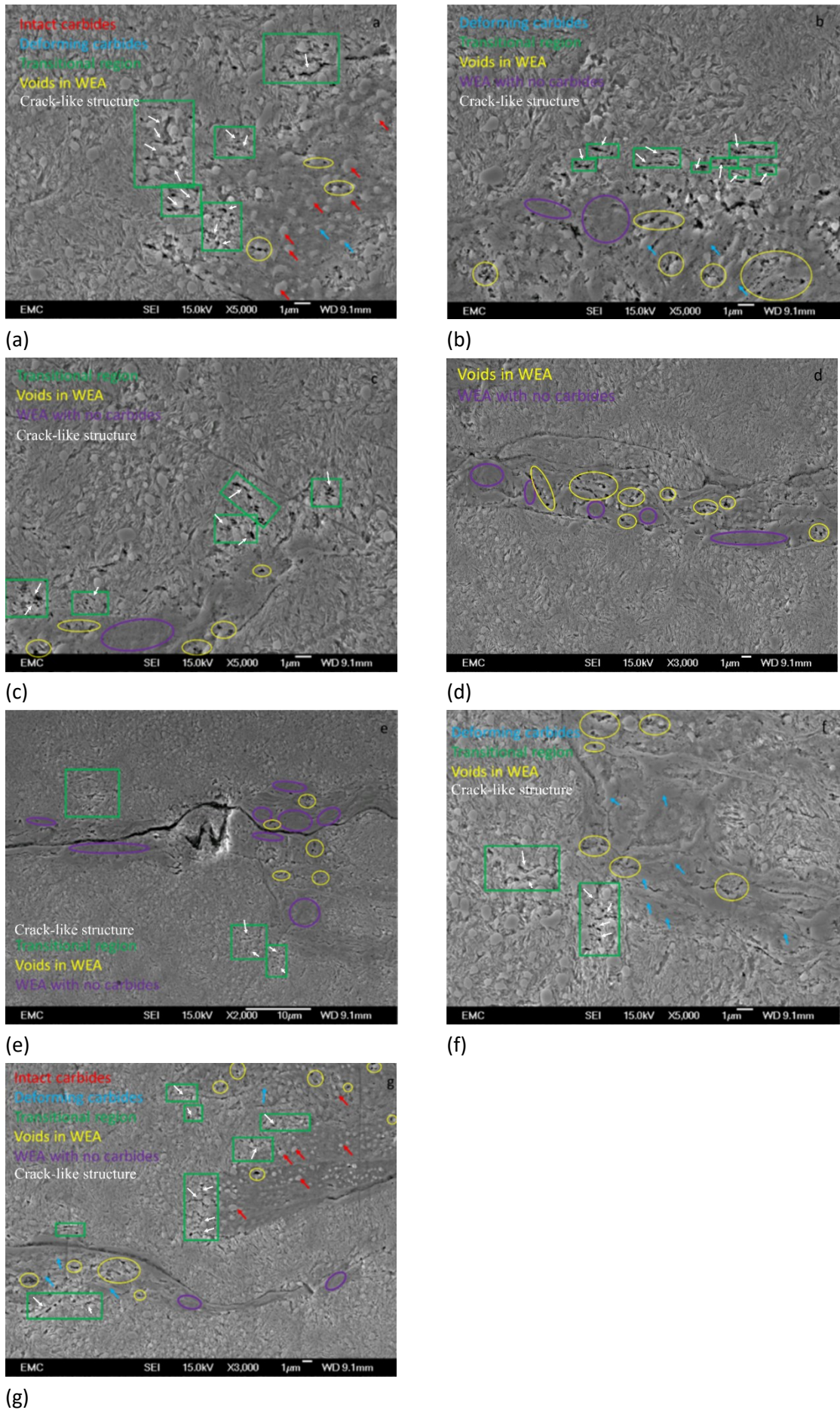
Figure 4-21. SEM images of the marked area in Figure 4-20.

Results and discussion
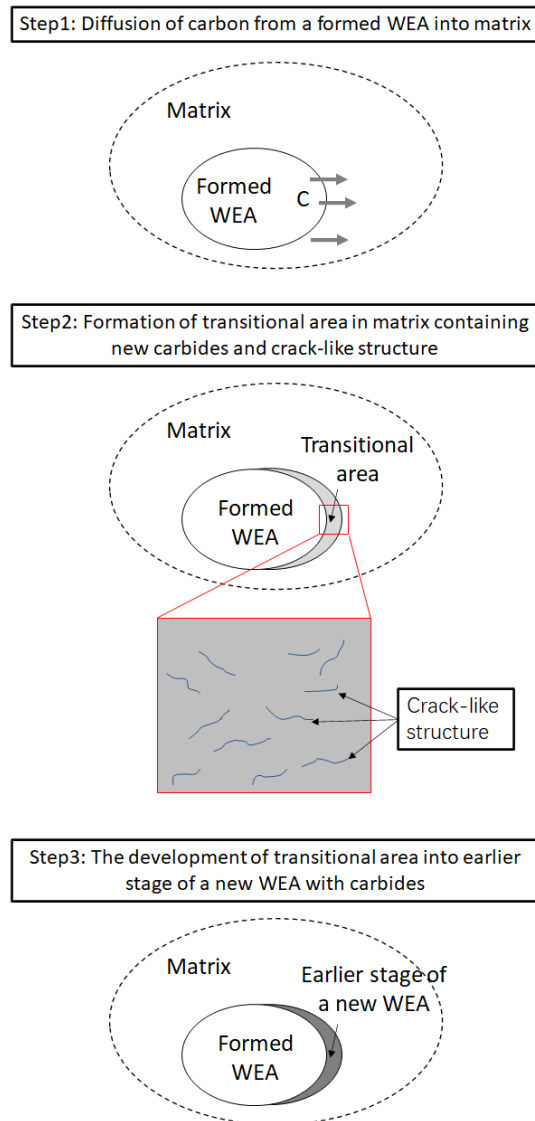
Figure 4-22. Flow chart of the proposed growth mechanisms of WEA.

4.5   Inclusions

WECs are found to be initiated by inclusions in many studies [9], [18], [19], [21], [144]. In this project, WECs also show a relationship to inclusions although there are no significant observation results showing large WECs containing inclusions nor butterflies eventually forming WECs. Inclusions are observed in 355 hour tested bearings, see Figure 4-23 and Figure 4-24. In Figure 4-23, an inclusion was found to be manganese sulphide (MnS) at a depth of 60 μm under the contact surface. Two cracks were formed on both sides of the MnS inclusion but "one wing" had already grown on one side. On the side without a WEA formed, voids or cavities were found near the crack. The size of the MnS inclusion was 6.4 μm × 3.5 μm, which was relatively small (<20 μm). Another inclusion was confirmed as aluminium oxide, shown in Figure 4-24. The inclusion was observed subsurface at 82 μm

depth. This was not a typical butterfly initiated with an inclusion because there is a distance (2.3 μm) between the oxide inclusion and crack. The size of the aluminium oxide inclusion was 2.4 μm × 2.3 μm. Because the inclusion did not contact with the crack and the region of WEA near the inclusion was less marked than the region of WEA near the crack, the crack was not initiated at that inclusion.
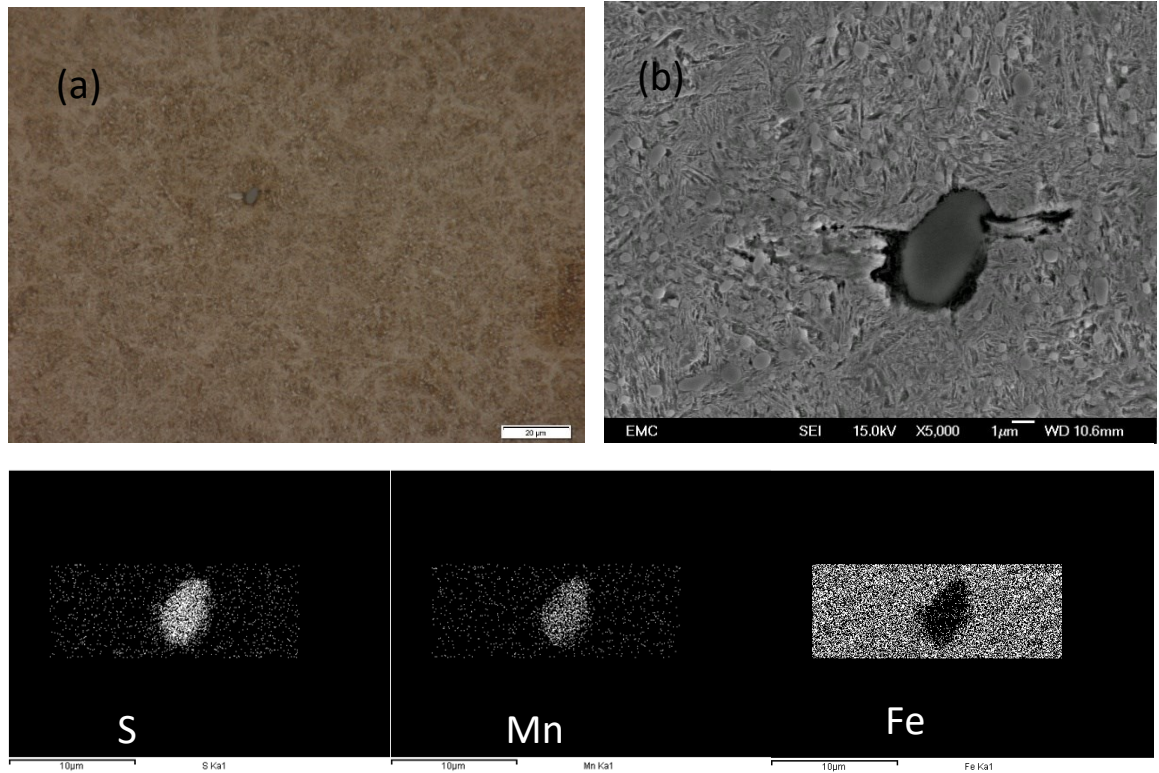
Figure 4-23. OM image (a), SEM (b) image and EDX results (c) of WECs initiated by MnS inclusion in 355 hours tested bearings.
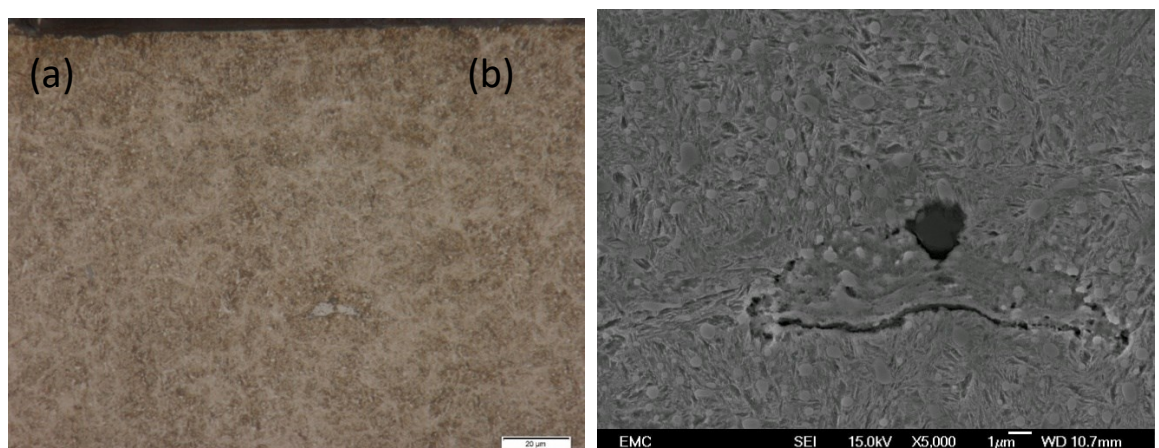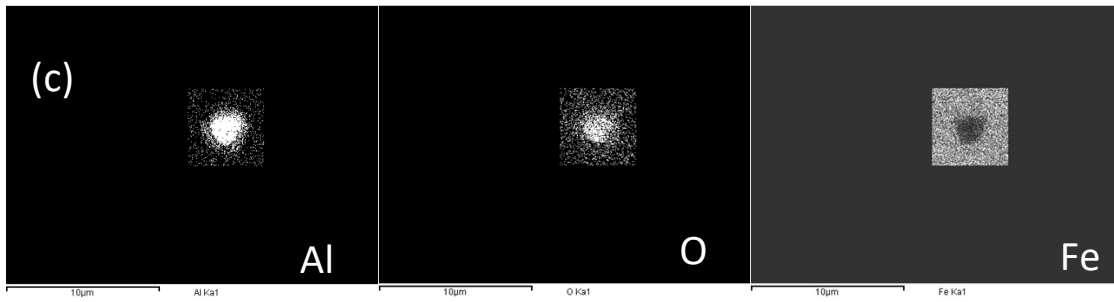
Figure 4-24. OM image (a), SEM (b) image and EDX results (c) of WECs related to aluminium oxide inclusion in 355 hours tested bearings.

In the 170 hours tested bearings, a multi-phase inclusion, containing aluminium, manganese, magnesium and sulphur, was observed at 82 μm depth from the contact surface, see Figure 4-25. A crack without WEA was formed within this inclusion and propagated into the matrix. The inclusion was located near the maximum shear stress region and the inclusion size was large (6.5 μm × 8.2 μm) which may lead to a higher localised stress level.
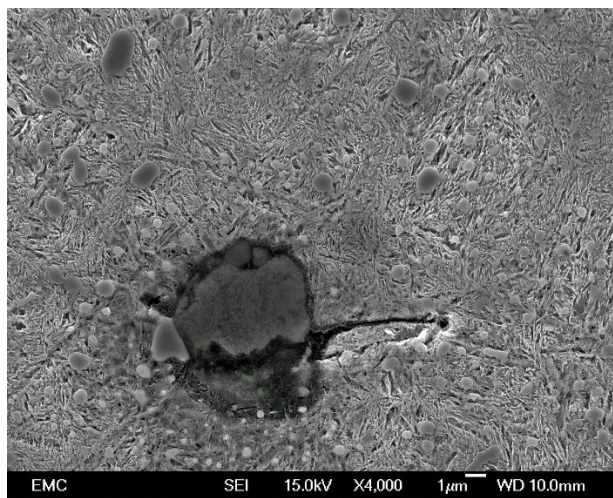
Figure 4-25. SEM image of multi-phase inclusion with WECs in 170 hours tested bearings.

The initiation of WECs related to inclusions is not a new theory. Evans et al [1] proposed that WECs were most likely initiated with small inclusions, which had an average length from 5 to 20 μm. The oxide part of the inclusion was proposed as an important part in initiating WECs or butterflies because they are unavoidable and usually cause a local stress concentration. Besides, they also easily cause debonding between the matrix and inclusion due to the hardness mismatch, tensile residual stresses and poor coherence [69].

In terms of inclusions observed in this project, their expected coefficients of thermal expansion and that of the corresponding matrix have been reported in ref [2] and [156] respectively. The coefficient of thermal expansion of MnS (the relatively soft inclusion) is larger while that of Al_2O_3 (hard inclusion) is smaller compared with that of the matrix. It is suggested that compressive stress is induced around the soft inclusions. When the matrix around the inclusion is forced and heat is generated, the soft inclusion will expand more due to its larger thermal expansion coefficient, then the soft inclusion is more likely to be subjected to compressive stress. Since the coefficient of thermal expansion of hard inclusion is smaller than that of matrix, the expansion of hard inclusion would be smaller than that of matrix. Therefore, in order to make the hard inclusion have the same expansion rate avoiding generation of new surface, a tensile stress would be induced on the hard inclusion from the matrix [2]. Combining with the cyclic shear stress field from rolling contact, these induced stresses may lead to the initiation of WECs.

Chapter 5   Conclusion and future work

5.1   Conclusion

This project mainly focused on investigating the initiation mechanism of white etching cracks (WECs) in AISI 52100 bearing steel. Microstructures of WECs at different stages were characterized by optical microscopy and scanning electron microscopy and compared with each other. The initiation mechanisms and evolution of microstructure changes of WECs were obtained for cylindrical roller thrust bearings under conditions of critical oil, slip and low pressure. All WECs were located in the subsurface, and had no direct relationship to surface damage. Carbide aggregation phenomenon and the transitional region between WEA and matrix were found firstly. A new WEC initiation mechanism and a growth mechanism of WEA were firstly proposed. The detailed findings of this report are listed as follows:

- WECs in the later stage contain fine and coarse structure, plastic deformation line and no carbides. They initiate near the region of maximum shear stress in the subsurface as most of the observed WECs/WEA (4/6) were found to be at or close to the depth of maximum shear stress. Their initiation may have no direct relationship to surface damage, which tend to locate at the edge of the rolling contact area due to the slippage on the washer, whereas only one WEC was found to be directly connected to the surface damage.

- In AISI 52100 bearing steel, some carbides are aligned or clustered over time and form a large carbide area eventually in regions with higher shear stress level. Based on the observed morphology and location of these carbide aggregations, it is possible that these are the earlier stage of WEA formation but this still requires further investigation.

- The transitional region between WEA and matrix is proposed to be the pre-stage of WEA. A growth mechanism of WEA related to the diffusion of carbon from dissolved carbides was proposed. The diffusion of carbon from the formed WEA to matrix will lead to the formation of a transitional area containing new carbides and crack like structures. This transitional area will develop into the earlier stage of a new WEA with the cessation of diffusion due to the decrease of differences in carbon content over time.

5.2   **Future work**

The current project has shown limited results to confirm the link between the carbide aggregation at the early stage and the WECs at the later stage. Therefore, firstly, more evidence showing a strong relationship between carbide aggregation and WECs is needed. Finding direct evidence like carbide aggregation with or within microcracks or small transformed regions in the middle will be helpful. If it confirmed that carbide aggregation can initiate cracks, then the mechanism of carbide aggregation needs to be further studied. At the same time, bearings under other test conditions are suggested to be analysed to assess whether the carbide aggregation phenomenon occurs, which could also be a further strong evidence to show the relationship between carbide aggregation and WECs.

Transitional regions found in the area between WEA and the matrix need to be further analysed in high resolution EBSD to see if there are ferritic grains formed. If the transitional region is not formed of ferritic grains, TEM are suggested to be conducted to check the dislocation density of this area. If the transitional region can be confirmed, then it will help to locate earlier WEA in earlier hours tested samples.

List of References

[1] M. H. Evans, "An updated review: white etching cracks (WECs) and axial cracks in wind turbine gearbox bearings," *Materials Science and Technology*, vol. 32, no. 11, pp. 1133-1169, 2016.

[2] M. H. Evans, "White structure flaking (WSF) in wind turbine gearbox bearings: effects of 'butterflies' and white etching cracks (WECs)," *Materials Science and Technology*, vol. 28, no. 1, pp. 3-22, 2012.

[3] K. Tamada and H. Tanaka, "Ohapccurrence of brittle flaking on bearings used for automotive electrical instruments and auxiliary devices," *Wear*, vol. 199, no. 2, pp. 245-252, Nov. 1996.

[4] M. N. Kotzalas and G. L. Doll, "Tribological advancements for reliable wind turbine performance," *Philosophical Transactions of the Royal Society A: Mathematical, Physical and Engineering Sciences*, vol. 368, no. 1929, pp. 4829-4850, Oct. 2010.

[5] V. Šmeļova, A. Schwedt, L. Wang, W. Holweger, and J. Mayer, "Microstructural changes in White Etching Cracks (WECs) and their relationship with those in Dark Etching Region (DER) and White Etching Bands (WEBs) due to Rolling Contact Fatigue (RCF)," *International Journal of Fatigue*, vol. 100, pp. 148-158, 2017.

[6] S. Hyde, "Improving Gearbox Reliability by Analyzing Axial Cracking on Bearings and Recommending a Solution," 2012.

[7] D. McVittie, "Wind Turbine Gearbox Reliability: The Nature of the Problem, "Gear Engineers, 2006.

[8] P. J. Tavner, J. Xiang, and F. Spinato, "Reliability Analysis for Wind Turbines," Wind Energy, vol. 10, pp. 1-18, 2007.

[9] M. H. Evans, A. D. Richardson, L. Wang, R. J. K. Wood, and W. B. Anderson, "Confirming subsurface initiation at non-metallic inclusions as one mechanism for white etching crack (WEC) formation," *Tribology International*, vol. 75, pp. 87-97, 2014.

[10] O. H. E. West, A. M. Diederichs, H. Alimadadi, K. V. Dahl, and M. A. J. Somers, "Application of complementary techniques for advanced characterization of white etching cracks," *Practical Metallography*, vol. 50, no. 6, pp. 410-431, 2013.

[11] H. Mikami and T. Kawamura, "Influence of electrical current on bearing flaking life," in *SAE World Congress & Exhibition*, 2007.

[12] K. Iso, A. Yokouchi, and H. Takemura, "Research work for clarifying the mechanism of white structure flaking and extending the life of bearings," in *SAE World Congress & Exhibition*, 2005.

[13] H. Harada, T. Mikami, M. Shibata, D. Sokai, A. Yamamoto, and H. Tsubakino, "Microstructural changes and crack initiation with white etching area formation under rolling/sliding contact in bearing steel," *ISIJ International*, vol. 45, no. 12, pp. 1897-1902, 2005.

[14] I. M. Widiyarta, F. J. Franklin, and A. Kapoor, "Modelling thermal effects in ratcheting-led wear and rolling contact fatigue," *Wear*, vol. 265, no. 9-10, pp. 1325-1331, Oct. 2008.

[15] J. Gegner and W. Nierlich, "The bearing axial cracks root cause hypothesis of frictional surface crack initiation and corrosion fatigue driven crack growth," in *NREL wind turbine tribology seminar*, 2011.

[16] J. Gegner, "Tribological aspects of rolling bearing failures," *Tribology-lubricants and lubrication*, IntechOpen, 2011.

[17] M. Paladugu, D. R. Lucas, and R. Scott Hyde, "Effect of lubricants on bearing damage in rolling-sliding conditions: Evolution of white etching cracks," *Wear*, vol. 398-399, pp. 165-177, 2018.

[18] M. H. Evans, A. D. Richardson, L. Wang, and R. J. K. Wood, "Serial sectioning investigation of butterfly and white etching crack (WEC) formation in wind turbine gearbox bearings," *Wear*, vol. 302, no. 1-2, pp. 1573-1582, 2013.

[19] M. H. Evans, A. D. Richardson, L. Wang, and R. J. K. Wood, "Effect of hydrogen on butterfly and white etching crack (WEC) formation under rolling contact fatigue (RCF)," *Wear*, vol. 306, no. 1–2, pp. 226-241, 2013.

[20] A. M. Diederichs, S. Barteldes, A. Schwedt, J. Mayer, and W. Holweger, "Study of subsurface

initiation mechanism for white etching crack formation," *Materials Science and Technology*, vol. 32, no. 11, pp. 1170-1178, 2016.

[21] T. Bruce, E. Rounding, H. Long, and R. S. Dwyer-Joyce, "Characterisation of white etching crack damage in wind turbine gearbox bearings," *Wear*, vol. 338-339, pp. 164-177, 2015.

[22] Rolling-element bearing. https://en.wikipedia.org/wiki/Rolling-element_bearing, 2020 (accessed 21 May 2020).

[23] M. Perez, C. Sidoroff, A. Vincent, and C. Esnouf, "Microstructural evolution of martensitic 100Cr6 bearing steel during tempering: From thermoelectric power measurements to the prediction of dimensional changes," *Acta Materialia*, vol. 57, no. 11, pp. 3170-3181, Jun. 2009.

[24] D. Scott, B. Loy, and G. H. ' Mills, "Metallurgical aspects of rolling contact fatigue," *Proceedings of the Institution of Mechanical Engineers*, vol. 181, no. 15, pp. 94-103, 1966.

[25] T. Endo, D. Dong, Y. Imai, and Y. Yamamoto, "Study on rolling contact fatigue in hydrogen atmosphere-improvement of rolling contact fatigue life by formation of surface film," *Tribology and Interface Engineering Series*, vol. 48, pp. 343-350, Jan. 2005.

[26] H. K. D. H. Bhadeshia, "Steels for bearings," *Progress in Materials Science*, vol. 57, no. 2, pp. 268-435, Feb. 2012.

[27] A. R. Marder and A. O. Benscoter, "Microcracking in plate martensite of AISI 52100 steel," *Metallurgical Transactions*, vol. 1, no. 11, pp. 3234-3237, 1970.

[28] J. Beswick, "Effect of prior cold work on the martensite transformation in SAE 52100," *Metallurgical Transactions A*, vol. 15, no. 2, pp. 299-306, Feb. 1984.

[29] H. Fu, E. Galindo-nava, and P. Rivera-diaz-del-castillo, "Modelling and characterisation of stress- induced carbide precipitation in bearing steels under rolling contact fatigue," *Acta Materialia*, vol. 128, pp. 176-187, 2017.

[30] International Standard ISO 281, "Rolling bearings - Dynamic load ratings and rating life," 2007.

[31] K. Johnson, *Contact mechanics*. Cambridge university press, 1987.

[32] E. V Zaretsky, "Rolling bearing life prediction, theory, and application," *National Aeronautics and Space Administration Technical Reports*, 2013.

[33] M. H. Evans, "White structure flaking failure in bearings under rolling contact fatigue," University of Southampton, 2013.

[34] A. V. Olver, "The mechanism of rolling contact fatigue: an update," *Proceedings of the Institution of Mechanical Engineers, Part J: Journal of Engineering Tribology*, vol. 219, no. 5, pp. 313-330, May. 2005.

[35] T. A. Harris, *Rolling bearing analysis*. John Wiley and sons, 2001.

[36] G. Lundberg and A. Palmgren, Dynamic capacity of rolling bearings. Generalstabens litografiska anstalts forlag, 1947.

[37] E. V. Zaretsky, J. V. Poplawski, and S. M. Peters, "Comparison of life theories for rolling-element bearings," *Tribology Transactions*, vol. 39, no. 2, pp. 237-248, Jan. 1996.

[38] G. W. Stachowiak and A. W. Batchelor, *Engineering tribology*. Butterworth-Heinemann, 2013.

[39] K. Ihata, T. Shiga, and A. Umeda, "Rolling bearing assembly having magnet to prevent brittle flaking," United States patent 7, pp. 520-675, Apr. 2009.

[40] H. Uyama and H. Yamada, "White Structure Flaking in rolling bearings for wind turbine gearboxes," *Wind systems*, 2014.

[41] A. Greco, S. Sheng, J. Keller, and A. Erdemir, "Material wear and fatigue in wind turbine Systems," *Wear*, vol. 302, no. 1-2, pp. 1583-1591, 2013.

[42] A. Ruellan, F. Ville, X. Kleber, A. Arnaudon, and D. Girodin, "Understanding white etching cracks in rolling element bearings: The effect of hydrogen charging on the formation mechanisms," *Proceedings of the Institution of Mechanical Engineers, Part J: Journal of Engineering Tribology*, vol. 228, no. 11, pp. 1252-1265, 2014.

[43] R. H. Vegter and J. T. Slycke, "The role of hydrogen on rolling contact fatigue response of rolling element bearings," *Journal of ASTM International*, vol. 7, no. 2, pp. 1-12, 2010.

[44] M. H. Evans, L. Wang, H. Jones, and R. J. K. Wood, "White etching crack (WEC) investigation by serial sectioning, focused ion beam and 3-D crack modelling," *Tribology International*, vol. 65, pp. 146-160, 2013.

[45] A. Grabulov, R. Petrov, and H. W. Zandbergen, "EBSD investigation of the crack initiation and TEM/FIB analyses of the microstructural changes around the cracks formed under Rolling Contact Fatigue (RCF)," *International Journal of Fatigue*, vol. 32, no. 3. pp. 576-583, 2010.

[46] A. Grabulov, U. Ziese, and H. W. Zandbergen, "TEM/SEM investigation of microstructural changes within the white etching area under rolling contact fatigue and 3-D crack reconstruction by focused ion beam," *Scripta Materialia*, vol. 57, no. 7, pp. 635-638, 2007.

[47] H. Uyama, H. Yamada, H. Hidaka, and N. Mitamura, "The effects of hydrogen on microstructural change and surface originated flaking in rolling contact fatigue," *Tribology Online*, vol. 6, no. 2, pp. 123-132, 2011.

[48] A. Muroga and H. Saka, "Analysis of rolling contact fatigued microstructure using focused ion beam sputtering and transmission electron microscopy observation," *Scripta Metallurgica et Materialia*, vol. 33, no. 1, pp. 151-156, Jul. 1995.

[49] A. M. Diederichs, A. Schwedt, J. Mayer, and T. Dreifert, "Electron microscopy analysis of structural changes within white etching areas," *Materials Science and Technology*, vol. 32, no. 16, pp. 1683-1693, 2016.

[50] R. Österlund, O. Vingsbo, L. Vincent, and P. Guiraldenq, "Butterflies in fatigued ball bearings-formation mechanism and structure," *Scandinavian Journal of Metallurgy*, vol. 11, no. 1, pp. 23-32, 1982.

[51] P. C. Becker, "Microstructural changes around non-metallic inclusions caused by rolling-contact fatigue of ball-bearing steels," *Metals Technology*, vol. 8, no. 1, pp. 234-243, 1981.

[52] M. H. Evans, J. C. Walker, C. Ma, L. Wang, and R. J. K. Wood, "A FIB/TEM study of butterfly crack formation and white etching area (WEA) microstructural changes under rolling contact fatigue in 100Cr6 bearing steel," *Materials Science and Engineering A*, vol. 570, pp. 127-134, 2013.

[53] W. Solano-Alvarez and H. K. D. H. Bhadeshia, "White-etching matter in bearing steel. Part 2: Distinguishing cause and effect in bearing steel failure," *Metallurgical & Materials Transactions A*, vol. 45, no. 11, pp. 4916-4931, 2014.

[54] J. H. Kang, B. Hosseinkhani, C. A. Williams, M. P. Moody, P. A. J. Bagot, and P. E. J. Rivera-Díaz-Del-Castillo, "Solute redistribution in the nanocrystalline structure formed in bearing steels," *Scripta Materialia*, vol. 69, no. 8, pp. 630-633, 2013.

[55] W. Liu, "The failure analysis of the repeat geartooth breakage in a 40 MW steam turbine load gearbox and the butterfly in the carburized case," *Engineering Failure Analysis*, vol. 46, pp. 9-17, Nov. 2014.

[56] J. L. O'Brien and A. H. King, "Electron microscopy of stress-induced structural alterations near inclusions in bearing steels," *Journal of Basic Engineering*, vol. 88, no. 3, pp. 568-571, 1966.

[57] H. Swahn, P. C. Becker, and O. Vingsbo, "Martensite decay during rolling contact fatigue in ball bearings," *Metallurgical Transactions A*, vol. 7, no. 8, pp. 1099-1110, Aug. 1976.

[58] Y. Murakami, M. Naka, A. Iwamoto, and G. Chatell, "Long life bearings for automotive alternator applications," in *International Congress & Exposition*, 1995.

[59] K. Hiraoka, M. Nagao, and T. Isomoto, "Study on flaking process in bearings by white etching area generation," *Journal of ASTM International*, vol. 3, no. 5, pp. 1-7, Apr. 2006.

[60] J. Martin, S. Borgese, and A. Eberhardt, "Microstructural alterations of rolling-bearing steel undergoing cyclic stressing," *Journal of Basic Engineering*, vol. 88, no. 3, pp. 555-565, 1966.

[61] K. Sugino, K. Miyamoto, M. Nagumo, and K. Aoki, "Structural alterations of bearing steels under rolling contact fatigue," *Transactions of the Iron and Steel Institute of Japan*, vol. 10, no. 2, pp. 98, 1970.

[62] M. Shibata, "Trends of studies on rolling contact fatigue life and recent results," *Koyo Eng. J.(English Edition)*, pp. 8-13, 2004.

[63] K. Hiraoka, T. Fujimatsu, N. Tsunekage, and A. Yamamoto, "Generation process observation of micro-structural change in rolling contact fatigue by hydrogen-charged specimens," *Journal of Japanese Society of Tribologists*, vol. 52, no. 12, pp. 888-895, 2007.

[64] J. Buchwald and R. W. Heckel, "An analysis of microstructural changes in 52100 steel bearings during cyclic stressing," *ASM Transactions Quarterly*, vol. 61, no. 4, pp. 750-756, 1968.

[65] A. D. Richardson, M. H. Evans, L. Wang, R. J. K. Wood, M. Ingram, and B. Meuth, "The evolution of white etching cracks (WECs) in rolling contact fatigue-tested 100Cr6 steel," *Tribology*

Letters, vol. 66, no. 1, 2018.

[66] H. K. D. H. Bhadeshia and W. Solano-Alvarez, "Critical assessment 13: elimination of white etching matter in bearing steels," *Materials Science and Technology*, vol. 31, no. 9, pp. 1011-1015, 2015.

[67] W. Musial, S. Butterfield, and B. Mcniff, "Improving wind turbine gearbox reliability," in *National Renewable Energy Lab.(NREL), Golden, CO (United States);*, 2007.

[68] A. Ruellan, "Tribological analysis of White Etching Crack (WEC) failures in rolling element bearings," Mechanics of materials, Institut National des Sciences Appliquées de Lyon, 2014.

[69] T. B. Lund, "Sub-surface initiated rolling contact fatigue-influence of non-metallic inclusions, processing history, and operating conditions," *Journal of ASTM International*, vol. 7, no. 5, pp. 1-12, 2010.

[70] A. Vincent *et al.*, "From white etching areas formed around inclusions to crack nucleation in bearing steels under rolling contact fatigue," in *Bearing Steels: Into the 21st Century*, ASTM International, West Conshohocken, pp. 109-123, 1998.

[71] A. E. Chard, "Deformation of inclusions in rail steel due to rolling contact," University of Birmingham, 2012.

[72] H. K. Danielsen *et al.*, "Multiscale characterization of White Etching Cracks (WEC) in a 100Cr6 bearing from a thrust bearing test rig," *Wear*, vol. 370, pp. 73-82, 2017.

[73] H. Muro and N. Tsushima, "Microstructural, microhardness and residual stress changes due to rolling contact," *Wear*, vol. 15, no. 5, pp. 309-330, May. 1970.

[74] J. Luyckx, "White Etching Crack Failure Mode in Roller Bearings: From Observation via Analysis to Understanding and an Industrial Solution," in *Rolling Element Bearings*, ASTM International, West Conshohocken, pp. 1-25, Oct. 2012.

[75] J. Luyckx, "Hammering wear impact fatigue hypothesis WEC/irWEA failure mode on roller bearings," in *Wind turbine tribology seminar*, CO(United States), pp. 15-17, 2011.

[76] W. Holweger *et al.*, "White etching crack root cause investigations," *Tribology Transactions*, vol. 58, no. 1, pp. 59-69, 2015.

[77] K. Stadler, J. Lai, and R. Vegter, "A review: the dilemma with premature white etching crack (WEC) bearing failures," In *Bearing Steel Technologies: 10th Volume, Advances in Steel Technologies for Rolling Bearings*, ASTM International, West Conshohocken, pp. 487-508, 2015.

[78] W. Solano-Alvarez, J. Duff, M. C. Smith, and H. K. D. H. Bhadeshia, "Elucidating white-etching matter through high-strain rate tensile testing," *Materials Science and Technology,* vol. 33, no. 3, pp. 307-310, 2017.

[79] M. Ščepanskis, A. Jakovičs, I. Kaldre, W. Holweger, B. Nacke, and A. M. Diederichs, "The numerical model of electrothermal deformations of carbides in bearing steel as the possible cause of white etching cracks initiation," *Tribology Letters*, vol. 59, no. 2, 2015.

[80] M. Ščepanskis, B. Gould, and A. Greco, "Empirical investigation of electricity self-generation in a lubricated sliding-rolling contact," *Tribology Letters*, vol. 65, no. 3, pp. 109, 2017.

[81] B. Gould and A. Greco, "Investigating the process of white etching crack initiation in bearing steel," *Tribology Letters*, vol. 62, no. 2, pp. 26, 2016.

[82] B. Gould and A. Greco, "The influence of sliding and contact severity on the generation of white etching cracks," *Tribology Letters*, vol. 60, no. 2, pp. 29, 2015.

[83] V. Rumpf, "A study on microstructural alterations in White Etching Cracks , Dark Etching Region , and White Etching Bands in rolling contacts," University of Southampton, 2018.

[84] F. Manieri, K. Stadler, G. E. Morales-Espejel, and A. Kadiric, "The origins of white etching cracks and their significance to rolling bearing failures," *International Journal of Fatigue*, vol. 120, pp. 107-133, 2019.

[85] R. Errichello, S. Sheng, J. Keller, and A. Greco, "Wind Turbine Tribology Seminar-A Recap," National Renewable Energy Lab. (NREL), Golden, CO (United States), 2012.

[86] S. Hyde, "White etch areas: metallurgical characterization & atomistic modeling," in *Wind Turbine Tribology Seminar,* Argonne, 2014.

[87] A. Ruellan, X. Kleber, F. Ville, J. Cavoret, and B. Liatard, "Understanding white etching cracks in rolling element bearings: Formation mechanisms and influent tribochemical drivers," in *Proceedings of the Institution of Mechanical Engineers, Part J: Journal of Engineering Tribology*,

vol. 229, no. 8, pp. 886-901, 2015.

[88] K. Stadler and A. Stubenrauch, "Premature bearing failures in wind gearboxes and white etching cracks," *Power Transmission Engineering*, vol. 10, pp. 34-40, 2014.

[89] Y. Kadin and M. Y. Sherif, "Energy dissipation at rubbing crack faces in rolling contact fatigue as the mechanism of white etching area formation," *International Journal of Fatigue*, vol. 96, pp. 114-126, 2017.

[90] W. Solano-Alvarez and H. K. D. H. Bhadeshia, "White-etching matter in bearing steel. Part I: Controlled cracking of 52100 steel," *Metallurgical and Materials Transactions A: Physical Metallurgy and Materials Science*, vol. 45, no. 11, pp. 4907-4915, 2014.

[91] M. Oezel *et al.*, "Formation of white etching areas in SAE 52100 bearing steel under rolling contact fatigue - Influence of diffusible hydrogen," *Wear*, vol. 414, pp. 352-365, 2018.

[92] J. Ćwiek, "Hydrogen degradation of high-strength steels," *Journal of Achievements in Materials and Manufacturing Engineering*, vol. 37, no. 2, pp. 193-212, 2009.

[93] L. Grunberg, "The formation of hydrogen peroxide on fresh metal surfaces," *Proceedings of the Physical Society. Section B*, vol. 66, no. 3, pp. 153-161, Mar. 1953.

[94] T. Imran, B. Jacobson, and A. Shariff, "Quantifying diffused hydrogen in AISI-52100 bearing steel and in silver steel under tribo-mechanical action: Pure rotating bending, sliding-rotating bending, rolling-rotating bending and uni-axial tensile loading," *Wear*, vol. 261, no. 1, pp. 86-95, Jul. 2006.

[95] J. A. Ciruna and H. J. Szieleit, "The effect of hydrogen on the rolling contact fatigue life of AISI 52100 and 440C steel balls," *Wear*, vol. 24, no. 1, pp. 107-118, Apr. 1973.

[96] L. Grunberg, D. T. Jamieson, and D. Scott, "Hydrogen penetration in water-accelerated fatigue of rolling surfaces," *Philosophical Magazine*, vol. 8, no. 93, pp. 1553-1568, Sep. 1963.

[97] H. K. Birnbaum and P. Sofronis, "Hydrogen-enhanced localized plasticity-a mechanism for hydrogen-related fracture," *Materials Science and Engineering: A*, vol. 176, no. 1-2, pp. 191-202, Mar. 1994.

[98] M. Grujicic, V. Chenna, R. Galgalikar, J. S. Snipes, S. Ramaswami, and R. Yavari, "Wind-turbine gear-box roller-bearing premature-failure caused by grain-boundary hydrogen embrittlement: a multi-physics computational investigation," *Journal of Materials Engineering and Performance*, vol. 23, no. 11, pp. 3984-4001, 2014.

[99] M. Grujicic, S. Ramaswami, R. Yavari, R. Galgalikar, V. Chenna, and J. S. Snipes, "Multiphysics computational analysis of white-etch cracking failure mode in wind turbine gearbox bearings," *Proceedings of the Institution of Mechanical Engineers, Part L: Journal of Materials: Design and Applications*, vol. 230, no. 1, pp. 43-63, 2016.

[100] B. A. Szost and P. E. J. Rivera-Díaz-del-Castillo, "Unveiling the nature of hydrogen embrittlement in bearing steels employing a new technique," *Scripta Materialia*, vol. 68, no. 7, pp. 467-470, Apr. 2013.

[101] M. Kohara, T. Kawamura, and M. Egami, "Study on mechanism of hydrogen generation from lubricants," *Tribology Transactions*, vol. 49, no. 1, pp. 53-60, Apr. 2006.

[102] H. Tanimoto, H. Tanaka, and J. Sugimura, "Observation of hydrogen permeation into fresh bearing steel surface by thermal desorption spectroscopy," *Tribology Online*, vol. 6, no. 7, pp. 291-296, 2011.

[103] Y. Imai, T. Endo, D. Dong, and Y. Yamamoto, "Study on rolling contact fatigue in hydrogen environment at a contact pressure below basic static load capacity," *Tribology Transactions*, vol. 53, no. 5, pp. 764-770, 2010.

[104] B. A. Szost and P. E. J. Rivera-Díaz-del-Castillo, "Unveiling the nature of hydrogen embrittlement in bearing steels employing a new technique," *Scripta Materialia*, vol. 68, no. 7, pp. 467-470, Apr. 2013.

[105] N. Kino and K. Otani, "The influence of hydrogen on rolling contact fatigue life and its improvement," *JSAE Review*, vol. 24, no. 3, pp. 289-294, Jul. 2003.

[106] E. Robert, B. Robert, and E. Rainer, "Investigations of bearing failures associated with white etching areas (WEAs) in wind turbine gearboxes," *Tribology Transactions*, vol. 56, no. 6, pp. 1069-1076, 2013.

[107] N. H. Forster, L. Rosado, W. P. Ogden, and H. K. Trivedi, "Rolling Contact Fatigue Life and

List of References

Spall Propagation Characteristics of AISI M50, M50 NiL, and AISI 52100, Part III: Metallurgical Examination," *Tribology Transactions*, vol. 53, no. 1, pp. 52-59, Dec. 2009.

[108] R. Errichello, S. Sheng, J. Keller and A. Greco, "Wind Turbine Tribology Seminar-A Recap," in *National Renewable Energy Lab.(NREL), Golden, CO (United States)*, 2012.

[109] A. W. Thompson and I. M. Bernstein, "The role of metallurgical variables in hydrogen-assisted environmental fracture," in *Advances in Corrosion Science and Technology*, Springer, Boston, MA: (United States), pp. 53-175, 1980.

[110] T. V. Liston, "Engine lubricant additives what they are and how they function," *Lubrication engineering*, vol. 48, no. 5, pp. 389-397, 1992.

[111] M. Paladugu, D. R. Lucas, and R. Scott Hyde, "Effect of lubricants on bearing damage in rolling-sliding conditions: Evolution of white etching cracks," *Wear*, vol. 398-399, pp. 165-177, 2018.

[112] N. Tsushima, "Crack propagation of rolling contact fatigue in ball bearing steel due to tensile strain," *Tribology Transactions*, vol. 47, no. 4, pp. 567-575, 2004.

[113] S. Tanaka, N. Mitamura, and Y. Murakami, "Influence of Sliding and Chromium Content in the Steel on the White Structural Change under Rolling Contact Fatigue," in *Proceedings of the global powertrain congress*, vol. 32, pp. 6-13, 2004.

[114] S. Fujita, N. Mitamura, and Y. Murakami, "Research of new factors affecting rolling contact fatigue life," in *World tribology congress III. American Society of Mechanical Engineers*, pp. 73-74, 2005.

[115] A. Umeda, T. Shiga, and K. Ihata, "Rolling bearing incorporated in auxiliary device for internal combustion engine," United States patent US 7,618,193, 2009.

[116] K. Iso *et al.*, "Rolling bearing, rolling bearing for fuel cell, compressor for fuel cell system and fuel cell system," United States patent US 7,265,080, 2007.

[117] W. Kruhöffer and J. Loos, "WEC formation in rolling bearings under mixed friction: influences and 'friction energy accumulation' as indicator," *Tribology Transactions*, vol. 60, no. 3, pp. 516-529, 2017.

[118] K. Nakayama and R. A. Nevshupa, "Plasma generation in a gap around a sliding contact," *Journal of Physics D: Applied Physics*, vol. 35, no. 12, pp. L53-L56, Jun. 2002.

[119] P. S. Y. Chu and A. Cameron, "Flow of Electric Current Through Lubricated Contacts," *ASLE Transactions*, vol. 10, no. 3, pp. 226-234, Jan. 1967.

[120] H. Prashad, "Magnetic Flux Density Distribution on the Track Surface of Rolling-Element Bearings-An Experimental and Theoretical Investigation," *Tribology Transactions*, vol. 39, no. 2, pp. 386-391, Jan. 1996.

[121] H. Prashad, "Determination of magnetic flux density on the surfaces of rolling-element bearings as an indication of the current that has passed through them-an investigation," *Tribology international.*, vol. 32, no. 8, pp. 455-467, 1999.

[122] K. Jablonka, R. Glovnea, J. Bongaerts, and G. Morales-Espejel, "The effect of the polarity of the lubricant upon capacitance measurements of EHD contacts," *Tribology International*, vol. 61, pp. 95-101, May. 2013.

[123] P. W. Huber and A. A. Sonin, "Theory for electric charging in liquid hydrocarbon filtration," *Journal of Colloid and Interface Science*, vol. 61, no. 1, pp. 109-125, Aug. 1977.

[124] J. Loos, I. Bergmann, and M. Goss, "Influence of Currents from Electrostatic Charges on WEC Formation in Rolling," *Tribology Transactions*, vol. 59, no. 5, pp. 865-875, 2016.

[125] W. J. Lu and R. S. Qin, "Stability of martensite with pulsed electric current in dual-phase steels," *Materials Science and Engineering A*, vol. 677, pp. 252-258, 2016.

[126] J. Rosinski and D. Smurthwaite, "Troubleshooting wind gearbox problems," *Gear Solutions*, vol. 8, pp. 22-33, 2010.

[127] H. Long, R. S. Dwyer-Joyce, and T. Bruce, "Dynamic modelling of wind turbine gearbox bearing loading during transient events," *IET Renewable Power Generation*, vol. 9, no. 7, pp. 821-830, Sep. 2015.

[128] B. Hamrock and D. Dowson, *Ball bearing lubrication: the elastohydrodynamics of elliptical contacts*. Wiley, 1981.

[129] T. Wright, *The physics and mathematics of adiabatic shear bands*. Cambridge University

Press, 2002.

[130] S. M. Walley, "Shear Localization: A Historical Overview," *Metallurgical and Materials Transactions A*, vol. 38, no. 11, pp. 2629-2654, Oct. 2007.

[131] T. Bruce, H. Long, T. Slatter and R. S. Dwyer-Joyce, "Formation of white etching cracks at manganese sulfide (MnS) inclusions in bearing steel due to hammering impact loading," *Wind Energy*, vol. 19, mo. 10, pp. 1903-1915, Oct. 2016.

[132] T. Bruce, H. Long, and R. S. Dwyer-Joyce. "Threshold maps for inclusion-initiated micro-cracks and white etching areas in bearing steel: the role of impact loading and surface sliding." *Tribology letters*, vol. 66, no. 111, 2018.

[133] S. Janakiraman, O. West, P. Klit, and N. S. Jensen, "Observations of the effect of varying Hoop stress on fatigue failure and the formation of white etching areas in hydrogen infused 100Cr6 steel rings," *International Journal of Fatigue*, vol. 77, pp. 128-140, 2015.

[134] F. B. Oswald, E. V. Zaretsky, and J. V. Poplawski, "Interference-Fit Life Factors for Roller Bearings," *Tribology Transactions*, vol. 52, no. 4, pp. 415-426, Jun. 2009.

[135] F. Oswald, E. Zaretsky, and J. Poplawski, "Interference-fit life factors for ball bearings," *Tribology Transactions*, vol. 54, no. 1, pp. 1-20, 2010.

[136] H. A. Al-Tameemi, H. Long, and R. S. Dwyer-Joyce, "Initiation of sub-surface micro-cracks and white etching areas from debonding at non-metallic inclusions in wind turbine gearbox bearing," *Wear*, vol. 406-407, pp. 22-32, 2018.

[137] A. Grabulov, "Fundamentals of rolling contact fatigue," Delft University of Technology, 2010.

[138] International Standard ISO 683-17, "Heat-Treated Steels, Alloy Steels and Free-Cutting Steels - Part 17: Ball and Roller Bearing Steels," 2014.

[139] M. Kuhn, P. W. Gold, and J. Loos, "Wear protection and low friction in roller bearings by different PVD-coating systems," *Tribology Series*, vol. 43, pp. 459-465, Jan. 2003.

[140] M. Reichelt, U. Gunst, T. Wolf, J. Mayer, H. F. Arlinghaus, and P. W. Gold, "Nanoindentation, TEM and ToF-SIMS studies of the tribological layer system of cylindrical roller thrust bearings clubricated with different oil additive formulations," *Wear*, vol. 268, no. 11-12, pp. 1205-1213, May. 2010.

[141] "AISI 52100 Alloy Steel (UNS G52986)." [Online]. Available: https://www.azom.com/article.aspx?ArticleID=6704. [Accessed: 05-April-2019].

[142] M. Paladugu, D. R. Lucas, and R. Scott Hyde, "Influence of raceway surface finish on white etching crack generation in WEC critical oil under rolling-sliding conditions," *Wear*, vol. 422, pp. 81-93, 2019.

[143] S. W. Ooi, A. Gola, R. H. Vegter, P. Yan, and K. Stadler, "Evolution of white-etching cracks and associated microstructural alterations during bearing tests," *Materials Science and Technology*, vol. 33, no. 14, pp. 1657-1666, 2017.

[144] B. Gould, A. Greco, K. Stadler, E. Vegter, and X. Xiao, "Using advanced tomography techniques to investigate the development of White Etching Cracks in a prematurely failed field bearing," *Tribology International*, vol. 116, pp. 362-370, 2017.

[145] M. Li and H. Zhang, "Effect of banded carbide structure on the rolling contact fatigue of GCr15 bearing steel, " in *2017 5th International Conference on Mechatronics, Materials, Chemsistry and Computer Engineering (ICMMCCE 2017)*, Atlantis Press, 2017.

[146] J. Guan, L. Wang, Z. Zhang, X. Shi, and X. Ma, "Fatigue crack nucleation and propagation at clustered metallic carbides in M50 bearing steel," *Tribology International*, vol. 119, pp. 165-174, 2018.

[147] KH. Kim, SD. Park, JH. Kim, and CM. Bae, "Role of Spheroidized Carbides on the Fatigue Life of Bearing Steel," *Metals and Materials International,* vol. 18, no. 6, pp. 917-921, 2012.

[148] E. Yu, H. Jung, KS. Kim, EJ. Kim, and J. Lim, "Influence of Carbide Formation on Tensile and Fatigue Properties of Carburized Steels," *Applied Microscopy*, vol. 43, no. 2, pp.81-87, 2013.

[149] M. Randelius, "Influence of microstructure on fatigue and ductility properties of tool steels," KTH Royal Institute of Technology, 2008.

[150] G. Guetard, I. Toda-Caraballo, and P. E. J. Rivera-Díaz-del-Castillo, "Damage evolution around primary carbides under rolling contact fatigue in VIM–VAR M50," *International Journal of Fatigue*, vol. 91, pp. 59-67, 2016.

List of References

[151] H. Fu, E.I. Galindo-Nava, and P.E.J. Rivera-Díaz-del-Castillo, "Modelling and characterisation of stress-induced carbide precipitation in bearing steels under rolling contact fatigue," *Acta Materialia*, vol. 128, pp.176-187, 2017.

[152] H. K. Danielsen et al., "3D X-ray computerized tomography of White Etching Cracks (WEC)," *Materials Characterization*, vol. 150, pp. 78-87, 2019.

[153] A.P. Voskamp, R. Österlund, P.C. Becker and O. Vingsbo, "Gradual changes in residual stress and microstructure during contact fatigue in ball bearings," *Metals Technology*, vol. 7, no. 1, pp.14-21, 1980.

[154] Y. Estrin, and A. Vinogradov, "Extreme grain refinement by severe plastic deformation: A wealth of challenging science," *Acta materialia*, vol. 61, no. 3, pp.782-817,2013.

[155] Y. J. Li, M. Herbig, S. Goto, and D. Raabe, " Atomic scale characterization of white etching area and its adjacent matrix in a martensitic 100Cr6 bearing steel, " *Materials Characterization*, vol. 123, pp. 349-353, 2017.

[156] D. Brooksbank, K. W. Andrews, "Stress fields around inclusions and their relation to mechanical properties, " *Production and Application of Clean Steels*, pp.186-198, 1972.